Effects of salinity on the leaching of ionic species from the Duvernay Formation, a Canadian hydraulic fracturing play

by

Katherine N. Snihur

A thesis submitted in partial fulfillment of the requirements for the degree of

Master of Science

Department of Earth and Atmospheric Sciences

University of Alberta

Abstract

Hydraulic fracturing combined with horizontal drilling has revolutionized the oil and gas industry in North America. The majority of Canada's hydraulic fracturing operations are in Alberta and British Columbia, with the Montney and Duvernay formations ranked highest in five hydraulically fractured formations in the Western Canadian Sedimentary Basin (WCSB). During fracturing, water, and chemical additives, are mixed to make hydraulic fracturing fluid (HFF), which is then injected into an oil and/or gas rich shale formation at high pressure to create fracture networks. The resulting fractures increase the formation permeability, allowing hydrocarbons to flow freely into the well bore. After fracturing, a portion of the injected HFF returns to the surface along with hydrocarbons and formation water. This wastewater, composed of HFF and formation water, is commonly referred to as flowback and produced water (FPW). FPW contains organic compounds from the HFF chemical additives, along with organic compounds from the target formation (e.g. polycyclic aromatic hydrocarbons (PAHs)), and potentially toxic heavy metals (PTHM) (e.g. As, Ba, and Sr). FPW often has high total dissolved solids (TDS) upwards of 200,000 ppm in many Formations including the Duvernay Formation. Recently, FPW from nearby wells, called recycled produced water (RPW), has been used to supplement fresh source water as part of the HFF to reduce the load hydraulic fracturing has on nearby freshwater sources, typically to a TDS of approximately 30,000 ppm. It is from the chemistry of FPW that much of our understanding of the subsurface interactions between HFF and the target geologic formation is derived. While the chemical analysis of FPW does provide information to understand water-rock interactions in the subsurface, the mechanisms by which various ions enter into FPW remain a topic of active study.

In this thesis, I simulated the geochemical processes occurring during hydraulic fracturing using benchtop reactors with a water:rock ratio of 18:1 at formation temperature of the Duvernay in the Eastern Shale basin (95 °C) and Western Shale basin (140 °C), to better understand reaction mechanisms in real time, such as the partitioning of metals between the solid and aqueous phases. I conducted these experiments in two different vessels to accommodate temperatures above and below 100 °C without violent boiling. Further, I aimed to assess if stirred batch reactors can be used to understand downhole water-rock interactions that occur during hydraulic fracturing and be used to predict the inorganic chemistry of FPW and be applied to commercial scale problems. I tested my approach by conducting simple experiments to determine how the higher initial salt content of RPW can affect the leaching of PTHM. My results indicated that elemental concentration data from reactor experiments can be used to predict the assemblage of solid phases that could precipitate downhole, such as quartz, barite, and celestite, through saturation indices modeling of these FPW minerals, with SI within ± 0.5, 0.3, and 2.0 of FPW, respectively. Results of experiments simulating the use of RPW to make up HFF, which had a higher initial salinity of 30,000 ppm, showed that the higher ionic strength results in a salting-in effect that increased the concentrations of many ions in solution such as As, Ba, and Sr by as much as 937%, 1874%, and 284%, respectively. My findings are corroborated by the geochemical modeling of FPW samples collected from the Duvernay Formation, using both freshwater and RPW source waters, that reveal that higher concentrations of many elements, including PTHM, occur in FPW from wells that used RPW for fracturing. My work both illustrated the potential risks of using RPW in hydraulic fracturing operations on the environment in the event of a spill during transport or at disposal sites and provided a robust benchtop approach to predict the leaching of elements from the host rock during hydraulic fracturing.

Acknowledgements

I would like to thank all the professors and colleagues have contributed to my research, with a special thank you to Dr. Daniel S. Alessi, my supervisor, and Dr. Shannon L. Flynn who contributed immensely to the improvement of my experimental method and this manuscript. A warm thank you to Dr. Murray K. Gingras for taking the time to assist me in my collection of outcrop samples from Jasper National Park, with the permission of Parks Canada (Permit # JNP-2018-28120), and Dr. Nicholas B. Harris, for assisting me in choosing my core samples and supplying much of the core material I needed, with the assistance of Alberta's Core Research Center. I would also like to thank Dr. Kurt O. Konhauser, Dr. Benjamin Rostron, and Dr. Siobhan (Sasha) A. Wilson without whose expertise this thesis would not have been possible.

I am grateful for all the help I received in my day-to-day research, particularly that of Dr. Konstantin von Gunten, who not only taught me many methods used in this thesis, but also contributed time in helping me conduct many of these analyses. A sincere thank you to both Logan R. Swaren and Christopher Noyahr who conducted supplemental analyses for this research and contributed greatly to the reliability of the results. I would also like to thank to our funding sources, from the Encana Corporation and NSERC Collaborative Research and Development and Discovery grants to Dr. Alessi. And finally, I would like to thank my sister and the rest of my family for their unwavering support during this process.

Table of Contents

List of Figures

List of Tables

1. Introduction

Hydraulic fracturing combined with horizontal drilling are methods for the recovery oil and gas that are used across the world, particularly in China, the United States, and western Canada. Hydraulic fracturing uses the injection of water and chemical additives into the subsurface at elevated pressures to produce fissures in the reservoir rock to increase permeability and allow hydrocarbon extraction into the wellbore (Alessi et al. 2017, He et al. 2017, Kim et al. 2016, Phillips 1972, Vidic et al. 2013). These fissures are held open by proppants, such as quartz sand or ceramic beads, which allow the hydrocarbons to flow after the fracture propagation stage has concluded. This technology has been employed to recover hydrocarbons from what are termed unconventional reservoirs such as low permeability shale-rich basins, where conventional oil and gas recovery would otherwise be uneconomic. In western Canada, there are 5 primary geological units that host unconventional reservoirs: the Nordegg Member, Muskwa Formation, Colorado Group, Montney Formation, and Duvernay Formation. To date the Montney and Duvernay formations have been targets for hydraulic fracturing, with the Duvernay Formation being the most developed (Alessi et al. 2017, Dong et al. 2018, Dong et al. 2019). In the United States, there are many formations that have been hydraulically fractured, but the Marcellus Shale has been the most studied (e.g. Abualfaraj et al. 2014, Arthur et al. 2008, Tasker et al. 2016, Xiong et al. 2018).

1.1 The Hydraulic Fracturing Water Cycle

Hydraulic fracturing requires considerable quantities of water, with a median volume of 15275 m^3 and 19425 m^3 of water to fracture an oil or gas well, respectively, in the United States (Gallegos et al. 2015). 5-60% of the injected water volume returns to the surface as a portion of the wastewater (Clark et al. 2013, Gregory et al. 2011, Tasker et al. 2016). The quantities of water used in hydraulic fracturing is on the rise, especially with horizontals are being drilling longer

distances, and therefore making the wells larger (Alessi et al. 2017, Gallegos et al. 2015). The water cycle of hydraulic fracturing can be divided into 5 steps: water acquisition, chemical mixing to produce fracturing fluids, fracturing fluid injection, flowback and produced water recovery, and the disposal or reuse of the recovered water (Fig. 1). Most commonly, water is acquired from nearby surface water bodies or shallow groundwater, but in some settings brackish groundwater has been used (Alessi et al. 2017). The water collected is mixed with chemical additives to make up hydraulic fracturing fluid (HFF) which is subsequently injected to fracture the reservoir host rock.

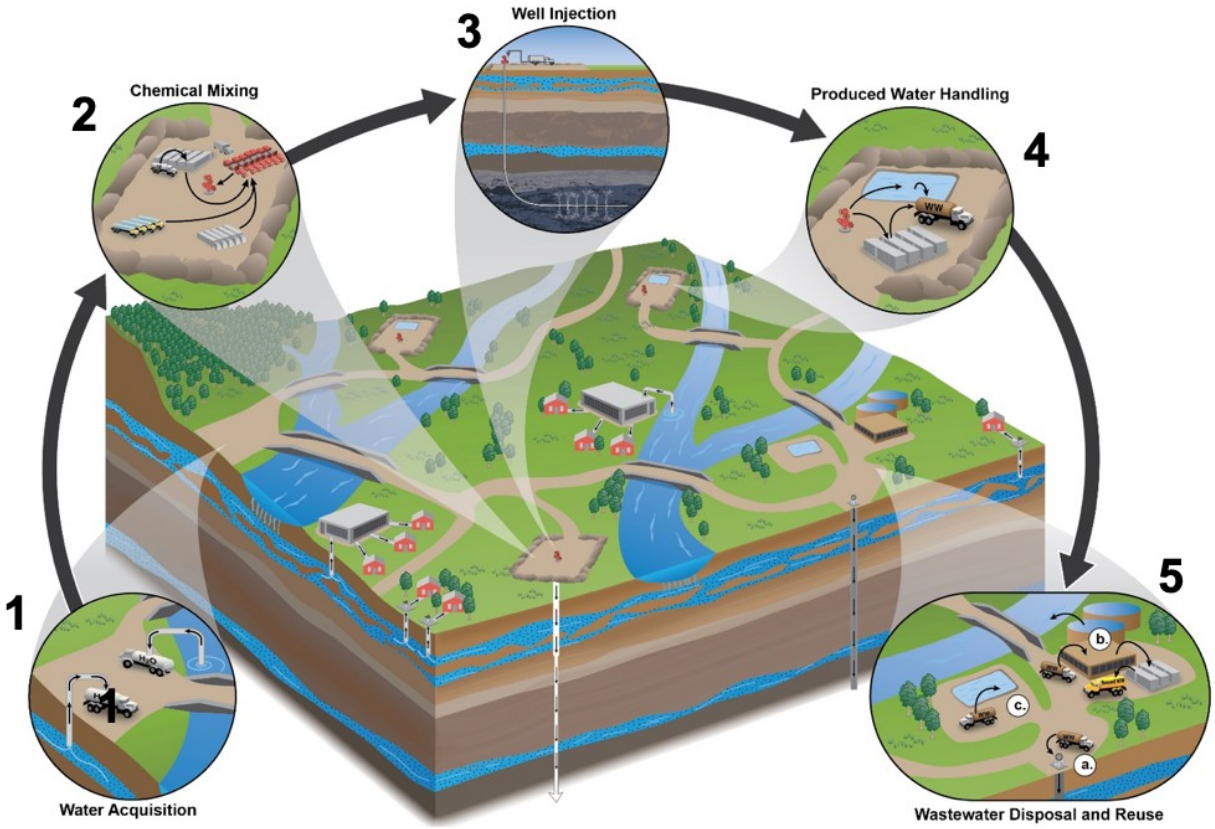

Figure 1: The hydraulic fracturing water cycle, illustrating the 5 major steps of hydraulic fracturing operations adapted from (US EPA, 2016)

The composition of HFF varies based on mineralogy and geochemistry of the target formation. However, broadly speaking it is a mixture dominated by water, with chemical additives

only contributing a small percentage (<1 %) of the bulk composition (Alessi et al. 2017; Arthur et al. 2008). In some cases, HFF is made using freshwater mixed with recycled wastewater from previous fracturing operations, typically referred to as flowback and produced water, and will be herein referred to as FPW (Zhong et al. 2019). FPW that has been recycled to be reused as a portion of HFF in fracturing in another well will be referred to as recycled produced water or RPW. There are also non-water fracturing processes that use nitrogen or hydrocarbons in place of water as the fracturing agent, but these are less common (Alessi et al. 2017). While chemical additives only constitute a small percentage of the overall volume of a typical HFF, each additive is added to improve the recovery of hydrocarbons from the well in some way, either by improving the fracturing process itself, or by extending the life of the well and equipment used. For example, biocides such as glutaraldehyde are added to inhibit bacterial growth and therefore extend the life of the infrastructure. Table 1 outlines the common additives, and their function in hydraulic fracturing.

Table 1: Common hydraulic fracturing additives, their common uses, and most common compounds. Adapted from Arthur et al. 2008.

Additive	Purpose	Main Compound
Acid	Dissolves minerals and assist in initial fissuring of rock	Hydrochloric acid or muriatic acid
Biocide	Eliminates bacteria that produce corrosive by-products	Glutaraldehyde
Breaker	Delays breakdown of polymer chains	Ammonium persulfate
Corrosion inhibitor	Prevents corrosion of pipes	N,n-dimethyl formamide
Crosslinker	Maintains fluid viscosity even with increased temperature	Borate Salts
Friction reducer	Reduces friction between fluid and pipes	Polyacrylamide and Mineral oil
Gel	Thickens water to suspend sand better	Guar gum or hydroxyethyl cellulose
Iron control	Prevents oxidation of metals	Citric acid
KCl	Carries brine fluids	Potassium chloride
Oxygen scavenger	Removes dissolved oxygen to prevent corrosion	Ammonium bisulphite
Ph adjusting agent	Maintains the optimum pH for the effectiveness of the other components	Sodium or potassium carbonate
Proppant	Holds fractures/fissures open	Silica sand
Scale inhibitor	Prevents scale deposits along the pipe	Ethylene glycol
Surfactant	Increases fracturing fluid viscosity	Isopropanol

Once mixed, a proppant (typically silica sand or ceramic beads) is added to the HFF, the mixture is injected into the well at high pressure to fracture the target formation, and then sealed in for a predetermined time; this is commonly referred to as fracturing period. During the fracturing period, the pressure causes fractures to propagate into target formation with HFF carrying the proppant into these small fissures. When the pressure is released, the newly formed fractures are held open by the proppant, which allows the HFF, formation water and hydrocarbons to escape the reservoir. Following fracturing, the formation waters (often saline brines), and fracturing fluid that returns to the surface are referred to as flowback water. Flowback water is produced for anywhere from a few weeks to a few months (Alessi et al. 2017). Once hydrocarbons are produced, the co-produced water is then referred to as produced water (Delompré et al. 2019, Kondash et al. 2017). FPW has variable total dissolved solids (TDS) content, depending on the formation of origin and time after flowback began. For example, FPW from the Marcellus shale in the Eastern USA ranges between 8000 – 360 000 ppm TDS (Abualfaraj et al. 2014, Shaffer et al. 2013), while FPW from the Duvernay Formation in Western Canada varies from less than 10,000 ppm in early flowback to greater than 200,000 ppm in produced waters (He et al. 2017, Zhong et al. 2019). The TDS is believed to be composed of salts in the formation brines and those that leached from the fractured formation (Ziemkiewicz & He 2015). In addition to the salts FPW contains potentially toxic heavy metals (PTHM), as well as organic compounds (e.g. polyaromatic hydrocarbons (PAHs)), residual HFF additives and their transformation products, and other hydrocarbon range organic compounds (He et al. 2017, Flynn et al. 2019).

The final two stages of the water cycle are, handling produced water and the disposal or reuse of the resulting FPW. FPW is reused to reduce cost and or mitigate potential environmental

impacts of the hydraulic fracturing water cycle. An important concern in produced water handling is the potential for surface releases of brackish to saline FPW. An FPW spill, containing salts, heavy metals, polyaromatic hydrocarbons, and other organic compounds, can have detrimental impacts on aquatic and soil ecosystems and can be costly to remediate (Delompré, et al. 2019, Folkerts et al. 2020, Goss et al. 2015). FPW is often transported to a deep injection well for disposal, which is expensive (Paktinat et al. 2011). During transportation there is a risk of a spill, which is amplified as the distance to the disposal site increases. FPW can also be treated and reused as a component of the HFF for the fracturing of a subsequent well. Recently, there have been developments to increase the efficiency of FPW treatment (Ahmadun et al. 2009, Freedman et al. 2017). Treatments, such as mechanical vapour compression (MVC), membrane distillation, and forward osmosis, target TDS reductions to levels that do not interfere with hydraulic fracturing additives, such as friction reducers (Shaffer et al. 2013, Sun et al. 2019). In Alberta, the targeted desalination is to approximately to seawater concentration of NaCl, which is about 30,000 ppm (Sun et al. 2019). While RPW was only used in 2 % of the hydraulic fracturing wells in Alberta in 2018 (AER 2019), the practice is on the rise and is common in areas of the of the United States. In Pennsylvania and Delaware, currently many wells are being fractured using RPW as a major component of the HFF (Shaffer et al. 2013). Using FPW and RPW instead of freshwater is viewed as an environmentally friendly practice, as it reduces withdrawals from freshwater resources, such as shallow groundwater, lakes, and rivers, which are also used for agricultural and drinking water (CAPP 2018). It also reduces the need for FPW disposal via deep well injection. Technological advancements in hydraulic fracturing have resulted in wells with longer horizontals, covering a larger area, and with larger fractures (Gallegos et al. 2015). In both cases there is an increase in

the water needed per well, which is driving the push towards using RPW in new hydraulic fracturing operations.

1.2 Previous Laboratory Experimental Simulations

Recently studies have begun to focus on the drivers of FPW geochemistry, by looking at the water-rock interactions between HFF, formation water, and the target formation (Flynn et al. 2019, Harrison et al. 2017, Li et al. 2019, Li et al. 2020, Owen et al. 2020, Sumner and Plata 2018, Tasker et al. 2016, Xiong et al. 2018). While some of these were focused solely on FPW chemistry (Flynn et al. 2019, Owen et al. 2020), there have also been attempts to experimentally replicate the formation temperatures and/or pressures achieved during hydraulic fracturing (Harrison et al. 2017, Li et al. 2019, Li et al. 2020, Sumner and Plata 2018, Tasker et al. 2016, Xiong et al. 2018). The reservoir temperatures and pressures for the Duvernay Formation are approximately 115 °C (Taylor et al. 2014) and between 600 to 850 bar (Shen et al. 2018); however, these values depend on the location within the formation and can vary between formations as well. For example, in the Marcellus Formation, the temperatures and formation pressures are substantially lower, up to 95 °C and 270-410 bar (Sumner and Plata 2018, Xiong et al. 2018).

Because FPW typically contains elements not used in hydraulic fracturing additives or found in abundance in fresh source waters, such as potentially toxic heavy metals (PTHM), there has been a push to investigate the source of these ions during hydraulic fracturing. The consensus is that either leaching from the formation or mixing with formation waters are the main sources of these ions to FPW (Owen et al. 2020, Rowan et al. 2015). While leaching from the formation and interactions with formation waters are likely the dominant drivers of the composition of FPW, it is still unknown which drivers contribute each ion and how these interactions occur during hydraulic fracturing. Some inverse modelling has been done to explain the interactions between

HFF, formation water and formation rock (Owen et al. 2020), but this is yet to be verified experimentally. Recent work with small benchtop reactors has begun to determine the organic and inorganic geochemical interactions that occur during hydraulic fracturing (Harrison et al. 2017, Li et al. 2019, Li et al. 2020, Sumner and Plata 2018, Tasker et al. 2016, Xiong et al. 2018).

Early studies by Tasker et al. (2016) and Xiong et al. (2018) focused on the Marcellus shale, and used commercially available stirred batch reactors to conduct experiments at elevated pressures and temperatures, 83 bar and 80 °C, respectively. Tasker et al. (2016) identified the behavior of both metals and organics when Marcellus shale samples were exposed to synthetic HFF over a range of pH values. Their major findings were that temperature and pressure did not influence the release of metals from the rocks, but did affect the degradation of the organic additives in the synthetic HFF. The minimal effect of temperature on the dissolution of the metals was inferred from the low concentrations of metals observed in the synthetic FPW following the experiments (with a max concentration of 14 mg/L observed for any one ion), and may have resulted from the relatively low temperatures studied (25 °C and 80 °C) or the low rock to water ratio compared to downhole conditions. They found increased degradation of organics and mobilization of metals occurred in lower pH experiments. Xiong et al.'s (2018) follow-up study, focused on polyacrylamide, a common friction reducer used in hydraulic fracturing (Arthur et al. 2008). They tested the effect of pressure, temperature, salinity, and rock heterogeneity on degradation glutaraldehyde. Their study agreed with the previous work that temperature, not pressure or salinity (ionic strength), played a major role in the degradation of organic compounds. Unfortunately, the effects of temperature on inorganics were not further analyzed in this study.

The next study, by Harrison et al. (2017), expanded the work of Tasker et al (2016) and Xiong et al. (2018) to encompass multiple formations, including the Barnett, Eagle Ford, and

Green River, in addition to the Marcellus Shale and focussed on the inorganic chemistry of leaching from these formations at elevated temperatures (80 °C). Their experiments, in agreement with the findings of Tasker et al. (2016), did not use elevated pressures, using the justification that mineral solubilities are far more sensitive to changes in temperature than in pressure in the ranges expected in hydraulic fracturing operations. These experiments looked at trends of element leaching over a period of up to 6 months, in short (3 weeks), intermediate (3 months), and long term (6 months) experiments conducted in borosilicate glass serum bottles. Their findings revealed that even over the course of 6 months the final metals and anions concentrations, which plateaued in the first 100 - 1000 hr, did not reach concentrations representative of FPW. For example, the maximum Ca concentrations observed were <400 mg/L, which is an order of magnitude lower than in FPW. Because of high heterogeneity in rock composition and leached elements between the formations studied, saturation index calculations were used to compare the data.

In the next most recent of these papers, Sumner and Plata (2018) used custom-made throughput reactors to simulate higher pressures (345 bar) with elevated temperatures (60 °C), to investigate the kinetics of the chemical additive-water-rock interactions. The purpose of the throughput reactors in this study was to enable computation of transformation pathways by allowing up to 15 simultaneous experiments or 5 triplicate experiments to be conducted under identical conditions. In their work, Sumner and Plata (2018) tested their reactor with 12 additives simultaneously and found that at increased pressures and temperatures there was no reactivity of these compounds. While this study's focus was on additives, there are potential applications for inorganic leaching from the shales as well. This study adds invaluable information for the scientific community but, I argue that an even simpler approach is possible to achieve the same ends. With previous studies reporting that pressure had an inconsequential effect on the interactions between

HFF and the rock formations, I hypothesized that a simple batch experimental approach, like that used by Harrison et al. (2017), can achieve the same goals as a reactor capable of achieving the high pressure and temperature conditions of hydraulic fracturing.

Most recently, some work by Li et al. (2019) focused on the thickness of the alteration zone along the fractures during hydraulic fracturing. They did this by submersing a core sample into simulated HFF into a reactor and increasing the temperature and pressure to 80 °C and 77 bar, respectively, and allowing to react for 3 weeks. They found that the alteration zone depends on the composition of the shale rock sample, especially on pyrite and carbonate dissolution. They concluded that the carbonate concentration dictated the alteration zone thickness, by increasing the acidic HFF pH and accelerating the iron and sulfur oxidation and subsequent precipitation of $Fe(OH)_{3(s)}$ and sulfate minerals, such as barite ($BaSO_4$). They tested two shales in their experiments, the low-carbonate Marcellus shale and the higher carbonate Eagle Ford shale, and determined that increased carbonate content resulted in a thinner chemically altered zone due to accelerated precipitation of iron oxides and sulfate minerals which blocked pathways for the HFF to penetrate into the core. Similar to Tasker et al. (2016) and Xiong et al. (2018), Li et al. (2019) used commercially available reactors to conduct their experiments. This work was then followed up in a subsequent paper, Li et al. (2020), which explored the depths specific reaction paths reached into the rock using active transport modelling. This second study found that chemical reaction between HFF and the host rock are likely occurring deeper than the visible chemically altered zone and that these reactions depended on both dissolved oxygen and extracted bitumen.

While formation leaching at elevated pressures and temperatures has been extensively addressed in the six studies I reviewed above, the relationship of these reactor chemical data to the chemistry of field-collected FPW has not. Thus, I tested if simple, low-cost, benchtop reactors

containing mixtures of water and target formation rock particles at reservoir temperatures could be used to predict the inorganic chemistry profile of FPW. Additionally, I aimed to constrain how the salinity of RPW impacts metals leaching from formation rocks during the hydraulic fracturing process, as well as the geochemical implications of using RPW during the hydraulic fracturing process. I finally assess if the reactors and methods developed here can be used to address the problem of scaling in-lab results to commercial scale questions.

2. Materials and Methods

2.1 The Duvernay Formation

The Devonian Duvernay Formation is the most developed hydraulic fracturing target in western Canada. The formation extends throughout central Alberta and is primarily composed of organic-rich mudstones commonly called “black shales” (Harris et al. 2018). It has a westward dip and ranges from 2 m to 99 m in thickness (AER 2016). The organic-rich mudstones originate from an intercontinental sea that covered portions of the western North American continent during the Upper Devonian, when the world was warmer and sea level was higher (Harris et al. 2018, Knapp et al. 2017). The stratigraphic members of the Duvernay Formation are: the Upper Duvernay, Middle Duvernay Carbonate, and Lower Duvernay. The Upper Duvernay Formation has been the primary zone targeted for hydraulic fracturing due to its high total organic carbon (TOC) content and brittleness (Dong et al. 2018).

The Duvernay Formation has been further subdivided into the Western Shale Basin (WSB) and the Eastern Shale Basin (ESB), separated by the Grosmont shelf. The WSB is primarily composed of silicate rich mudstones high in Al and Si with some calcite. While the ESB is richer in carbonate minerals and is dominated by Ca and Mg (Dong et al. 2018, Dong et al. 2019). Because the Duvernay Formation is a west-leaning sloped deposit, like most of the stratigraphy in western Canada, the WSB is buried deeper and therefore warmer and under greater lithostatic pressure than the ESB. Despite differences in lithology, both basins have been targeted by hydraulic fracturing operations. The Duvernay Formation extends to the Cordilleran deformation belt where its name is changed to the Perdrix Formation (Pilkington et al. 2006). The Perdrix Formation, is the metamorphosed equivalent to the Duvernay Formation. The Perdrix, originally of the same composition as the Duvernay formation, is composed of organic rich shaley

mudstones, and outcrops in a few locations in the Jasper area of the Rocky Mountains, near the Pyramid Thrust. In previous hydraulic fracturing studies, outcrop samples have been used in place of core samples from target formations as proxies for subsurface samples (MacKay et al. 2018, McKean et al. 2018). The assumption has been made that outcrop samples are reasonable proxies, except when weathering appears on the surface.

In this study, a core from each basin (WSB and ESB) was accessed from Core Research Centre (CRC) in Calgary, Alberta, as well as an outcrop sample of the Perdrix Formation, were used to determine how HFF salinity and formation composition impacts the mobilization of metals (Fig. 2). The two cores were previously characterized for thermal maturity, hardness index, and oxide composition (see Dong et al. 2018, Dong et al. 2019, Harris et al. 2018). The well ID's for the two cores sampled are 100/08-20-038-28W4/00 (Eastern Shale Basin) and 100/11-04-058-23W5/00 (Western Shale Basin) for Core 1 and 2, respectively. Core 1 was sampled over a depth range of 2600-2615 m and Core 2 was sampled over a depth range of 3985-3985.5 m. Further, visibly unweathered outcrop samples from Perdrix Formation were used to determine if outcrop samples were suitable proxies for the subsurface Duvernay Formation by comparing their experimental results, such as mineral composition and solid and aqueous element compositions, to the core samples (Fig. 2). Outcrop samples were used for reactor experiment method development and temperature-dependent reactor experiments due to the larger quantities available.

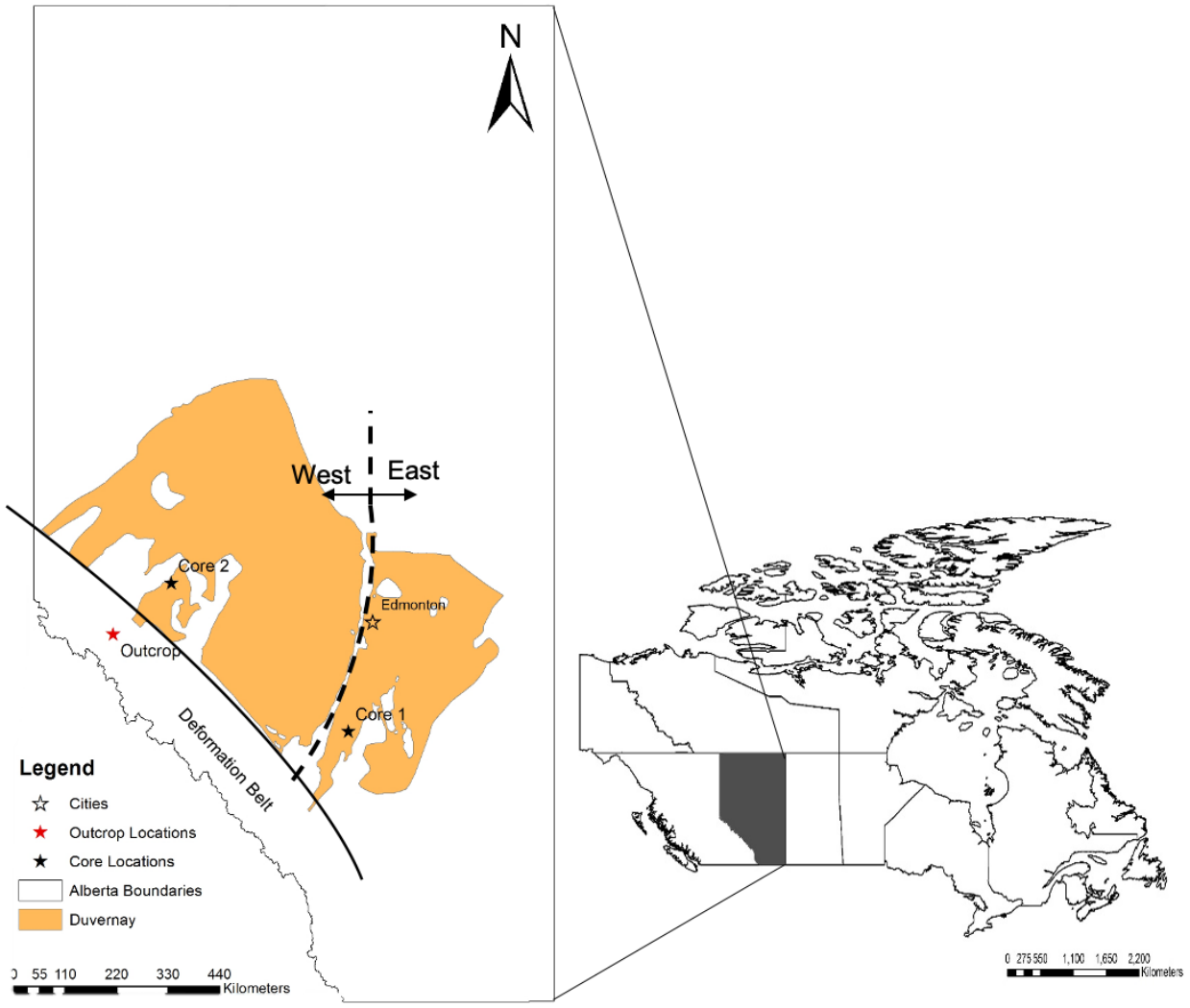

Figure 2: The Duvernay Formation and sampling locations in Alberta, Canada. Core 1 is from the Eastern Shale Basin, Core 2 is from the Western Shale Basin, and the outcrop sample is from the Perdrix Formation.

2.2 Experimental Design

Reservoir temperatures were calculated by Christopher Noyahr, a MSc student in the EAS department, from available well log data using "Time-Since" or the "Constant Addition" corrections for drilling fluid cooling (Weides and Majorowicz 2014, Zetaware Utilities 2003a,

Zetaware Utilities 2003b). Once reservoir bottom-hole temperatures were determined, the values were adjusted for the Upper Duvernay Formation, using the local geothermal gradient and were estimated to be 93.7 °C and 137.4 °C for Cores 1 and 2, respectively. For simplicity, the temperatures used in reactor experiments were rounded to 95 °C and 140 °C. Additionally, room temperature (25 °C) experiments were conducted with the outcrop sample to investigate the impact of temperature on the leaching of ions from the rocks. These 25 °C experiments were also useful in establishing a baseline for the mineral solubility constants (K_{sp}), of which many were determined at room temperature, before extrapolating to the higher temperatures (95 °C and 140 °C).

Reactor experiments using the Perdrix Formation outcrop samples were conducted to assess the kinetics of leaching and the mobilization of ions at all three temperatures, 25 °C, 95 °C, and 140 °C, prior to experiments using limited core samples. Experiments with core materials from the Duvernay Formation were conducted at the corresponding reservoir temperatures for each core: 95 °C and 140 °C for Core 1 and 2, respectively. Experiments were conducted in two bespoke benchtop reactors. For the low temperature experiments (<100 °C), a sealed 500 mL glass media bottle with a lid septum, hereafter referred to as Vessel A, was used and allowed for periodic sampling with a 1 mm needle (18G) (Fig. 3A). For experiments with temperatures >100 °C, a 420 mL thick-walled, glass, round-bottom flask (Chemglass, CG-1800-R-04) was used with a stainless-steel ball valve inserted into a Teflon lid to withstand higher pressure, hereafter referred to as Vessel B (Fig 3B). As a standard thermometer could not be inserted into Vessel B at sampling, a laser thermometer (Fisherbrand™ CON4485) was used to measure the temperature of the glass. The measured glass temperature was calibrated using irreversible temperature dots (Omega #TL-C5-240-10) located inside of the vessel (see Appendix A-1 for calibration parameters).

Additionally, in Vessel B the natural build-up of pressure (~3.6 bar at 140 °C) was allowed to occur in the headspace to prevent boiling during the experiment. In both reactors, a constant stir rate (250 rpm in Vessel A and 500 rpm in Vessel B) was maintained using magnetic stir bars to ensure continuous mixing. The differing stir rates reflected the different sized stir bars used due to the flat bottom of vessel A and the rounded bottom of Vessel B.

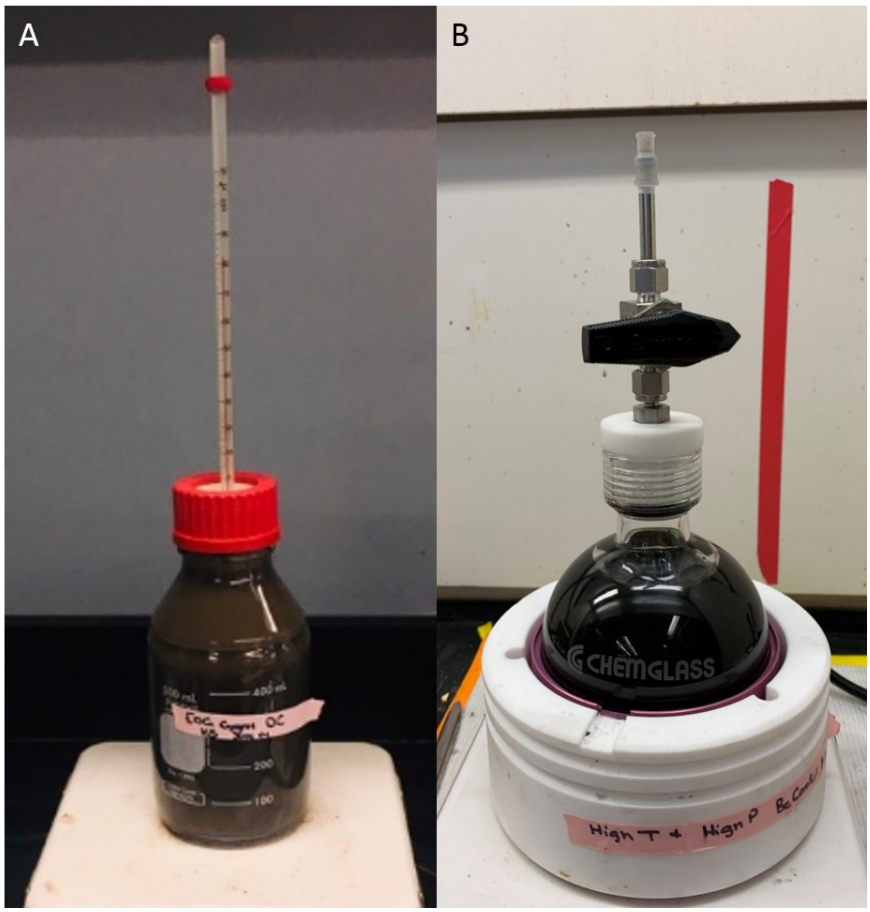

Figure 3: Benchtop reactor vessels used to conduct experiments at A) <100 °C and B) >100 °C.

Outcrop and core samples were prepared using an agate mortar and pestle, followed by sieving between 0.5 and 0.09 mm. This particle size range was chosen to ensure the solids would pass through the needle (18G or 1 mm) used to sample the low temperature apparatus, while excluding ultrafine powders with high surface reactivity. For all experiments a water-rock ratio of

18:1 was used, although due to a smaller maximum volume for Vessel B, a smaller amount of solid and water was used to attain this ratio. The exact volumes, masses and temperatures are provided in Table 2. Two types of experiments were conducted, in order to balance the need for a more sampling points, especially in the beginning of the experiment (Type I), with the need for a more balanced sampling to a later timepoint, T_{96hr} or T_{168hr} (Type II) (Table 3). To reduce potential kinetics effects due to the sampling of different amounts of material (15 mL vs. 30 mL) experimental types I and II, the sample aliquot volume was adjusted to end each experiment with approximately the same residual volume.

Table 2: Summary of Reactor Parameters used in experiments.

	Vessel A	**Vessel B**
Volume of Solution used	450mL	420mL
Mass of Solids used	25g	23.5g
Temperature of experiments	25 °C and 95 °C	140 °C

Table 3: Sampling times and aliquots from each type of experiment.

Experiment Type	**Number of Samples**	**Sample aliquot**	**Sampling Times**
I	11	15 mL	$T_{0'}$, $T_{30min'}$, $T_{1hr'}$, T_0, T_{1hr}, T_{2hr}, T_{4hr}, T_{8hr}, T_{16hr}, T_{24hr}, $T_{48hr.}$
II	8	30 mL	$T_{0'}$, T_0, T_{4hr}, T_{8hr}, T_{24hr}, T_{48hr}, T_{96hr}, *T_{168hr}

*T_{168hr} was only sampled with experiments using Vessel A

All 18 ΩM ultrapure water and 30,000 ppm NaCl experiments were conducted in duplicate, with one experiment of each type, I and II, (Table 3) to simulate the interaction between the rock formation and hydraulic fracturing fluids made from either freshwater, or a mixture of freshwater and recycled produced water or brackish-saline groundwater. Following sampling, the slurry aliquots were filtered using 0.8 μm cellulose acetate membranes. The solids retained on the filters were dried and weighed to account for the mass change within the reactor. The mass and pH of

the filtrate was recorded, before it was separated into two vials, one unacidified and one acidified with 12μL 70 % nitric acid per 10mL of sample. Both samples were then refrigerated until analysis.

2.3 Aqueous Analyses

2.3.1 ICP-MS/MS

Filtrates were analysed for major and trace elements using an Agilent 8800 inductively coupled plasma mass spectrometer (ICP-MS/MS). In the freshwater experiments, the total dissolved solids (TDS) in the filtrate was low enough (<2000ppm) to allow direct analysis. Experiments conducted with 30,000 ppm NaCl required a 15x dilution with 18 ΩM ultrapure water and were re-acidified with 12 μL 70 % HNO_3 per 10 mL solution, prior to ICP-MS/MS analysis. During analysis, no-gas mode was used for low mass elements and heavy metals, while a gas collision/reaction cell was utilized for most of the elements – either He, O_2, or H_2 depending on the element, with all using MS/MS (Table 4). An internal standard mix containing 2 ppm Sc, Ge, In, Lu, and Bi, was introduced using an inline addition to account for instrumentation drift; and were measured using the applicable gas collision/reaction mode. The internal standard drift correction for each element was determined by mass of the element and available gas collision/reaction cells (Table 4).

Table 4: ICP-MS/MS parameters used in aqueous sample measurements.

Element	Q1 → Q2	Gas	Internal Std.	Element	Q1 → Q2	Gas	Internal Std.
Li	7 → 7	-	Sc 45	Mn	55 → 55	He	Ge 74
B	11 → 11	-	Sc 45	Fe	56 → 56	He	Ge 74
Na	23 → 23	He	Sc 45	Ni	60 → 60	He	Ge 74
Mg	24 → 24	He	Sc 45	Cu	63 → 63	He	Ge 74
Al	27 → 27	He	Sc 45	Zn	66 → 66	He	Ge 74
Si	28 → 28	H2	Se 45	As	75 → 91	O2	Ge 74
P	31 → 47	O2	Ge 74	Br	79 → 79	H2	Ge 74
S	32 → 48	O2	Ge 74	Sr	88 → 88	He	Ge 74
Cl	35 → 37	O2	Ge 74	Mo	95 → 95	He	Ge 74
K	39 → 39	He	Sc 45	Cd	111 → 111	-	In 115
Ca	40 → 40	H2	Sc 45	Ba	137 → 137	-	In 115
Ti	47 → 47	He	Ge 74	Pb	208 → 208	-	Lu 175
Cr	52 → 52	He	Ge 74	U	238 → 238	-	Bi 209

2.3.2 Alkalinity Measurements

The alkalinity of each sample for Core 2 and the outcrop experiments were measured using the unacidified portion of the filtrate following the method outlined in Flynn et al. (2019). For each measurement, 5-7 mL of filtrate was titrated with 0.1 M HCl to a pH of 4.2 using a Metrohm Titrando 905. The milliequivalents of acid used to lower the pH were then used to calculate the alkalinity of each sample in ppm CO_3^{2-}. These analyses revealed that there was a relatively constant ratio of 7:5 for Ca^{2+}:CO_3^{2-} that was used to calculate alkalinity in experiments with Core 1 for later modelling and mass balance checks.

2.3.3 Colorimetry Measurements

For Core 1 experiments Cl concentrations were measured with colorimetry, using EPA method 325.2. For this method, ferricyanide is used to form a colored complex and was measured with a Thermo Gallery Plus Beermaster Autoanalyzer.

2.4 Solids analysis

Filtered solids were dried at room temperature in a fume-hood and then weighed. Analyses were conducted when there was enough sample to allow for proper analysis. To conduct all of the analyses at least 1.0 g was needed, the breakdown of mass requirements for analysis were as follows: for acid digestions, 0.1 g was needed, and for XRD between 1 g and 0.5 g.

2.4.1 Total Acid Digestions

A total acid digestion of each solid sample was conducted to determine inorganic content. I used a modified method based on that of Wang et al. (2016). Briefly, 0.1 g of sample was pre-digested with 5 mL 70% HNO_3 and 5 mL 30% H_2O_2 and heated at 80 °C for 1 hour and 150 °C for an additional hour, then allowed to cool. After, 2.5 mL 50% HF was added to the cooled solution and then heated at 150 °C for 2 hours. The method was modified to include an introduction of 20 mL boric acid to the solution and the heated for an additional 2 hours at 150 °C. Boric acid was used to prevent the formation of insoluble fluoride precipitates, such as CaF_2, LiF, and AlF_3 (Wilson et al. 2006). The resulting solution was cooled to room temperature and diluted to a final volume of 50 mL with aqua regia. Following complete digestion, digestate composition was determined using an ICP-MS/MS following method similar to that used to analyze aqueous samples. Before analysis, the samples were diluted an additional 20x with 18 ΩM ultrapure water and reacidified with 12 µL 70 % HNO_3 per 10 ml. In the digestates, additional trace elements considered relatively insoluble we measured, V, Co, Se, Rb, Ce, and Th, and thus unlikely to be detected in the filtrates. Because the introduction of boric acid and hydrochloric acid during the digestion, B and Cl were not measured. Br was also not measured in the digestates, as it was found

to have not leached during the experiments. A complete list of ICP-MS/MS parameters and metals measured for the digested solids is listed in Table 5.

Table 5: ICP-MS/MS parameters for digested solids measurements.

Element	Q1 → Q2	Gas	Internal Std.	Element	Q1 → Q2	Gas	Internal Std.
Li	7 → 7	-	Sc 45	Ni	60 → 60	He	Ge 74
Na	23 → 23	He	Sc 45	Cu	63 → 63	He	Ge 74
Mg	24 → 24	He	Sc 45	Zn	66 → 66	He	Ge 74
Al	27 → 27	He	Sc 45	Se	78 → 78	H2	Sc 45
Si	28 → 28	H2	Se 45	As	75 → 91	O2	Ge 74
P	31 → 47	O2	Ge 74	Rb	85 → 85	He	Ge 74
S	32 → 48	O2	Ge 74	Sr	88 → 88	He	Ge 74
K	39 → 39	He	Sc 45	Mo	95 → 95	He	Ge 74
Ca	40 → 40	H2	Sc 45	Cd	111 → 111	He	In 115
Ti	47 → 47	He	Ge 74	Ba	137 → 137	He	In 115
V	51 → 51	He	Ge 74	Ce	140 → 140	-	In 115
Cr	52 → 68	O2	Ge 74	Pb	208 → 208	-	Lu 175
Mn	55 → 55	He	Ge 74	Th	232 → 232	-	Bi 209
Fe	56 → 56	He	Ge 74	U	238 → 238	-	Bi 209
Co	59 → 59	He	Ge 74				

Digestions were done in sets of 12 of which 10 were new samples, 1 was a replicate of one of the 10 samples, and 1 was a reference standard of comparable total organic carbon (TOC) content. The repeated sample was used to determine a standard error for the digestions associated with heterogeneity. The reference standard was used to determine error in the methodology. The USGS reference used for these experiments was the Boquillas Shale, ShBOQ-1 which has a TOC of 4.61 % (Birdwell 2017).

2.4.2 Powder X-Ray Diffraction (XRD)

XRD analyses and peak fitting were conducted by Logan Swaren, a PhD student in the EAS department. Each sample having a total mass >1 g was ground with anhydrous ethanol using agate elements with a McCrone Micronizing Mill for 7 minutes, and samples with 0.5-0.99 g were milled for 5 minutes (using the design of Locock et al., 2012). All samples were dried overnight, collected, and disaggregated using an agate mortar and pestle.

Samples were prepared in front-loading cavity mounts for analysis. Patterns were collected using a Bruker AXS D8 Advance powder X-ray diffractometer equipped with LYNXEYE XE-T linear position sensitive detector and a cobalt source that was operated at 35 kV and 40 mA. XRD patterns were collected from 3–80° 2θ using a step size of 0.02° 2θ and a dwell time of 1s/step. Mineral phase identification was conducted using the DIFFRAC.EVA XRD phase analysis software (Bruker) with reference to the International Center for Diffraction Data Powder Diffraction File 4+ database (ICDD PDF4+). Rietveld refinement (Bish and Howard 1988, Hill and Howard 1987, Rietveld 1969) with XRD data utilized to determine mineral abundances with TOPAS 5 (Bruker). Fundamental parameters peak fitting (Cheary and Coehlo 1992) was used for all phases.

2.5 Modelled Saturation Indices

Chemical speciation modelling for saturation indices was conducted using PHREEQC (Parkhurst & Appelo 2013). Due to the high ionic strength of the NaCl experiments (0.2-0.35 M), the pitzer.dat database was used, while for the experiments conducted in 18 ΩM ultrapure water and a lower ionic strength (<0.1 M), the phreeqc.dat database was used. The pitzer.dat database uses a series of analytical equations, called the Pitzer equations, to calculate the activity of ions in solution while phreeqc.dat uses the extended Debye-Hückel equation. Saturation indices based on aqueous sample concentrations (Appendix B-1) were calculated using an approach similar to Flynn et al. (2019). Saturation indices of amorphous silica ($SiO_{2(am)}$), quartz (SiO_2), barite ($BaSO_4$), celestine ($SrSO_4$), and gypsum ($CaSO_4$) were calculated as a time-series dataset for the duration of each experiment. Elements of concentration >0.5 mmol/L, or important trace elements such as Ba and Sr, in the experimental solutions and available in both databases were used (Appendix A-2), as well as the temperature recorded during the reactor experiments. A list of the elements used in

modelling is available in Appendix A-2; of the elements present and of interest in solution, only Al was not available in one of the databases (pitzer.dat), which was of little concern due to its low solubility in silicate minerals, the anticipated greatest source of Al for the experiments. Hörbrand et al. (2018), studying the performance of common databases used in PHREEQC at extreme conditions, showed that the Pitzer database most closely resembles the results of the phreeqc.dat database, used for the freshwater experiments, and so those were the databases I chose. Temperature corrections of solubility constants in PHREEQC are made using a polynomial correction function when correction parameters were available and using Van't Hoff's extrapolation when not (Hörbrand et al. 2018).

3. Results

3.1 Characterization of Rock Samples

3.1.1 Initial Characterization

Previous characterizations of the two well cores studied found significant chemical and mineralogical composition differences. Dong et al. (2018) and Harris et al. (2018) reported samples from the Eastern Shale basin of the Duvernay Formation are typically higher in carbonates and lower in silicate minerals than samples from the Western Shale basin which is typically dominated by quartz. The mineralogical content of both cores was dominated by the carbonate minerals calcite and dolomite. While Core 1 from the Eastern Shale Basin had a higher proportion of calcite; 61.2 % by mass verse 56.0 % in Core 2 from the Western Shale Basin, their total carbonate mineral contents were roughly equal (66.2 % in Core 1 and 68.5 % in Core 2). Additionally, the analysis of core material by total digestion showed Ca + Mg to comprise a similar fraction by mass of both cores (Fig. 4). Core 1 was found to have a higher content of clay minerals, with illite, clinochlore and kaolinite making up 13.3 % by mass of the total rock composition, while only illite was the only clay found in Core 2, comprising 3.7 %. Of the elements measured by ICP-MS/MS, the major metals identified by total acid digestion made up 99.9 % or more of the rock composition, with trace metals making up the remainder 0.1 %. Consistent with the mineralogical data, the dominant cations were, Ca and Mg, consistent with the carbonate mineralogy determined by XRD, making up a sum of 48.8 % and 55.8 % in Core 1 and Core 2, respectively. Si, the dominant cation in quartz and other silicate minerals, made up another 30 % of the overall measured composition of the cores. The remainder of the major ions are cations commonly found in silicate minerals, such as Na, Al, and K, cations ions commonly found in sulfide/sulfate minerals, such as Fe, S, Sr, and Ba, and other accessory oxides, such as Ti and Mn.

Na, Al and K were the next most abundant elements and likely from feldspars (11.7 %, 6.0 %, and 15.9 % in Core 1, Core 2, and the outcrop, respectively). The sulfur-bearing mineral ions were the next most concentrated ions, with Fe taking up the greatest proportion (2.4 %, 2.6 %, and 2.1 % in Core 1, Core 2 and Outcrop, respectively), which correlated with the only sulfide mineral identified by XRD, pyrite.

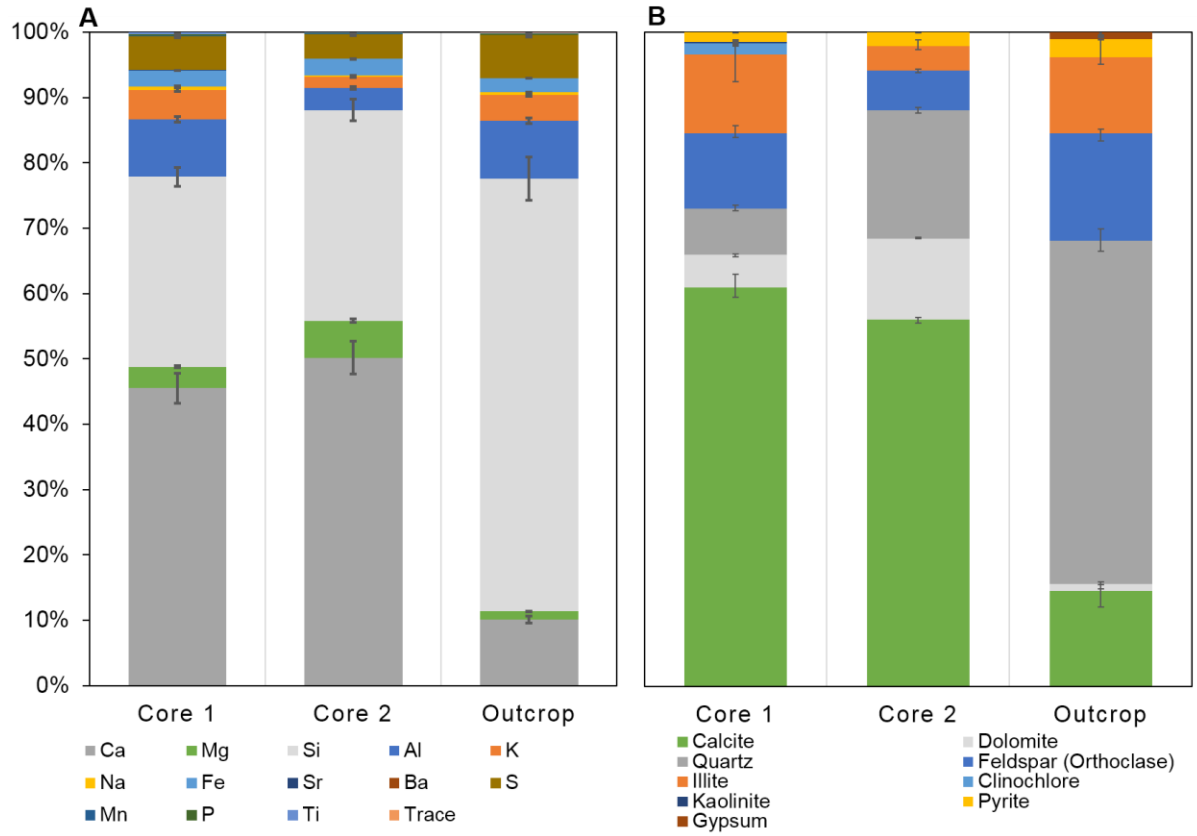

Figure 4: Composition of rock samples used in experiments. The major metals (>1 %) and mineralogy are presented in A) and B), respectively. Major metals represent >99.9 % by mass of the total composition of the rock samples, the trace metals are defined as making up less than 0.01 % of the rock composition. Metal concentrations were determined by total acid digestion, mineralogy was determined with quantitative XRD analysis.

Trace elements, PTHM, were measured by complete acid digestion. An element was identified as trace if it made up less than 0.01 % of the digested rock composition. The detectable trace metals were Zn, Cu, Li, Ni, Cr, Co, As, Pb, Mo, and U, composing in total 0.1 % of the rock samples. The core samples had similar concentrations of most of the trace metals, with the exception of Zn which had a 10-fold greater concentration in Core 1 than Core 2.

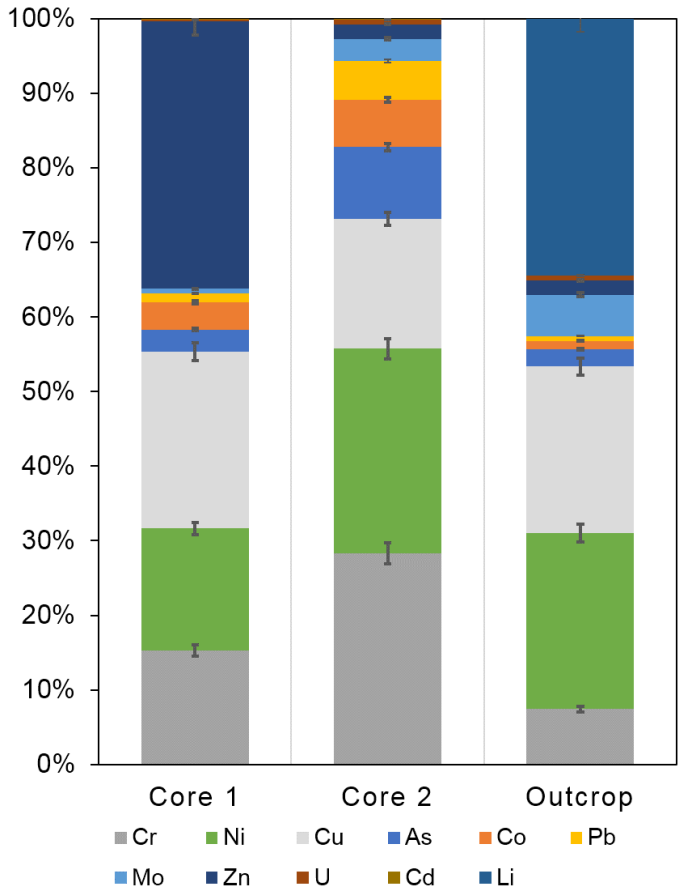

Figure 5: Trace metals fractions in the rock samples used in reactor experiments. Trace metals comprise at total of <0.1 % by mass of the rock samples. As the digestion process modified the oxidation state of redox sensitive metals, no oxidation state is reported. Errors and concentrations are not included in the figure but reported in Appendix B.

While there were differences in both the chemical and mineral composition of the two core samples, these differences were minimal when compared to the outcrop sample (Fig. 4 and Fig. 5). Gypsum was the only mineral found in the outcrop sample, that was absent in both cores. The gypsum was found to be heterogeneously distributed in the outcrop sample (Appendix B-3). Illite was the only clay present in the outcrop and comprised 11.9 % of the overall sample. The outcrop had higher fraction of quartz (52.4 % vs 7.3 % and 19.6 % for Core 1 and Core 2, respectively) and led us to believe the outcrop sample was weathered before collection. This was despite our attempts to remove the visibly weathered exterior. The higher proportion of quartz was possibly due to the weathering of mineral phases with higher solubilities from the rock, such as calcite and dolomite (Szramek et al. 2007), resulting in an increased proportion of quartz. Another possibility is that there was an introduction of Si by Si-rich hydrothermal fluids carried by the nearby Pyramid Thrust. Despite the presence of weathering products, such as gypsum, pyrite was still present in the outcrop (2.8 % ± 0.2). Pyrite forms in reducing/anoxic environments, such as the bottom of the Western Interior Seaway during the Devonian, and typically weathers in oxidizing environments (Rimstidt and Vaughan 2003). Under oxidizing conditions, it is possible that an oxidisation rind of ferric iron oxide could have formed on the exterior of the pyrite crystals and thereby prevent or slow down further weathering (Nicholson et al. 1989). The mineralogical differences were reflected in the measured elemental composition, with 3-fold higher concentrations of Si in the outcrop samples when compared with the cores (Fig. 4 and Fig. 5). Although the trace element fractions in the outcrop samples were different than the core samples, they were not any more substantial than the variations between the core samples themselves. This smaller deviation in elemental concentrations from the core samples, coupled with the consistent pyrite fraction with

the core samples, allowed for the outcrop sample to be used for method development and temperature dependence test experiments.

3.1.2 Post Experiment Characterization

3.1.2.1 Mineralogical Changes in the Core Samples

There were minimal changes in the mineral compositions during the leaching experiments. No new phases were detected in either of the core or the outcrop samples (Fig. 6 and Fig. 7). With Core 1, there were minor changes (<15 % of their initial fraction) in the proportion of primary minerals (quartz, feldspar, calcite, and pyrite), but a more substantial changes (34-60 % of their initial fraction) in the secondary and accessory minerals, such as dolomite, illite, and kaolinite. The differences between the freshwater and 0.5 M NaCl experiments were also minor (<7 %) for all mineral phases with the exceptions of dolomite and kaolinite (25 % and 21 % respectively). Both minerals were found to have a larger decrease in the NaCl experiments (Fig. 6C); however, these differences were small relative to the overall rock mineralogy (Figs. 6A and 6B). While the addition 0.5 M NaCl did not have a major impact on the minerology of the samples, it did impact the kinetics of the leaching/dissolution reactions (Figs. 6A and B). In the NaCl experiments, changes in rock mineralogy occurred earlier in the experiments, at T_0, when the reactor first reached the target temperature (95 °C for Core 1, 140 °C for Core 2). While both the freshwater and spiked experiments had changes in the proportions of the minerals between the addition of the solution to the reactor and T_0, the change in their fractions was more pronounced in the NaCl experiments. The changes continued throughout the experiment, with another change in the mineral fractions between T_0 and T_{4hr} that was not seen in the freshwater experiments. The fractions of the primary minerals and clinochlore decrease in their fractions, while the two other clays, illite and kaolinite, both increased modestly in their fractions, making up 5.8 % and 0.2 %

more, respectively, at T_{48hr} than in the initial rock. The mineralogical changes observed by XRD were likely due to alteration of the primary minerals to clay minerals. Further analysis via total digestions of the rock samples was conducted to determine the cause(s) of these changes.

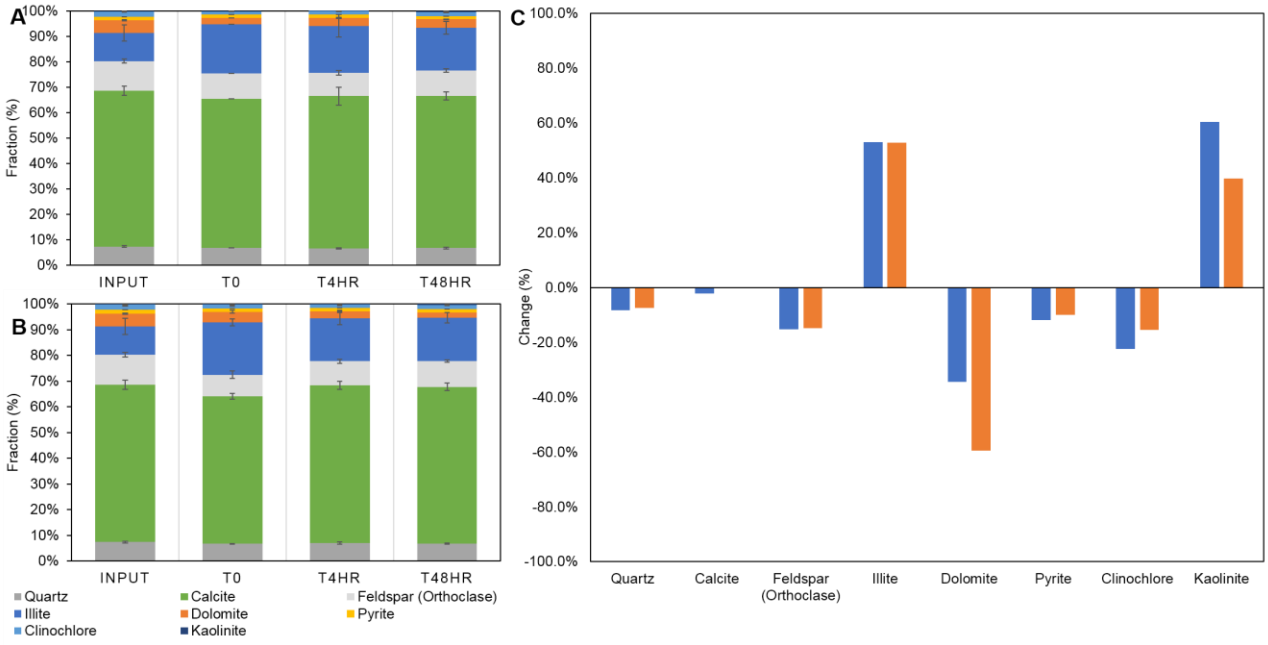

Figure 6: Mineralogical changes in Core 1 from freshwater experiments (A) and experiments spiked with 0.5 mol/L NaCl (B) and the resulting percent change comparison (C) between the freshwater (blue) and NaCl spiked (orange) experiments. Error bars indicate quantitative errors of ± 1 σ.

Similar to Core 1, Core 2 had only minor changes in the proportions of the minerals during the experiments, with all mineral changes being <17 % of their initial fraction (Fig. 7). There was a reduction in the dolomite, feldspar, and pyrite fraction in both the freshwater and 0.5 M NaCl of experiments (Fig. 7C), but totaling <16 % for each mineral. In contrast to Core 1, Core 2 had an increase in its fraction of calcite, by 1.8 % and 2.2 % in the freshwater and NaCl experiments, respectively. The increase was likely due to either the dissolution of dolomite, the formation of

illite from the degradation of feldspar, or both. The most important difference between the freshwater and the saline experiments for Core 2 was the kinetics of the changes in mineral fractions. Similar to the results for Core 1, it happened quicker in the NaCl experiments (Fig. 7A and B). In both cases there were small observed changes from the initial rock characterizations was, but those changes were not substantial and so it was assumed that the bulk mineralogy remained unchanged throughout the experiments.

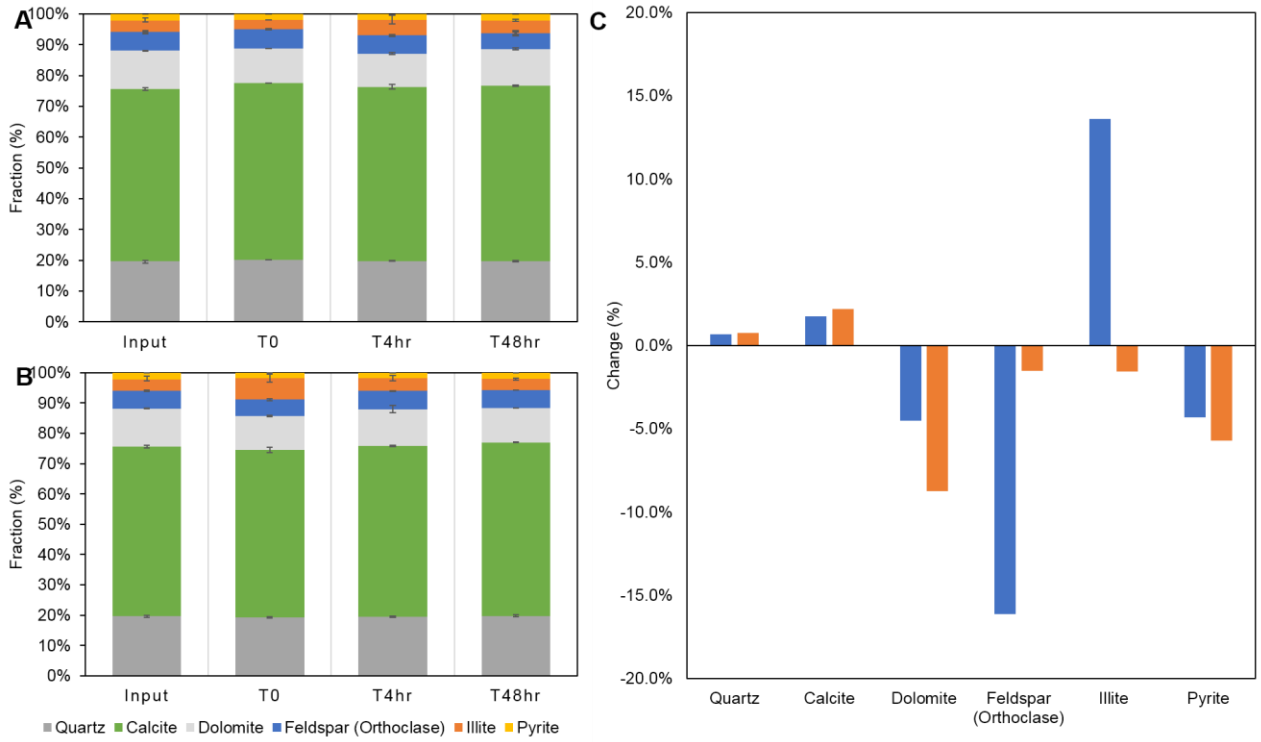

Figure 7: Mineralogical changes in Core 2 from both freshwater experiments (A) and 0.5 mol/L NaCl experiments (B) and the resulting percent change comparison (C) between the freshwater (blue) and NaCl spiked (orange) experiments. Error bars indicate quantitative errors of ± 1 σ.

3.1.2.2 Mineralogical Changes in the Outcrop Samples

Similar to the core samples, the mineralogical changes in the outcrop sample were minimal, the exception was the total loss of gypsum in all the experiments by T_0 (Fig. 8 and Fig. 9). This

was likely due to the high solubility of gypsum at the temperatures of the reactors during the initial temperature ramp, between 25 °C and 95 °C (Krumgalz 2018, Rosenbauer et al. 2005). The changes in the fractions of the remaining minerals were more pronounced in the 0.5 M NaCl experiments (up to 53 % change from their initial fraction vs 45 % in the freshwater experiments), consistent with the results of the core experiments. There were no clear temperature dependence trends observed in the mineralogical data.

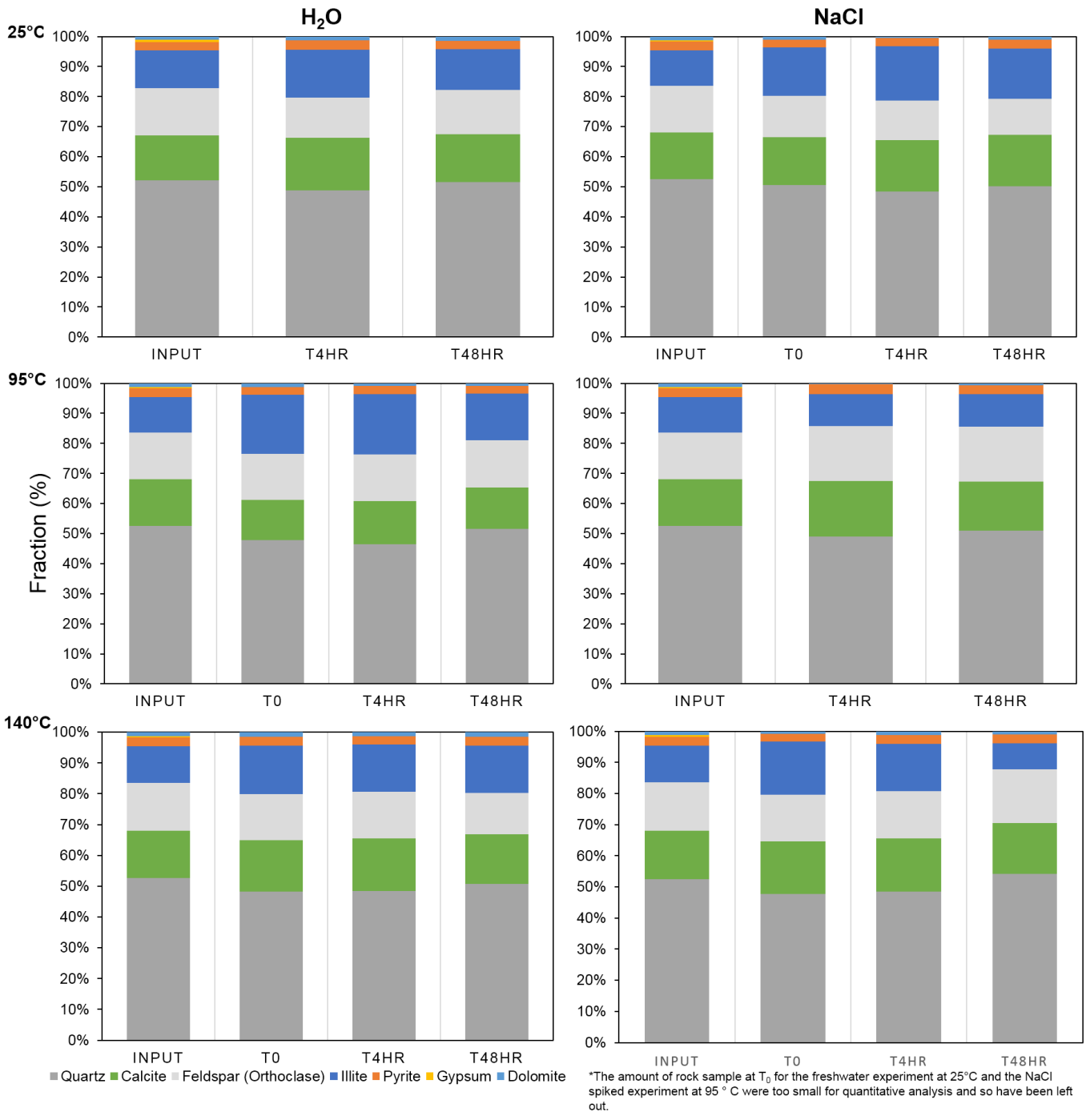

Figure 8: Mineralogical changes in the outcrop samples from both freshwater experiments and 0.5 mol/L NaCl experiments at 25 °C, 95 °C, and 140 °C.

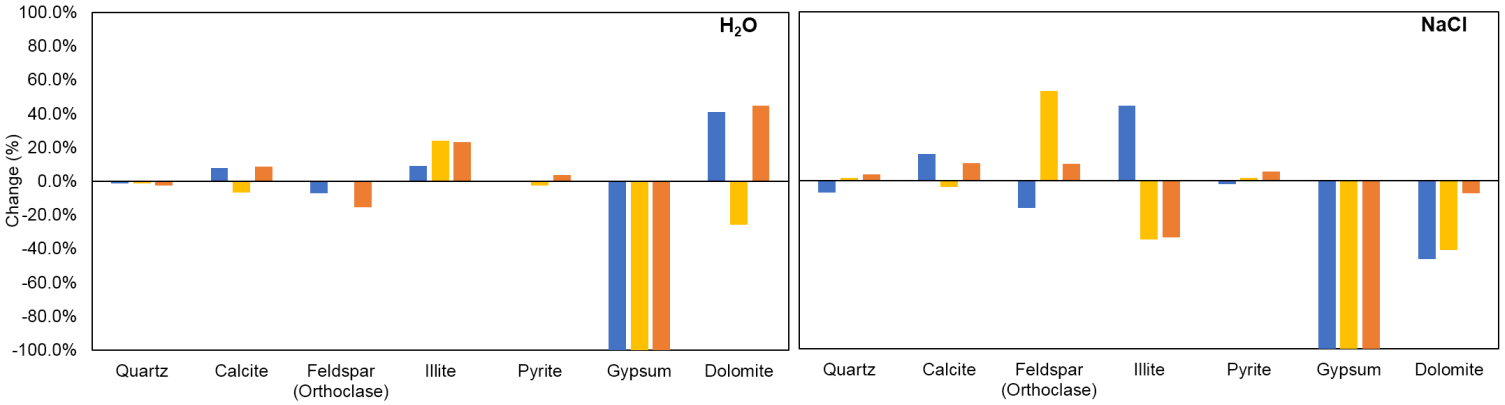

Figure 9: Percent changes in mineral fractions for the temperature-dependent experiments at 25 °C (blue), 95 °C (yellow), and 140 °C (orange).

3.1.2.3 Element Concentration Changes

The total digestion data gave a better understanding of which elements leached from the rock and the reactions that occurred during the experiments than the mineralogical data. The elemental concentrations show minor decreases in abundances of the elements measured in agreement with the mineralogical data. The only element to show a substantial decrease in concentration was Mo, with up to 10 % of the Mo leaching during the 0.5 M NaCl experiments of Core 1. For comparison, less than 0.1 % of most other transition metals was leached during the experiments. As the proportion of each element leached was small compared to the portion in the rock fraction, the aqueous geochemical data was more valuable than the solid chemistry to illustrate trends and determine the effect of temperature, rock composition, and salinity on leaching of elements.

Table 6: Fractions of elements remaining in the rock at the T_{48hr} sampling point, in percent. Calculations were done using the rock input composition and the aqueous concentration of elements at T_{48hr}.

	Fresh water (%)					NaCl Spiked (%)				
	Outcrop			Core 1	Core 2	Outcrop			Core 1	Core 2
Temp. (°C)	25	95	140	95	140	25	95	140	95	140
Li	100.0	100.0	100.0	*NDS	100.0	100.0	NDS	100.0	*NDS	100.0
Na	99.8	99.4	99.5	98.1	99.1	+N/A	+N/A	+N/A	+N/A	+N/A
Mg	99.7	99.6	99.9	99.8	100.0	99.7	99.6	99.9	99.7	99.8
Al	100.0	100.0	100.0	100.0	100.0	100.0	100.0	100.0	100.0	100.0
Si	100.0	100.0	100.0	100.0	100.0	100.0	100.0	100.0	100.0	100.0
K	100.0	99.9	99.9	99.9	99.9	99.9	99.9	99.9	99.9	99.9
P	100.0	100.0	100.0	100.0	100.0	100.0	100.0	100.0	100.0	100.0
S	99.6	99.6	99.6	99.6	99.7	99.5	99.7	99.5	99.8	99.4
Ca	99.9	99.7	99.9	100.0	100.0	99.8	99.8	99.8	100.0	99.9
Ti	100.0	100.0	100.0	100.0	100.0	100.0	100.0	100.0	100.0	100.0
Cr	100.0	100.0	100.0	100.0	100.0	100.0	100.0	100.0	100.0	100.0
Mn	100.0	100.0	100.0	100.0	100.0	100.0	100.0	99.8	100.0	100.0
Fe	100.0	100.0	100.0	100.0	100.0	100.0	100.0	100.0	100.0	100.0
Co	100.0	100.0	100.0	100.0	100.0	100.0	100.0	100.0	100.0	100.0
Ni	100.0	100.0	100.0	100.0	100.0	100.0	100.0	100.0	100.0	100.0
Cu	100.0	100.0	100.0	100.0	100.0	100.0	100.0	100.0	100.0	100.0
Zn	100.0	98.9	100.0	100.0	99.9	100.0	*NDS	100.0	100.0	100.0
As	100.0	100.0	99.9	100.0	99.9	100.0	99.7	99.7	99.9	99.9
Sr	99.8	99.5	99.7	99.7	99.7	100.0	99.4	98.7	99.2	97.5
Mo	98.3	97.6	97.9	97.9	99.8	98.2	96.1	97.7	89.8	99.8
Cd	100.0	100.0	100.0	100.0	100.0	100.0	100.0	100.0	100.0	100.0
Ba	100.0	100.0	100.0	100.0	100.0	99.9	99.8	99.9	99.3	99.4
Pb	100.0	100.0	100.0	100.0	100.0	100.0	99.9	100.0	100.0	100.0
U	100.0	100.0	100.0	100.0	100.0	99.8	99.9	99.9	100.0	100.0

*NDS= Not detected in the rock fraction
+N/A applies to Na in the NaCl spiked, of which those values are compromised due to the introduction of 0.5 mol/L NaCl to the aqueous fraction.

3.2 Aqueous Chemistry of Experiments

The aqueous elemental concentrations from reactor experiments provided a clearer picture of the leaching of both major and trace elements, than the rock digestion data. Additionally, the effect of the ionic strength of the solution on leachability was tested by comparing freshwater leaching experiments to 0.5 M NaCl experiments. The aqueous elemental concentrations were used to determine the saturation indices of both prominent minerals in the formation, such as

quartz, calcite, and gypsum, and common accessory minerals found in the solid fraction of FPW, such as barite and celestite. Only the concentration profiles of elements that are associated with these minerals are provided below; other elemental profiles are found in Appendix B as well as aqueous chemistry of all the experiments.

3.2.1 Major Cations

Time series of the leaching of major cations from the core samples, including Mg, Ca, Al, Si, and K (Fig. 9, Fig. 10, Appendix B-4, Fig. 11, and Appendix B-5 respectively), were determined for both Core 1 and Core 2 samples, and at both experimental conditions (freshwater and in 0.5 M NaCl). Experiments for Core 1 were conducted at 95 °C and 140 °C for Core 2, matching the formation temperature at the depth and location from which they were extracted. Al and K, although not used in modelling, are components of some of the major minerals present in the rock samples, so their concentration profiles can be found in Appendix B. Fe was not found to leach from the rocks to a measurable degree (Appendix B-1), likely because of the rapid oxidation of Fe^{II} and precipitation of insoluble Fe-oxide minerals, at near neutral pH values, as was the case in these experiments (Jew et al. 2017, Li et al. 2019).

In both cores, calcite was the most abundant mineral as determined by XRD, with a substantial presence of dolomite as well (5.0 % ± 0.2 % and 12.4 % ± 0.2 % for Core 1 and 2, respectively; Fig. 4). There was greater leaching of both Mg and Ca in Core 1 than Core 2 and the outcrop sample (Fig. 10 and Fig. 11), which is consistent with the greater proportion of calcite, as Mg can substitute for Ca ions in calcite (Fig. 4). After 168 hours of reaction, Ca and Mg in solution were found to be supersaturated with respect to calcite in the Core 1 experiments, however, their concentrations were stable by 4 hours in Core 2, indicating that an equilibrium had been reached. This could be a product of the higher temperature of the experiments for Core 2, accelerating the

kinetics and allowing equilibrium with calcite and dolomite to be reached sooner. Although Core 2 reached equilibrium faster than Core 1, it was at a lower Ca and Mg concentration than Core 1, consistent with the retrograde solubilities of calcite and dolomite at increased temperature (Rosenbauer et al. 2005). Also observed in the concentration profiles was a difference between the freshwater experiments and the 0.5 M NaCl experiments, with the spiked experiments having higher concentrations earlier on (<2 hours), due to accelerated kinetics. In most cases, the higher ionic strength resulted in a salting in effect that resulted in higher the equilibrium concentrations of Ca and Mg. The one instance where this was not the case was with Mg in Core 1, where the freshwater concentrations increased to match the NaCl experiments by 168 hours (7 days), although these values were not yet in equilibrium and the concentrations were still increasing, and so later time points could result in a reappearance of a difference in the concentration profiles between the freshwater and NaCl experiments. Finally, the differences between the two experiment types, I and II, (48 hours and 96/168hours duration, respectively) was minimal, indicating the experimental results are reproducible.

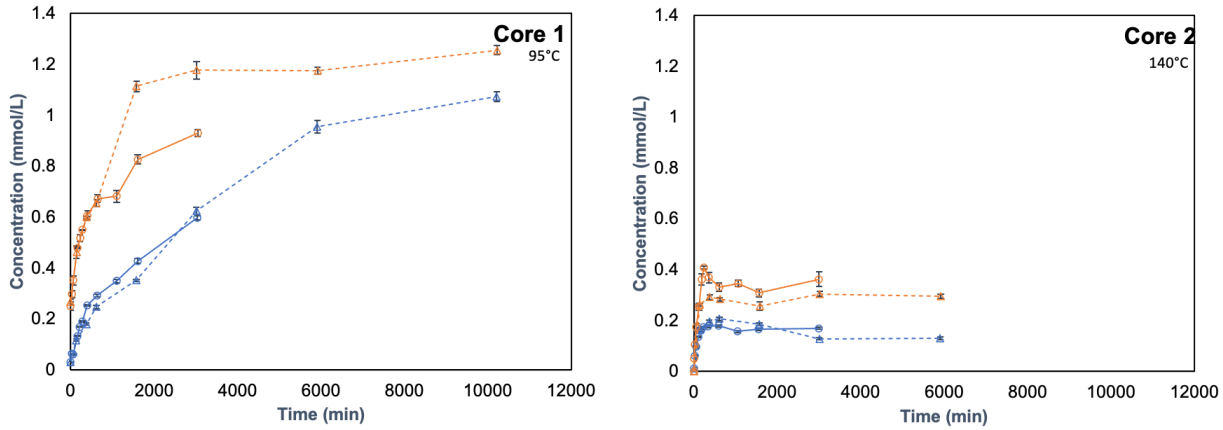

Figure 10: Aqueous geochemical profiles of Mg for both Core 1 and Core 2 experiments, freshwater (blue) and 0.5 mol/L NaCl (orange) experiments. Experiment type I (solid line) and II (dashed line), are shown, as well as quantitative errors of ± 1 σ.

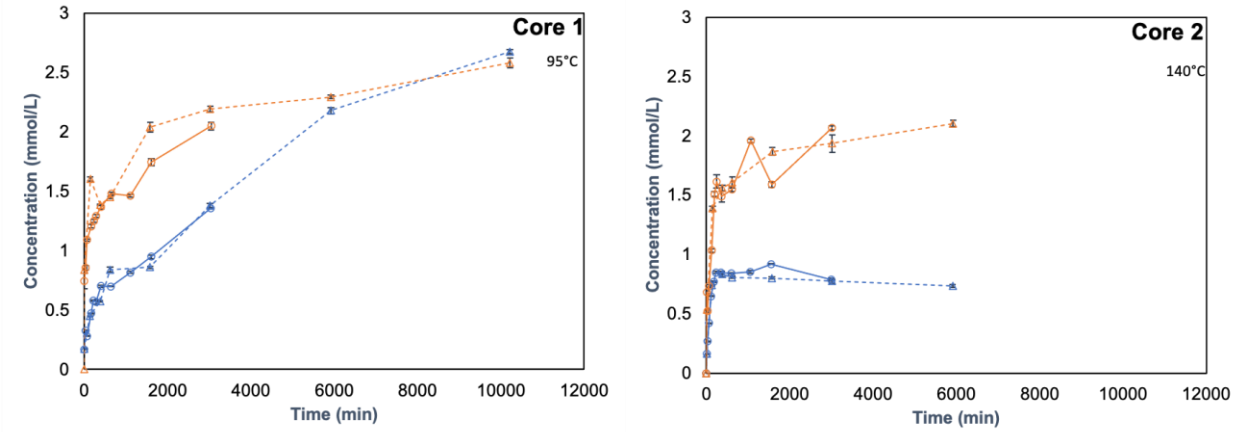

Figure 11: Aqueous geochemical profiles of Ca for both Core 1 and Core 2 experiments, freshwater (blue) and 0.5 mol/L NaCl (orange) experiments. Experiment type I (solid line) and II (dashed line), are shown, as well as quantitative errors of ± 1 σ.

As quartz was the next most abundant mineral in both the cores (Fig. 4B), the concentration profile for dissolved Si was determined (Fig. 12). The Si in solution was found to not reach equilibrium with the rock during experiments with either core, this was consistent with previous

reactor experiments which found Si to not reach equilibrium with quartz even after 500 hours (20.8 days) (Harrison et al. 2017, Morey et al. 1962). The increased leaching of Si, resulting in higher concentrations in solution, observed in the Core 2 experiments was due to the increased temperature of those experiments, which either accelerated the kinetics, as with Ca and Mg, or increased the solubility of quartz and other silicates (Siever 1962). Despite the low solubility of quartz and other silicates, there was substantial leaching of Si (10 % and 41 % of the total leached ions of Core 1 and Core 2, respectively) from the rock. Ionic strength had no discernible effect for either the Core 1 or Core 2 experiments. The dissolution of quartz is known to be affected by ionic strength between 40 °C and 250 °C (Icenhower and Dove 2000, Worley et al. 1996).

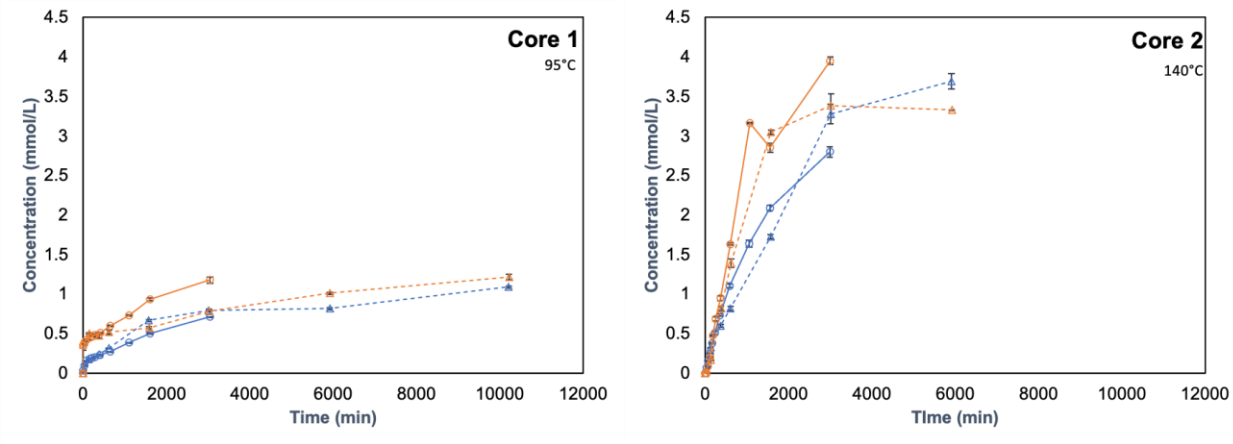

Figure 12: Aqueous geochemical profiles of Si for both Core 1 and Core 2 experiments, freshwater (blue) and 0.5 mol/L NaCl (orange) experiments. Experiment type I (solid line) and II (dashed line), are shown, as well as quantitative errors of ± 1 σ.

3.2.2 Trace Cations

The concentration profiles of three trace metals were plotted due to their potential to form scale in hydraulic fracturing infrastructure (Ba and Sr) and/or their toxicity (As). Ba and Sr are components of the sulfate minerals, celestite and barite, which may form scale in hydraulic

fractured wells, only these elements are reported here (Fig. 13 and Fig. 14 respectively). Barite and celestite were of interest due to concerns about their potential to form celestite and/or barite scale in oil and gas infrastructure and they have been found in the suspended solids fraction of unfiltered FPW (Brower 1973, He et al. 2014, Flynn et al. 2019, Plata Enriquez 2018, Krumgalz 2018, Xiong et al. 2020, Zhang et al. 2017). The concentration profile of As, which is important due to its potentially toxic effect on aquatic life at low concentrations (Delompré et al. 2019, Folkerts et al. 2020, Mehler et al. 2020), can be found in Appendix B. Because the detected concentrations of As are low, any trends observed between the freshwater and 0.5 M NaCl experiments were less than the error in quantification, and therefore not significant.

Celestite has been found in the suspended solids fraction of FPW and high concentrations of Sr and sulfate are often found in FPW indicate it may precipitate out of solution once the FPW returns to the surface and begins cooling (He et al. 2014, Flynn et al. 2019, Zhong et al. 2019). However, in my experiments the concentration of Sr in solution was consistently below 40 µmol/L. In contrast to our experiments, in target geologic formations for hydraulic fracturing, Sr is commonly found not only in the formation rock but also in interstitial formation water. This additional source of Sr in the subsurface could explain the lower Sr concentration in the simulated reactor experiments. Recent work by Owen et al. (2020) modeling the sources of metals in FPW, found Sr concentrations could be explained by both the input of formation water and ion exchange, or as trace metal replacing divalent cations in carbonate minerals, such has Ca^{2+} in calcite. Both core samples leached similar Sr concentrations of between 3.5-4 mmol/L. Additionally, the concentration of Sr increased with ionic strength, with a 3-fold greater release in the 0.5 M NaCl experiments. In the freshwater experiments, there was a rapid initial increase in Sr concentration to 8.5 µmol/L over the first 2 hours and subsequently plateaus at 10-15 µmol/L after 24 hours for

both cores. In contrast, for the saline experiments the aqueous Sr concentrations in experiments using Core 1 plateaued rapidly at 30 µmol/L after 24 hours while those with Core 2 increased more slowly, reaching the same concentration only after 96 hours and did not reach a plateau in the duration of the experiments. While this could be due to Sr being associated with different minerals in the cores, it is more likely to reflect the effects of higher temperature (140 °C) of Core 2, as strontianite ($SrCO_3$) is less soluble at higher temperatures (Helz and Holland 1965).

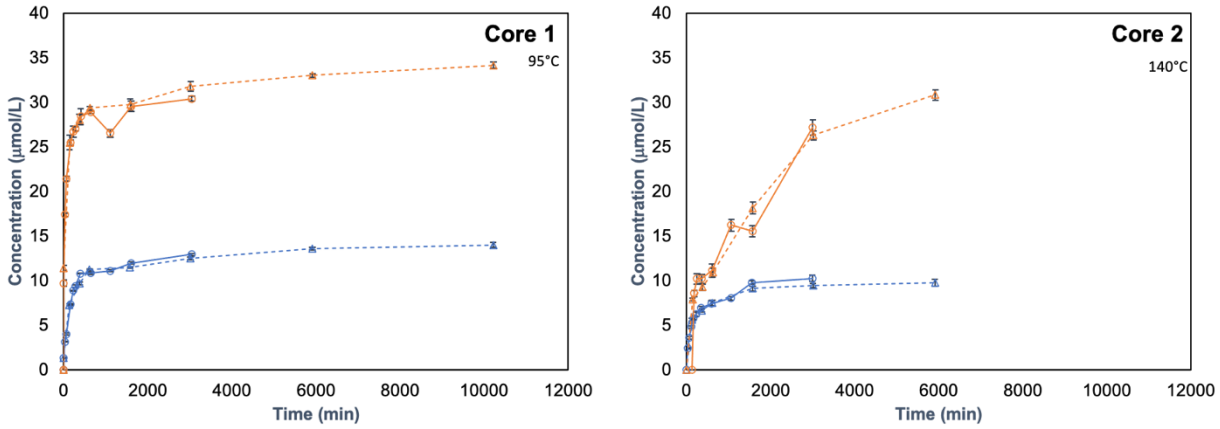

Figure 13: Aqueous geochemical profiles of Sr for both Core 1 and Core 2 experiments, freshwater (blue) and 0.5 mol/L NaCl (orange) experiments. Experiment type I (solid line) and II (dashed line), are shown, as well as quantitative errors of ± 1 σ.

Another common mineral in FPW solids is barite, which can form an acid-resistant scale that can inhibit productivity by reducing flow, and ultimately reducing the lifespan of the equipment and the well (Dyer and Graham 2002, Krumgalz 2018, Zhang et al. 2017). Further, Ba can be a PTHM that is often also associated with environmental problems such as bioaccumulation in aquatic life in the event of FPW spills (Mehler et al. 2020). My experiments had low concentrations of barium leached into solution during experiments with both cores (<30 µmol/L) (Fig. 14). Similar to Sr, Ba had a strong salting-in effect in the 0.5 M NaCl experiments, of 17x

and 12x compared to the freshwater experiments for Core 1 and Core 2, respectively, after 96 hours. The freshwater experiments for both cores show an early peak in Ba concentration at the time the reactor reaches the target temperature, 95 °C for Core 1 and 140 °C for Core 2 (1.8 µmol/L and 1.6 µmol/L, respectively). These are followed by a stabilization of the Ba concentration at lower levels. This trend was also observed in the saline experiments of Core 1 in a more exaggerated manner, with a higher initial peak concentration of 27 µmol/L. The initial peak, reached at T_0 of the experiment, is approximately 2.5x higher than the final concentrations measured after 168 hours. In Core 2, this trend was not observed in the saline experiments. This could be explained by quick leaching of barium from the original core and subsequent precipitation of barium minerals, such as barite ($BaCO_3$, and $BaSO_4$) (Blount 1974, Krumgalz 2018). Because the mineralogy between the two cores is not markedly different, the differing behavior of Ba between the two cores was likely due to lower solubility of a barium containing mineral (either as a substitution in calcite or as a dominant cation witherite or barite) in the higher temperature experiments. As no barium minerals were detected by the XRD analyses, either a barium-containing mineral such as barite is present but at trace amounts, or Ba is substituting for other cations in minerals detected by XRD, such as for calcium in calcite. It is possible that barium is not associated with calcite in Core 2, and therefore does not demonstrate the same trends. This hypothesis was tested by modelling barite saturation indices (Fig. 25).

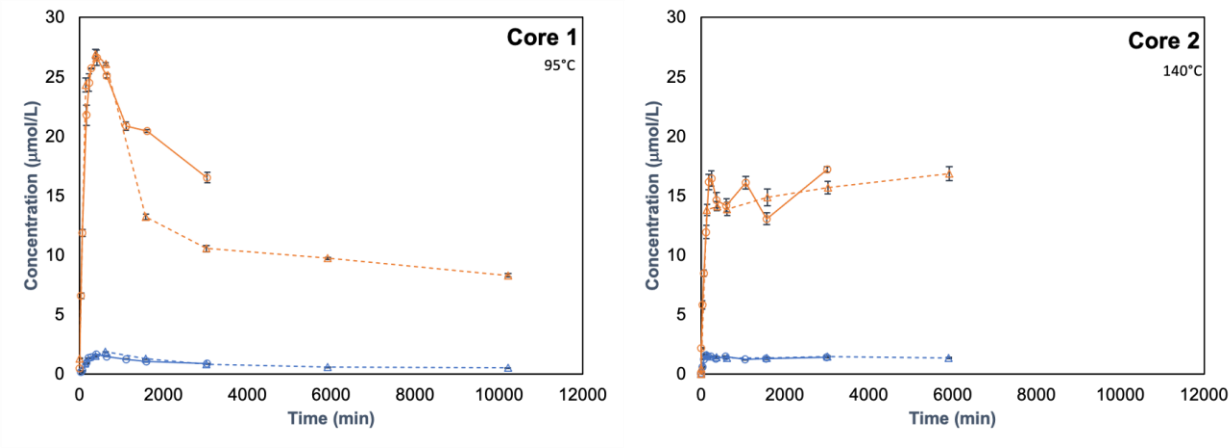

Figure 14: Aqueous geochemical profiles of Ba for both Core 1 and Core 2 experiments, freshwater (blue) and 0.5 mol/L NaCl (orange) experiments. Experiment type I (solid line) and II (dashed line), are shown, as well as quantitative errors of ± 1 σ.

3.2.3 Major Anions

The three major anions typically found in FPW are chloride, sulfate and carbonate. While aqueous Cl concentrations were measured for all experimental solutions, due to the 0.5 mol/L NaCl in the saline experiments, only the freshwater experiments showed quantifiable leaching of Cl, up to 873 µmol/L (Appendix B-1). Because Cl is not associated with common minerals found in FPW, the concentration profiles are plotted in Appendix B-7.

Sulfate minerals including celestite and barite are among the most common minerals found in the solids associated with FPW (Flynn et al. 2019); therefore, the geochemical profiles of sulfate were calculated for experiments conducted with both cores (Fig. 15). Due to the initially oxic conditions of the reactor experiments, the total sulfur determined by ICP-MS/MS was assumed to be in the oxidized form, sulfate (Appendix D). It is possible that over the duration of the experiments that the initial oxygen could have been consumed and the reactors became anoxic, although through sampling small amounts of oxygen may have been introduced. Another possibility is that microbial communities could have formed in the lower temperature experiments

(25 °C and 95 °C) and began reducing sulfate. As neither dissolved oxygen or microbial activity were determined during the experiments and only the total sulfur was measured and the initial conditions of the experiment were oxic, we assumed sulfur was in the oxidized form for the purposes of subsequent modelling. This assumption is supported by the fact that Fe as not detected in measurable amounts in the aqueous phase despite its considerable source concentrations in the host rock. As Fe is oxidized it would rapidly precipitate out at the pH of the experiments (pH 6-8), in the form of $Fe(OH)_{3(s)}$ but would be in its soluble phase, $Fe^{2+}_{(aq)}$ in reducing conditions (Jew et al. 2017, Li et al. 2019). Unlike Ba and Sr, the concentration of sulfate released into solution varied considerably between the two cores. Core 1 showed an inverse salting-in effect, with lower concentrations of sulfate in the higher ionic strength experiment. Core 1 had 2.5x more sulfate leached in the freshwater experiments compared to the NaCl experiments. It is unlikely that the leaching behavior was due to heterogeneity, as the experiments had a high level of reproducibility. As the bulk mineralogy and inorganic elemental composition was indistinguishable between the two core samples, the difference in sulfate profiles between the two cores was likely not due to the major mineralogy, although some trace minerals that were not identified could cause changes in the leaching of sulfate. Core 2 had a rapid initial increase in concentration over the first 2-4 hours to a plateau at 0.4 mmol/L and 0.7 mmol/L in the freshwater and NaCl experiments, respectively, showing a distinct salting-in effect of approximately 1.75x in the NaCl spiked experiments. Additionally, there was a salting out effect of sulfate observed in the Core 1 experiments (95 °C) that was that was not observed in the Core 2 experiments (140 °C). While the leaching trends of the NaCl experiments of both cores are comparable, there is a substantial increase in leaching in the freshwater Core 1 experiments, when compared with that ore Core 2. The increased leaching is likely because of a peaked solubility of many sulfate minerals at temperatures between 75-100°C

(Krumgalz 2018). I interpret the subdued leaching in saline Core 1 experiments to be because of either a lag in the kinetics due to water hydrating Na and Cl in solution (Azimi 2010), or sulfate is precipitating out in an amorphous phase with the excess Na in solution at that temperature (95 °C).

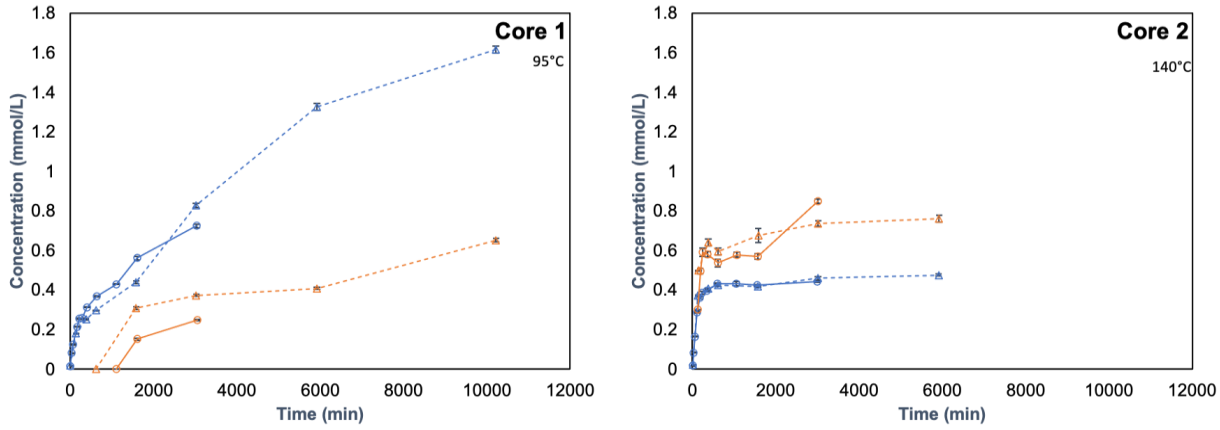

Figure 15: Aqueous geochemical profiles of SO_4 for both Core 1 and Core 2 experiments, freshwater (blue) and 0.5 mol/L NaCl (orange) experiments. Experiment type I (solid line) and II (dashed line), are shown, as well as quantitative errors of ± 1 σ.

Another important anion group is dissolved inorganic carbon (DIC), produced during the dissolution of carbonate minerals such as calcite and dolomite. The bicarbonate concentrations were determined as alkalinity, but due to sample volume limitations, alkalinity was only measure for Core 2. In subsequent modelling, the average ratio of Ca to DIC determined from Core 2 of 1.4 to 1, and was used to calculate DIC concentrations in the Core 1 experiments. These calculated values are shown in Fig. 16. This assumption was made because the major carbonate sources, calcite and dolomite, were present in excess in both core samples. For core 2, the DIC concentrations increased rapidly over the first 2 hours, and then began to plateau after approximately 24 hours. Unsurprisingly due to their common source in calcite, a similar salting-in effect was observed to that of Ca (Fig. 12 and Fig. 15).

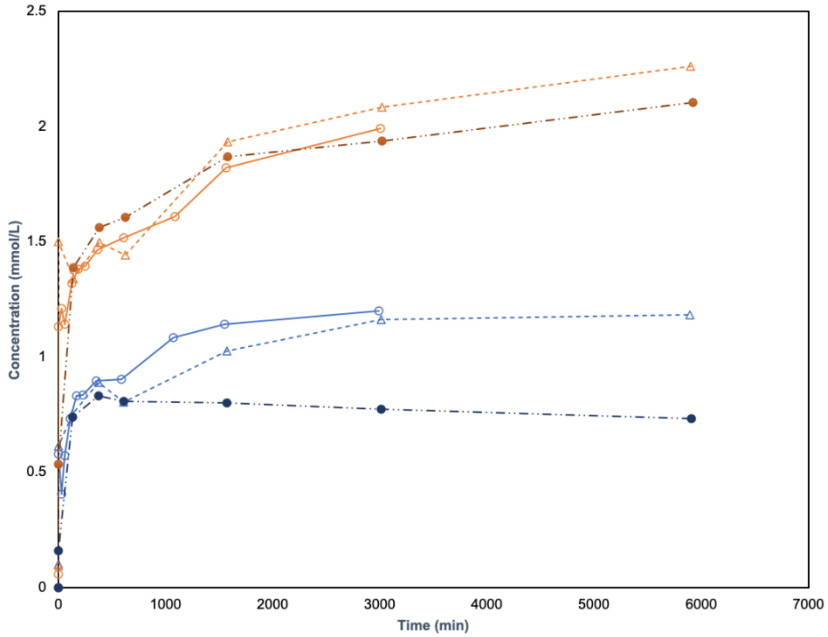

Figure 16: Aqueous geochemical profiles of DIC for Core 2 experiments (140°C), freshwater (blue) and 0.5 mol/L NaCl (orange) experiments. Experiment type I (solid line) and II (dashed line), are shown, as well as the calculated DIC values for the Core 1 experiments (95°C) (dot-dashed line) in mmol/L.

3.3 Temperature profiles of outcrop reactor experiments

As the outcrop samples are shales of similar mineralogical and geochemical composition to the core samples and are of a stratigraphically equivalent formation, we considered them similar enough to be used to analyze the dependence of temperature leachability of the ions of interest in the core experiments. Although there are some mineralogical and geochemical differences, the small amounts leached during the experiments were not impacted considerably by these changes (Table 6). Here the outcrop samples were used to estimate expected temperature effects on the release of elements from the rock samples. While most of the mineralogy was the same between the core samples and the outcrop, the exception was the presence of gypsum ($CaSO_4 \bullet 2H_2O$) in the

outcrop samples, which was not present (in amounts measurable by XRD) in either of the core samples. Because of the presence of gypsum, which is highly soluble in water, aqueous concentration trends from the outcrop experiments in both ions, Ca and SO_4, are less reliable than for elements from other minerals, as gypsum is highly soluble and could accelerate the release of Ca and SO_4 considerably.

3.3.1 Major Cations

The aqueous concentrations of Mg, Ca, and Si showed a dependence on temperature, although those changes were not uniform (Fig. 17). Si increased leaching at higher temperatures, while Mg and Ca had the highest leaching from 25 °C to 95 °C, and declined when the temperature increase to 140 °C. This behaviour of a peaked solubility between 25 °C and 95 °C, with a rapid decline as temperature increases above 100 °C, is common of many sulfate mineral solubilities, such as gypsum and kieserite ($MgSO_4 \bullet H_2O$) (Krumgalz 2018, Rosenbauer et al. 2005), but there was some inconsistency between the freshwater and saline experiments. At 95 °C the concentrations of Ca in the freshwater experiment exceeding those in the NaCl experiments. It was expected that the higher ionic strength of the saline experiments would result in greater leaching of Ca, as is seen at 25 °C and 140 °C. Instead, a salting-out effect was prevalent. This salting-out effect is likely due to the presence of gypsum, which has its peak solubility between 50 °C and 100 °C, as there was nearly 4x as much gypsum (2.2 % vs 0.5-0.9 %) in the input rock for the freshwater experiment at 95 °C than in the 0.5 M NaCl experiment (Appendix B-3). It is worth noting that not all of the Ca or SO_4 from the dissolved gypsum was observed in solution, only 1/40. It is therefore likely that although gypsum fully dissolved, there were subsequent precipitations of minerals bearing Ca and SO_4 and as they were not detected with XRD at later timepoints during the experiments, they were either in the form of numerous minerals below the detection limit of

XRD or in a poorly crystallographic phase that was not distinguishable in the diffraction pattern and are therefore considered amorphous. While differences in the concentration trends of Ca and Mg in reactor experiments were likely the result of temperature, our results show that they may be impacted by heterogeneities in the outcrop samples.

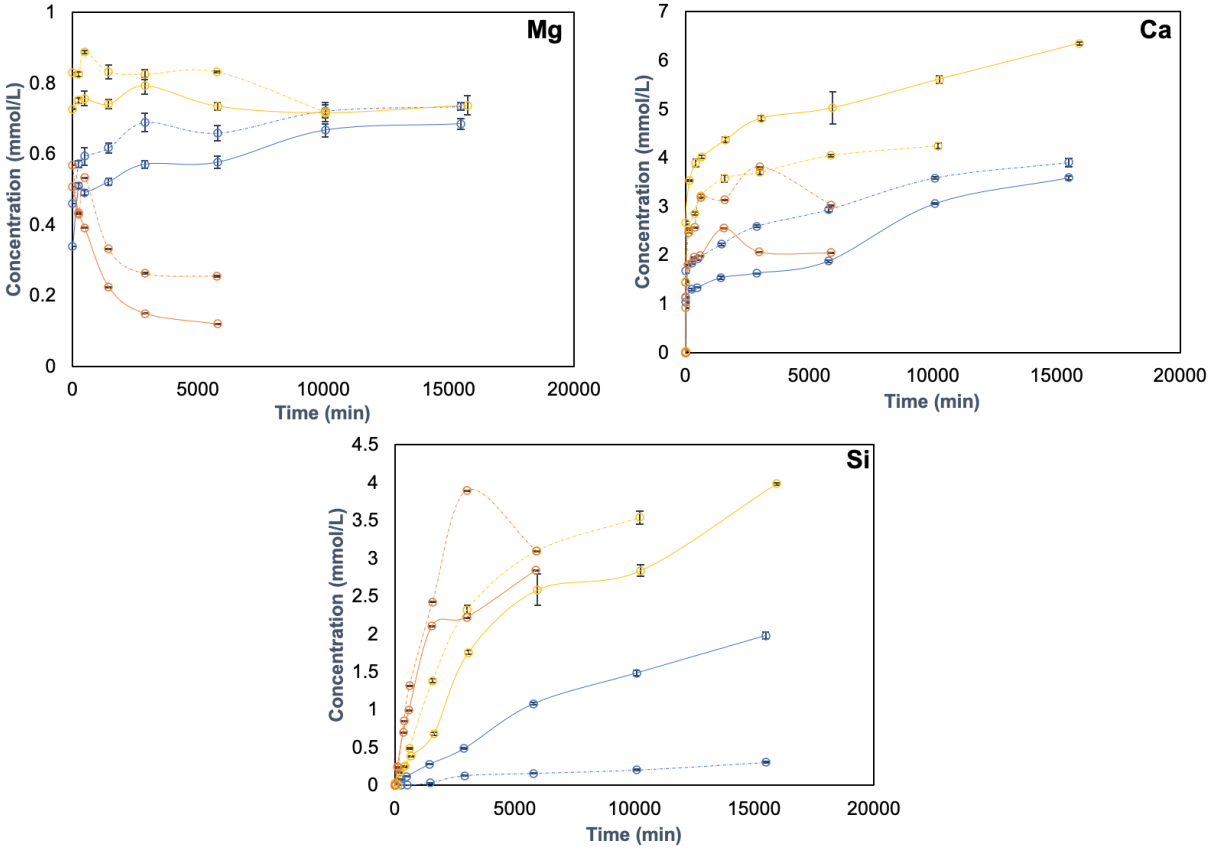

Figure 17: Aqueous chemical profiles of Mg, Ca, and Si in outcrop experiments, 25 °C (blue), 95 °C (yellow), and 140 °C (orange) for both freshwater (solid lines) and 0.5 mol/L NaCl spiked (dashed lines). All experiments were type II style with associated errors reported as ± 1 σ.

3.3.2 Minor Cations

The geochemical profiles of Ba and Sr were measured to determine the effect of temperature on their leachability, due to their potential to form scale (Fig. 18). The behaviors of Sr and Ba were different, with Sr concentrations showing a strong temperature dependence while

Ba exhibited little temperature dependence. Sr appeared to be influenced by both temperature and the ionic strength of the solution, increasing its leaching, which is inconsistent with the solubility of strontianite and celestite, which typically decrease with temperatures greater than 25 °C (Busenberg et al. 1984, Krumgalz 2018). This indicates that leaching from a different mineral may be the source of Sr, such as Sr substituted for Ca in carbonate minerals such as calcite. As with Ca, there is some inconsistency in Sr concentrations in the 95 °C freshwater experiments when compared with the saline experiment at the same temperature, indicating at least some of the Sr may be incorporated in gypsum crystals in the rock. Sr was below the instrument detection limit in the saline experiment at 25 °C, due to the increased dilution factor required to bring the TDS of these samples to levels low enough to analyze by ICP-MS/MS. Ba, on the other hand, was not significantly affected by temperature, and showed a more significant change due to ionic strength, indicating Ba leaching is mostly temperature independent between 25 °C and 140 °C. A few of the saline experiments showed an early spike in Ba concentration similar to Core 1 experiments, but they later decreased and plateaued or increase in concentration, like the Ba behavior observed in the Core 2 experiments.

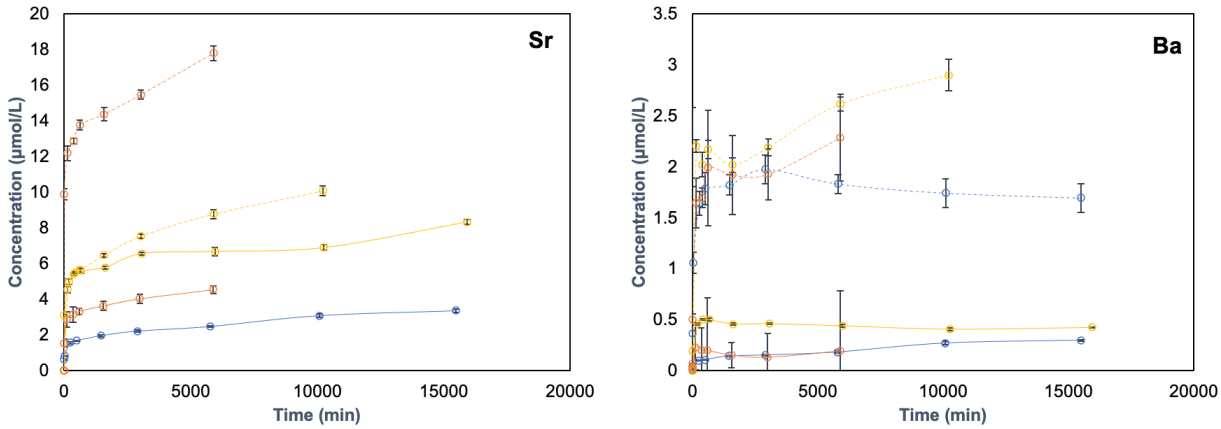

Figure 18: Aqueous chemical profiles of Sr and Ba in outcrop experiments, 25 °C (blue), 95 °C (yellow), and 140 °C (orange) for both freshwater (solid lines) and 0.5 mol/L NaCl spiked (dashed lines). All experiments were type II style with associated errors reported as ± 1 σ.

3.3.3 Major Anions

Both alkalinity and sulfate were measured in all outcrop experiments (Fig. 19). The measured sulfate concentrations supported earlier indications with Ca and Mg linked to sulfate minerals, such as gypsum or epsomite ($MgSO_4 \bullet 7H_2O$). The 95 °C experiments show a salting out effect, likely linked to the higher proportion (4x greater) of gypsum, which was 4x higher in the 95 °C freshwater experiment than in the 0.5 M NaCl experiment as well as the experiments conducted at 25 °C and 140 °C. The sulfate trends seen in the 140 °C experiments, mirror those of Mg, indicating some connection to a Mg-sulfate mineral, such as epsomite, was present. DIC, on the other hand, was not closely linked to trends in the Ca profile, even though calcite is present in the rock samples at about 12-15 % (Fig. 4). There was some resemblance between the trends seen in Mg and DIC in the freshwater experiments at 140 °C, which agrees with the finding of a preferred dissolution of dolomite over calcite during the experiments (Fig. 9).

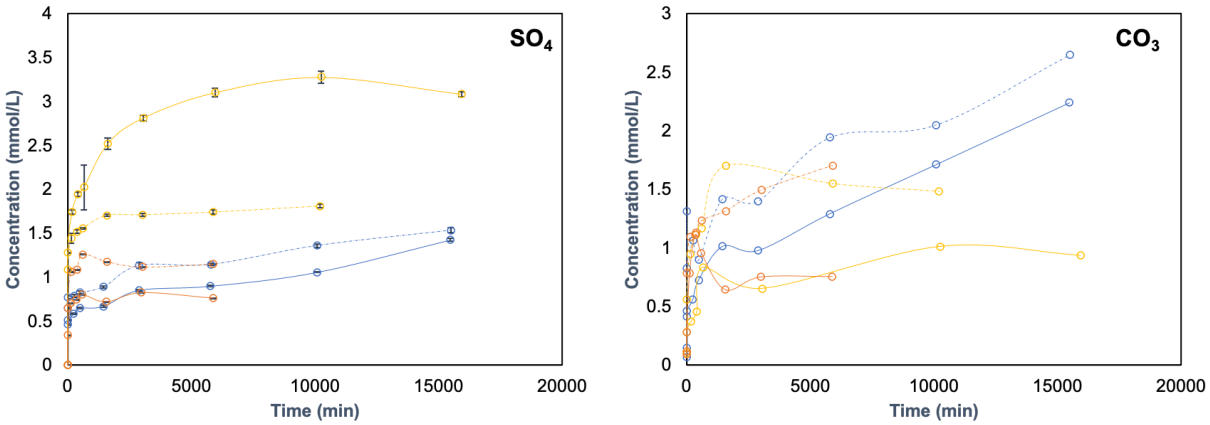

Figure 19: Aqueous chemical profiles of SO_4 and CO_3 in outcrop experiments, 25 °C (blue), 95 °C (yellow), and 140 °C (orange) for both freshwater (solid lines) and 0.5 mol/L NaCl spiked (dashed lines). All experiments were type II style with associated errors reported as ± 1 σ.

4. Discussion

4.1 Comparison of Fluids from Reactor Experiments with FPW

The results from the reactor leaching experiments were compared to the FPW from two hydraulically fractured wells from the Duvernay Formation, one that used RPW to make up the injected HFF (Well ID: 103/01-12-063-21W5), while the other exclusively used freshwater (Well ID: 100/12-30-063-21W5). The FPW from these wells will be referred to as RPW FPW and freshwater FPW, respectively. The percent of the source water composed of RPW for the RPW FPW was proprietary information and therefore not disclosed. Both wells are located in the Western Shale Basin, approximately 55 km from the borehole where Core 2 was obtained, near Fox Creek, AB (Fig. 20). The wells, although not of equal thermal maturity to either core, represent more similar thermal maturity to Core 2 than with Core 1. Geochemical data for the FPW from these wells is published in Zhong et al. (2019) with detection limits reported in Appendix C.

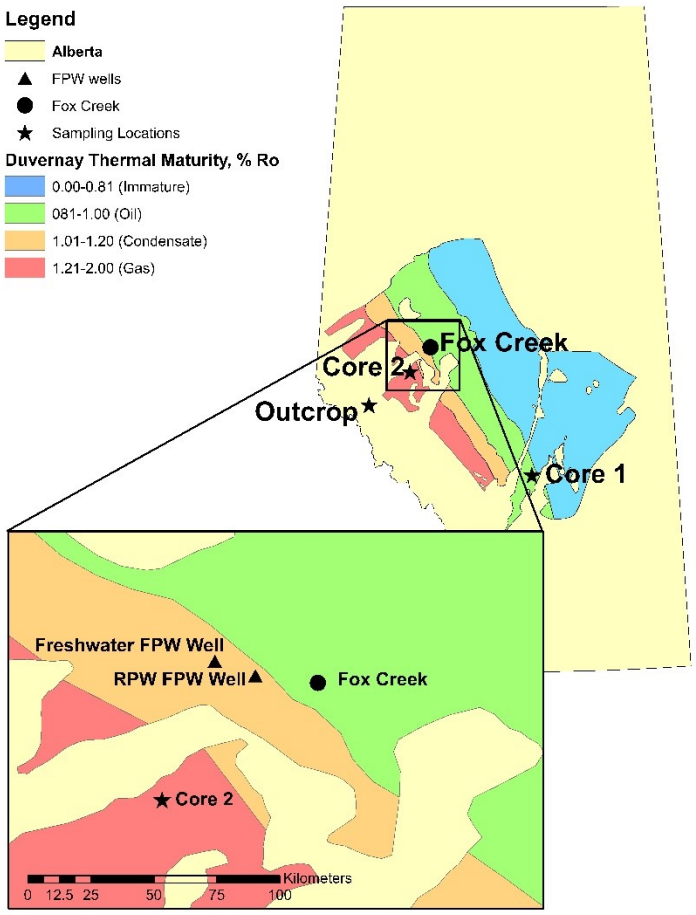

Figure 20: Map of the locations of the wells the FPW samples were collected from with respect to Core 2. Thermal maturity boundaries based off of Hackley and Cardott (2016).

4.1.1 Chemical Data

Both FPW samples had higher aqueous concentrations of all measured elements than the reactor experiments. While absolute concentrations and some order of abundances vary slightly between the FPW and the leaching experiments, the grouping of major (B, Ca, K, Mg, Na, and Sr) and minor/trace cations (Al, As, Ba, Fe, Mn, Mo, Ti, Zn) were identical with the exception of Si. Si was not above the detection limit for either FPW samples but were detected in both freshwater

and NaCl experiments in substantial quantities (1-3mmol/L). This consistency with FPW indicates that the methodology used in our experiments replicated the major water-rock interactions that occur during hydraulic fracturing, despite the differing water-rock ratios and implies that metals found in FPW are primarily sourced from the leaching and dissolution of minerals in the host rock during hydraulic fracturing. For example, Ca and Mg, among the highest concentrations in our reactor experiments (1-5 mmol/L and 0.1-1 mmol/L, for Ca and Mg, respectively) were likely sourced from the dissolution of carbonate minerals, such as calcite and dolomite, both found in high proportions in the rock samples (~65 % for the cores and ~15 % for the outcrop). Additionally, the dissolution of some silicate minerals, such as feldspar and quartz, and clay minerals, such as clinochlore, illite, and kaolinite, would provide common elements associated with these minerals, such as Si, Na, K, and Al, all of which were measured in our experimental solutions (Table 7 and 8).

While there are contending theories for the source of the TDS in FPW, there is a growing consensus that the formation water and leaching that occurs as a result of HFF interactions with reservoir rock are the primary contributors (Owen et al. 2020, Rowan et al. 2015). The bulk of the FPW TDS is made up of salt forming ions, particularly Na and Cl. As the freshwater reactor experiments (with no added NaCl) had considerably smaller fractions of Na and Cl than either FPW sample, it is likely that most of the Na and Cl in the FPW samples originated from pore water brines that were released during fracturing, and those brines were not present in large quantities in the core samples, likely due to the heterogeneous presence of formation water in the host rock, that would be connected during fracturing but not present in large amounts in the small core sample used for these experiments. It seems these brines could also be a source of other metals as well, such as Br, which was almost exclusively present in measurable amounts in the FPW samples and

not in the reactor experiments. As the detection limit for Br is ~3.5 µmol/L and the expected amount of Br would be considerably less than that, at ~1.5-2.5 µmol/L (700-800x less than the leached Na in FPW), it is likely there is some Br present at less than measurable amounts with ICP-MS/MS. The presence of formation water, which is often a brine, could explain the excess Na^+ and Cl^- present in the FPW not present in the injected water and that was found in the freshwater reactor experiments. Regardless of the mixing water used to make the HFF, Na and Cl make up over 90 % of the ions measured in both FPW samples, indicating their presence in the Duvernay Formation's formation brine waters. The brine formation water contributes other major and trace metals to FPW, likely accounting for differences in the concentration of elements between FPW and reactor experiments as well as a lower water:rock ratio of real hydraulic fracturing, when compared with that of the reactor experiments. For example, Br was present in both FPW samples (>3000µmol/L), however, it was below the detection limit (<3.5 µmol/L) in all reactor experiments. It could be argued that either the reactor experiments were of an insufficient duration to reach the same degree of dissolution as during fracturing, or that the formation water is the source of Br. At least in the case of Na and Cl, where halite could be assumed to be the mineral source of these ions in solution, the solubility and kinetics of dissolution are sufficiently high that 48 hours would allow for dissolution and equilibrium to be reached. Since no halite was identified with XRD (Fig. 4), it is strong evidence for formation waters being their source and that the brines were not present in the cores materials at the time of the experiments.

Table 7: Concentration data at T_{48hr} from pure water experiments values in comparison with Freshwater FPW 48 hours after water began to flow (Data from Zhong et al. 2019).

Element	Units	T_{48hr} Freshwater FPW	Outcrop			Core 1 95°C		Core 2 140°C	
			25 °C	95 °C	140 °C	I	II	I	II
Cl	mmol/L	2688.32	BDL	BDL	BDL	1.13	0.95	BDL	BDL
Na	mmol/L	2205.83	0.15	0.45	0.35	1.18	1.15	0.53	0.59
Ca	mmol/L	182.29	1.63	4.81	2.07	1.36	1.38	0.79	0.77
K	mmol/L	43.03	0.29	0.41	0.42	0.40	0.37	0.33	0.31
Mg	mmol/L	29.92	0.57	0.79	0.15	0.60	0.62	0.17	0.13
B	mmol/L	7.18	0.18	0.46	0.46	0.34	0.47	0.90	1.10
SO_4	mmol/L	3.02	2.56	8.43	2.48	2.17	2.48	1.33	1.38
DIC	mmol/L	NM	0.72	0.48	0.55	0.97*	0.99*	0.88	0.85
Si	mmol/L	BDL	0.49	1.76	2.22	0.71	0.79	2.80	3.28
Li	µmol/L	5245.79	BDL	BDL	BDL	16.23	BDL	BDL	BDL
Br	µmol/L	3346.17	BDL	BDL	BDL	BDL	BDL	BDL	BDL
Sr	µmol/L	8940.15	2.21	6.56	4.03	12.96	12.50	10.26	9.46
Fe	µmol/L	1155.33	BDL	BDL	BDL	BDL	BDL	BDL	BDL
Ba	µmol/L	150.13	0.15	0.46	0.13	0.84	0.81	1.39	1.43
Mn	µmol/L	84.90	BDL	0.50	0.44	0.16	0.27	0.28	0.96
Mo	µmol/L	NM	14.51	15.54	18.20	0.71	0.72	0.69	0.70
Cu	µmol/L	BDL	BDL	0.45	BDL	0.12	0.13	0.01	BDL
P	µmol/L	NM	BDL	0.32	0.53	0.68	BDL	BDL	BDL
Al	µmol/L	BDL	0.29	1.49	1.41	0.76	0.63	0.82	0.95
Ti	µmol/L	NM	BDL	0.18	BDL	4.06	0.18	0.00	0.00
Zn	µmol/L	BDL	BDL	0.16	0.18	0.97	BDL	0.31	BDL
Ni	µmol/L	BDL	0.14	BDL	0.15	BDL	BDL	0.04	0.02
As	µmol/L	BDL	0.06	0.14	0.43	0.02	0.05	0.13	0.17
Pb	µmol/L	0.05	BDL	BDL	0.002	BDL	BDL	BDL	BDL
Co	µmol/L	NM	BDL	BDL	0.02	BDL	BDL	BDL	BDL
U	µmol/L	NM	0.04	0.01	0.01	BDL	BDL	BDL	BDL
Cr	µmol/L	NM	BDL	BDL	BDL	BDL	BDL	BDL	BDL
Cd	µmol/L	BDL	BDL	BDL	BDL	BDL	BDL	BDL	BDL

BDL = below detection limit, detection limits provided in Appendix C
NM = not measured
*DIC was not measured for Core 1, but calculated based on the results from Core 2

Table 8: Concentration data at T_{48hr} from NaCl spiked experiments values in comparison with RPW FPW 48 hours after water began to flow (Data from Zhong et al. 2019).

Element	Units	T_{48hr} RPW FPW	Outcrop			Core 1 95 °C		Core 2 140 °C	
			25 °C	95 °C	140 °C	I	II	I	II
Cl	mmol/L	3609.72	425.07	378.85	387.44	549.88	557.99	502.48	409.05
Na	mmol/L	2470.50	476.37	492.30	396.44	446.88	461.31	426.90	452.11
Ca	mmol/L	212.58	2.59	3.70	3.81	2.05	2.20	2.07	1.94
K	mmol/L	52.07	0.45	0.68	0.55	0.55	0.54	0.59	0.47
Mg	mmol/L	32.02	0.69	0.82	0.26	0.93	1.18	0.36	0.30
B	mmol/L	7.36	0.19	1.20	1.50	0.55	0.25	2.54	2.02
SO_4	mmol/L	2.11	3.40	5.13	3.34	0.75	1.12	2.55	2.21
DIC	mmol/L	0.83	1.03	1.19	1.10	1.47*	1.57*	1.46	1.53
Si	mmol/L	BDL	0.13	2.32	3.89	1.17	0.78	3.95	3.38
Li	µmol/L	6237.37	BDL	BDL	BDL	BDL	BDL	BDL	BDL
Br	µmol/L	3110.27	BDL	BDL	BDL	BDL	BDL	BDL	BDL
Sr	µmol/L	10764.21	BDL	7.53	15.47	30.45	31.83	27.21	26.32
Fe	µmol/L	883.05	BDL	BDL	BDL	BDL	BDL	BDL	BDL
Ba	µmol/L	138.39	1.97	2.19	1.93	16.51	10.53	17.20	15.68
Mn	µmol/L	259.99	BDL	BDL	3.93	BDL	BDL	BDL	BDL
Mo	µmol/L	NM	15.34	20.36	19.67	3.41	3.45	0.75	0.60
Cu	µmol/L	BDL	BDL	BDL	BDL	BDL	BDL	0.12	BDL
P	µmol/L	NM	BDL	BDL	BDL	BDL	BDL	BDL	BDL
Al	µmol/L	BDL	BDL	BDL	BDL	BDL	BDL	BDL	BDL
Ti	µmol/L	NM	BDL	1.52	BDL	2.16	BDL	BDL	BDL
Zn	µmol/L	BDL	BDL	BDL	BDL	BDL	BDL	BDL	BDL
Ni	µmol/L	BDL	BDL	BDL	BDL	BDL	BDL	BDL	BDL
As	µmol/L	BDL	BDL	0.83	0.87	0.22	0.17	0.31	0.15
Pb	µmol/L	BDL	BDL	0.08	BDL	BDL	BDL	BDL	BDL
Co	µmol/L	NM	BDL	BDL	BDL	BDL	BDL	BDL	BDL
U	µmol/L	NM	0.14	0.07	0.10	BDL	BDL	BDL	0.05
Cr	µmol/L	NM	BDL	BDL	BDL	BDL	BDL	BDL	BDL
Cd	µmol/L	BDL	BDL	BDL	BDL	BDL	BDL	BDL	BDL

BDL = below detection limit, detection limits provided in Appendix C
NM = not measured
*DIC was not measured for Core 1, but calculated based on the results from Core 2

Unlike salts and Br, Fe is not believed to be in formation water, and as pyrite was identified in (~2 %) in all the rock samples for our experiments, there was a source of Fe in all of the experiments. Recent work by Jew et al. (2017) and Li et al. (2019) found that aqueous Fe concentrations in simulated hydraulic fracturing experiments were linked to the pH of the experiments Lower pH values prevented the rapid oxidation of leached Fe and formation of relatively insoluble Fe-oxy(hydr)oxide minerals. My experimental solutions were consistently between pH 6-9, and any leached Fe would have rapidly oxidized and precipitated. No Fe-

oxy(hydr)oxide minerals were identified in the rock samples following the experiments, however, they would have been difficult to identify as amorphous Fe^{III} minerals typically have poor diffraction patterns. The small amount of Fe that was leached from pyrite during the experiments, resulting in trace minerals in too low of concentration, or poor of crystallographic structure, for detection by XRD. The pH of FPW from the Duvernay Formation is generally lower, around 4-5 (Flynn et al. 2019, He et al. 2017) and so Fe oxidation precipitates, such as $Fe(OH)_{3(s)}$ would be less inhibited in hydraulic fracturing operations in the field.

The relative abundance of five selected major elements, Mg, Si, K, S, and Ca found in both FPW samples (after 48 hours of FPW flow) and our experiments (48 hours after the target temperature was reached) were compared (Fig. 21). Elements such as Sr, Ba, and S are dominant components of precipitates that formed in Duvernay FPW after it returned to the surface (Flynn et al. 2019, He et al. 2017). There was a substantially greater fraction of aqueous Ca in the FPW samples (68-70 % vs 12-24 % in reactor experiments, after the exclusion of Na and Cl), likely owing to its presence in formation water or increased dissolution from the formation due to the low initial pH of HFF due to the addition of acids, such as KCl and/or HCl (Table 1). As K is also a component of typical additives in HFF, its higher relative abundance in both FPW samples can also be explained in this way, although the composition of the additives was proprietary information and not disclosed. The primary S species in oxidized water is SO_4^{2-}, and as the experiments were are assumed to be conducted in oxidizing conditions, it is reasonable to assume that sulfate was the form of S in solution in the experiments (Appendix D). In the recent study conducted by Owen et al. (2020), it was found that SO_4^{2-} could only be modelled as coming from the dissolution of pyrite, likely the mechanism by which sulfur was entering into solution in both the FPW and reactor experiments here. A study by Li et al. (2019) also found that pyrite oxidation

was a significant source of sulfate during reactor experiments of similar design to those we conducted. In another study, Xiong et al. (2018), suggested the primary source of sulfate could be from another chemical additive, ammonium persulfate, which is often used as a breaker in HFF. However, as the reactor experiments only had one potential source of SO_4, the rock samples, either leaching of already oxidized sulfur or through oxidation of leached reduced sulfur. Despite this and the far higher water-rock ratio in the reactor experiments, they had absolute S concentrations comparable to FPW: 1-5 mmol/L (Table 7 and 8). As the TDS of the reactor experiments was far lower than that of true FPW, the relative fraction of S in those experiments was far greater: 18-50 % in freshwater experiments and between 0.07-0.58 % in NaCl spiked experiments. As the absolute concentrations of S in my experiments are consistent with those measured in both FPW samples, it is likely that modelling by Owen et al. (2018) was correct in stating that the majority of sulfate ions in FPW are sourced from pyrite oxidation during hydraulic fracturing. As the experiments were conducted at atmospheric oxygen concentration and not anoxic, there was a greater oxidation of pyrite, although the speciation remained much the same as hydraulic fracturing (Appendix D).

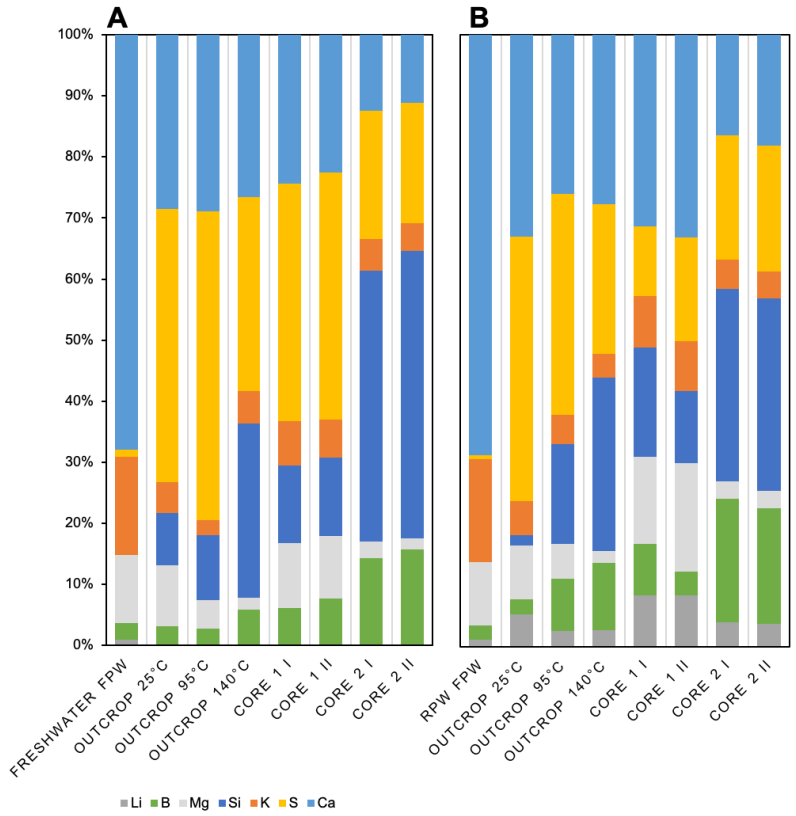

Figure 21: Element distribution of major ions in solution (>1 %) with the exclusion of Na and Cl. (A) Freshwater FPW was compared with pure water reactor experiments (B) and RPW FPW was compared with NaCl spiked reactor experiments.

4.1.2 Saturation Indices of Core Samples vs FPW

The saturation indices (SI) of both major and trace minerals were calculated using PHREEQC (Parkhurst & Appelo 2013) to determine whether equilibrium was reached with in the reactor experiments and whether the mineral sources of the dissolved constituents could be determined. For the NaCl spiked experiments, the Pitzer equations and database was used, while calculations for freshwater experiments were conducted using the extended Debye-Hückel

equation and the phreeqc.dat database. Major minerals such as quartz (SiO_2), $SiO_{2(am)}$ and calcite ($CaCO_3$) were modeled as well as minor or trace minerals such as gypsum ($CaSO_4 \cdot 2H_2O$), anhydrite ($CaSO_4$), barite ($BaSO_4$), and celestite ($SrSO_4$). Modelling with Al minerals was not done as Al is not included in the Pitzer database of PHREEQC; however, we can infer that the role of Al bearing minerals, dominantly silicates such as feldspars, would have been minor due to their low solubility. This inference was further supported by the low concentrations of Al after the reactors reached equilibrium (approximately 0.6 µmol/L and <1.48 µmol/L in the freshwater and NaCl experiments, respectively). Saturation indices were calculated at the temperature of the reactor experiments, 95 °C and 140 °C for Core 1 and 2, respectively. The FPW saturation indices were also calculated and compared at the same temperatures as the experiments or 95 °C and 140 °C, to ensure temperature was not a cause for difference in SI.

Saturation indices were used to determine the stability of minerals as they reacted with the fluids and to determine whether they were likely to have dissolved or precipitated and if equilibrium between a given mineral and dissolved constituents was reached. The saturation index (SI) of a mineral was calculated by:

$$\mathrm{SI} = \log \frac{\mathrm{IAP}}{\mathrm{K}_{sp}}$$

Where IAP is the ion activity product, and K_{sp} is the solubility product. A saturation index of 0 indicates that solution equilibrium with respect to a mineral has been met. Saturation indices greater than 0 indicate the mineral is supersaturated and may precipitate out of solution, while an SI less than 0 indicates the mineral is undersaturated and further dissolution is thermodynamically favored.

4.1.2.1 Major Minerals

In all three rock samples, quartz and calcite were found to be the dominant minerals comprising greater than 67 % of each sample. Because of this, both were adequate minerals to compare with FPW solution chemistry using the SI approach. Because quartz also has an amorphous counterpart that is more soluble, $SiO_{2(am)}$, both were modelled (Fig. 22). From the concentration data, Si makes up a much smaller proportion in FPW than the reactor experimental solutions (Fig. 21). In fact, Si was below the detection limit in both T_{48hr} FPW samples (Table 7 and 8), but was in relatively high abundance in our experiments at the same time point, ranging 0.1-4 mmol/L. Flynn et al. (2019) demonstrated that there were high concentrations of Si in secondary precipitates that form in FPW; however, due to the overall lower TDS, this did not occur in our experiments and Si increased in concentration over the entire duration of the experiment (Fig. 12). Si was only detected in the freshwater FPW at one time-point, and so a SI could only be calculated for that time. Despite the chemical profiles of Si not reaching steady state during the experimental timeframe in both core sample experiments, the SI of quartz was near equilibrium, ranging from -0.33 to 0.07, while the solution was undersaturated with respect to $SiO_{2(am)}$ (-1.24 to -0.71), indicating the solution was in equilibrium with quartz, and not with $SiO_{2(am)}$. The higher ionic strength of the NaCl spiked experiments caused an early increase in SI, but for both cores the experimental Si concentrations converged to show the ionic strength did not have a significant effect on the equilibrium of either mineral.

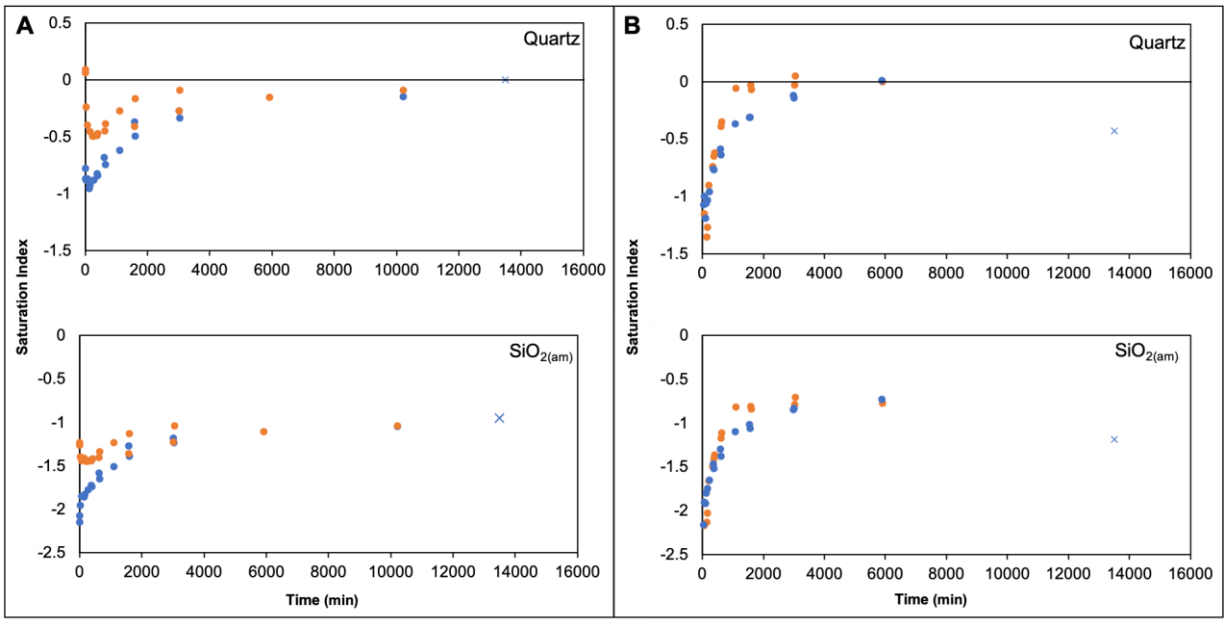

Figure 22: Saturation indices of quartz and $SiO_{2(am)}$ for both A) Core 1 at 95 °C and B) Core 2 at 140 °C experiments. Both freshwater (●) and NaCl spiked (●) experiments are shown as well as Freshwater FPW (×).

The most abundant mineral in both core samples was calcite. The SI for calcite was calculated for all cores and FPW that had measured Ca and DIC concentration values (Fig. 23). As the Freshwater FPW component concentrations reported in Zhong et al. (2019) did not include DIC concentrations, the SI for calcite was not determined for that sample. The calcite SI for both cores showed an initial dip in SI to less than 0 (that is, an increase in undersaturation with respect to calcite), followed by a return to near equilibrium conditions, with SI values ending between 0 and 0.5 (at or near equilibrium). As with Si in quartz, Ca did not reach steady state during some of the experiments, but the SI was still near equilibrium for calcite. The initial dip in SI is likely a product of the reactor reaching temperature at around 120-180min, with a lag in the kinetics to reach equilibrium.

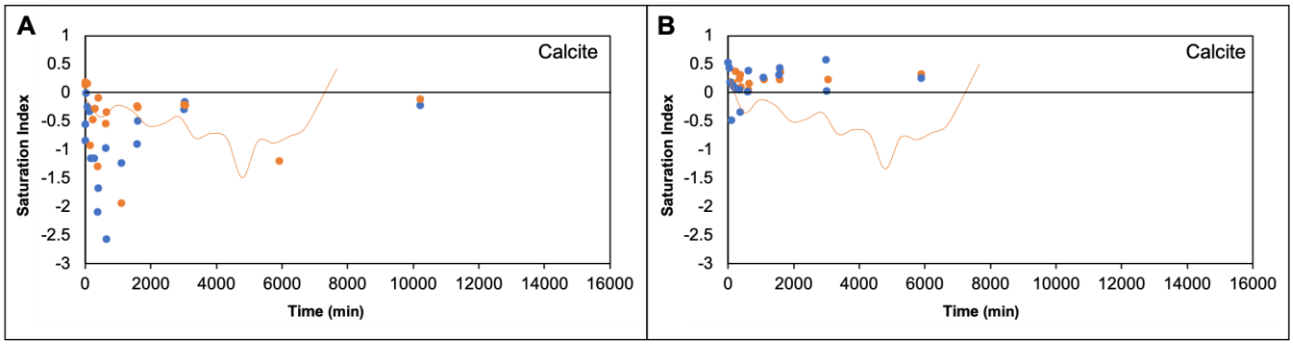

Figure 23: Saturation indices of Calcite for both A) Core 1 at 95 °C and B) Core 2 at 140 °C experiments. Modelling was conducted at the temperatures of experiments. Both freshwater (●) and NaCl spiked (●) experiments are shown as well as RPW FPW (orange line).

4.1.2.2 Minor and Trace Minerals

While not present in measurable amounts in either core sample, gypsum, anhydrite, barite, and celestite are all common accessory minerals found as precipitates in FPW (Flynn et al. 2019, Paukert Vankeuren et al. 2017). These minerals are known to pose problems in oil and gas infrastructure by forming unwanted scaling on drilling equipment or even precipitating in fractures within the formation, reducing the productivity of the well (Dyer and Graham 2002, Li et al. 2019, Paukert Venkeuren et al. 2017, Krumgalz 2018, Zhang et al. 2017). As all four of these phases are sulfate minerals, they are thought form as the result of the oxidization of pyrite (found in both core Fig. 4) and subsequent release of dissolved sulfate (Harrison et al. 2017). As the concentration of Fe was below the detection limit for all experiments, the SI relationship for pyrite could not be calculated (Appendix B).

Sr and Ba are two trace elements present at low relative concentrations in both FPW samples (0.16-0.17 % and 0.0021-0.0028 % for Sr and Ba, respectively), These elements are found at low concentrations in the rock samples (1-5 mmol/L and 1-3 mmol/L for Sr and Ba,

respectively), and no common Ba or Sr minerals, such as witherite, strontianite, barite, or celestite were identified in the rock samples (Fig. 4). Instead, it is likely their source was Sr^{2+} and Ba^{2+} that substituted for Ca^{2+} or Mg^{2+} as impurities in carbonate minerals (Pingitore 1987). Although both elements were found in similar concentrations in the rock samples, the ratio of Sr to Ba in both FPW samples was high (60:1 and 78:1 for Freshwater FPW and RPW FPW, respectively). This was also reflected to a lesser degree in the experiments, with the ratios ranging from 6:1 to 31:1 in the freshwater experiments and 1.6:1 to 8:1 in the NaCl spiked experiments. This suggests that most of the Sr and Ba in FPW leaches from the rocks themselves, and that the differences in concentrations are most likely the result of the higher water:rock ratio in the experiments than at downhole hydraulic fracturing conditions. There may also be a small contribution of Sr from formation waters in both FPW samples, as Owen et al. (2019) modelled. It is unsurprising that more Sr than Ba leached from the rock samples, owing to the smaller ion size of Sr and therefore greater solubility (Finch and Allison 2007).

Although not detected by XRD in the core samples, gypsum is a common accessory mineral known form as the result of oxidative weathering in the presence of calcium bearing minerals (e.g. calcite) and sulfide bearing minerals (e.g. pyrite). Both of these mineral types were present in substantial quantities (>2 %) in the core samples, therefore it would be reasonable to hypothesize that gypsum could form during the experiments. Gypsum and its dehydrated endmember, anhydrite, are both Ca sulfate minerals with their highest solubility of approximately 0.02 mol/L around 25 – 50 °C (Krumgalz 2018). In the core experiments, the SI values of both gypsum and anhydrite remained less than 0, indicating undersaturation and that conditions were favorable for dissolution, not precipitation (Hörbrand et al. 2018, Meijer and Van Rosmalen 1984) (Fig. 24). In contrast with quartz and calcite, gypsum and anhydrite show a lag in the kinetics of

the NaCl experiments (-1.2 vs -3 in Core 1, and -1.8 vs -2.4 in Core 2 for gypsum), which is likely a product of the kinetic lag of sulfate leaching observed in the aqueous chemistry (Fig. 15). For both cores, gypsum and anhydrite were more undersaturated than the FPW samples for the 1 week (168 hr or 10080 min) experimental timeframe. In contrast to the cores, there was no discernible difference in the calculated SI values for gypsum and anhydrite between the freshwater FPW and RPW FPW. This is likely due to the shut-in period during hydraulic fracturing that allowed the HFF to reach equilibrium with the formation before any wastewater was allowed to flow from the well. The SI calculation results from the pure water experiments for both gypsum and anhydrite coincided well with the SI values calculated in the FPW samples for both minerals (-1.4 for gypsum and -0.8 for anhydrite for Core 1 and -1.6 for gypsum and -1 for anhydrite for Core 2). The SI values in the laboratory NaCl experiments were all significantly more undersaturated than calculated for the field-collected RPW FPW for both gypsum and anhydrite. Since none of the laboratory reactor experiments reached equilibrium in the duration of the experiments, it is likely that slower mineral dissolution kinetics at the higher ionic strength of the NaCl experiments is the cause of this difference between the RPW FPW and NaCl experimental SI (Azimi 2010).

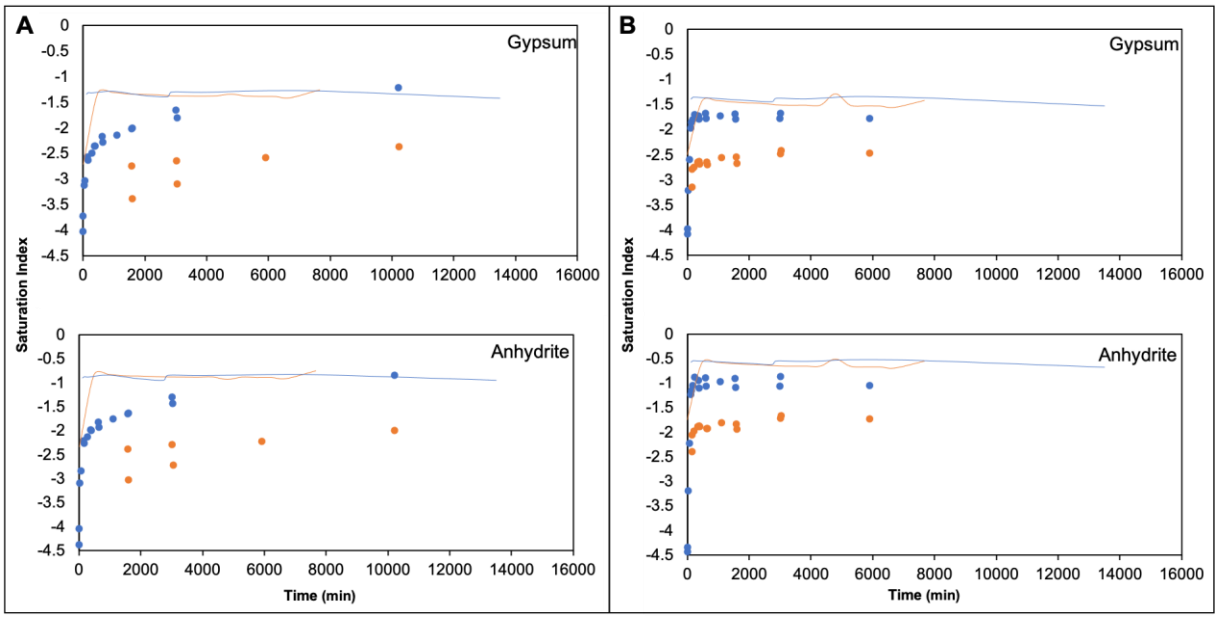

Figure 24: Saturation indices of gypsum and anhydrite for both A) Core 1 at 95 °C and B) Core 2 at 140 °C experiments. Modelling was conducted at the temperatures of experiments. Both freshwater (●) and NaCl spiked (●) experiments are shown. FPW is shown as solid lines for both Freshwater FPW (blue) and RPW FPW (orange).

Barite and celestite are both of high interest for the oil and gas industry as they can form unwanted scale on equipment or in downhole fissures when sulfate rich formation water is present (Li et al. 2019, Li et al. 2020, Xiong et al. 2020). The most common sources of the sulfate that leads to their formation are the sulfide minerals present in the target formation, or sulfur-containing water used to make up the drilling mud or HFF. Significant effort has been invested in determining sources of the sulfate, Sr and Ba, and how these minerals nucleate (Blount et al. 1974, Li et al. 2020, Zhang et al. 2017). As the reactor experiments did not include formation water or sulfate-rich source waters, they are useful in determining if the presence of barite crystals in the FPW are derived from the formation or are truly precipitates as proposed by Flynn et al (2019). In both FPW

samples, both barite and celestite were close to equilibrium, with their SI values plateauing around ±0.2 and -0.5, respectively (Fig. 25). There was very little difference in SI values calculated for the Freshwater FPW and RPW FPW (<0.5). In the reactor experiments, the SI values for barite closely resembled those of the corresponding FPW, but were largely undersaturated with respect to celestite (-1.5 for freshwater experiments and -2.0 for NaCl experiments). Similar to gypsum, ionic strength had an observable effect on celestite's SI in the reactor experiments, and perhaps a longer experimental duration would allow for celestite to reach similar SI values as those of the FPW samples (-0.5). More likely, however, the aqueous Sr in the FPW samples did not come solely from the dissolution or leaching from the formation. Similarly, Owen et al. (2020) found that to explain Sr concentrations, both ion exchange and formation water mixing with HFF was required to accurately model the observed Sr concentrations in FPW. As the barite SI hovered around equilibrium in both FPW samples, it would make sense that it precipitated out during or after hydraulic fracturing, which is what is observed in FPW precipitates from the same formation (Flynn et al. 2019), as well as others (Li et al. 2019). In our experiments, barite is near equilibrium, (SI of -0.4 to -0.1 for freshwater experiments and -0.7 to -0.1 for NaCl experiments) and so the prevalent issue of barite scaling during hydraulic fracturing can be explained mostly from the interactions between the rock and source water. With celestite on the other hand, which is much more soluble than barite, the SI indicates that celesite is still under-saturated, although it is still increasing at the end of the experiments. It is possible that given more time in the reactor, the SI of celestite in both freshwater and NaCl experiments could reach an SI of -0.5 to match both FPW samples. Other possibilities are during hydraulic fracturing as second source of Sr is present, in the form of formation brines that was not present in our reactor experiments or the addition of some chemical additives to the HFF effects the saturation indices of celestite. The effect of

additives on the leaching of inorganics has not been studied extensively yet and so this hypothesis cannot be verified in the literature.

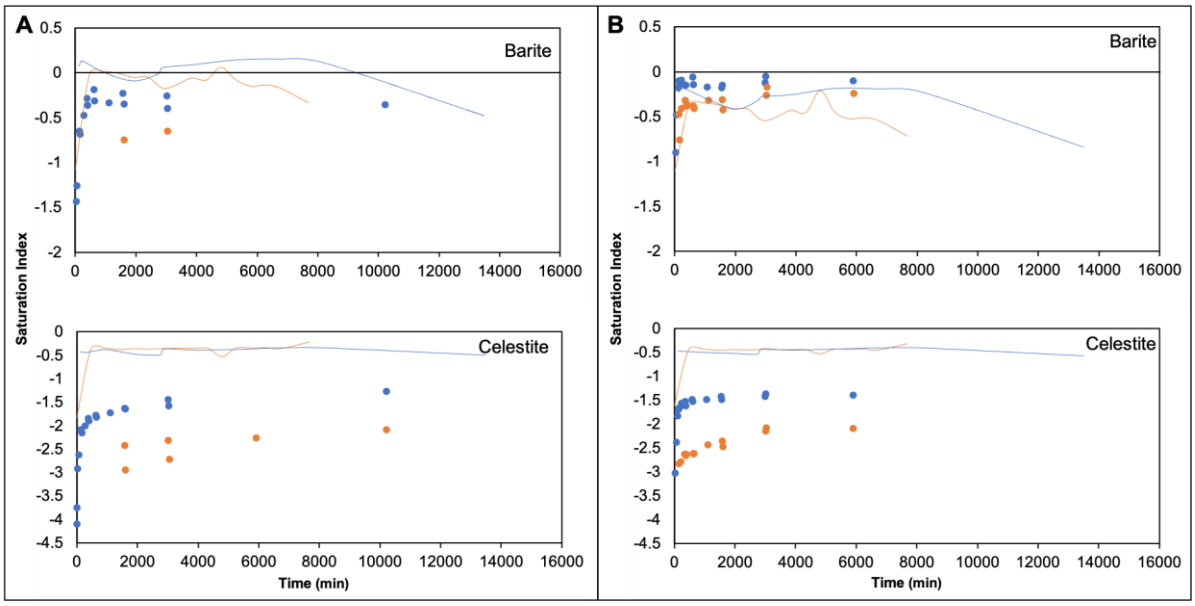

Figure 25: Saturation indices of barite and celestite for both A) Core 1 at 95 °C and B) Core 2 at 140 °C experiments. Modelling was conducted at the temperatures of experiments. Both freshwater (●) and NaCl spiked (●) experiments are shown. FPW is shown as solid lines for both Freshwater FPW (blue) and RPW FPW (orange).

Overall, the calculated SI values from reactor experiments with the core material more closely match the FPW than the elemental concentrations. In most cases, the pure water experiments agreed well with the SI values from the Freshwater FPW. Despite the higher concentration of most elements reported in the RPW FPW, the SI values from the NaCl spiked experiments were found to not be a suitable proxy (e.g., in the cases of celestite and gypsum). It may be that there is sufficient formation water so that when HFF mixes with it, the resulting FPW becomes saturated with Na and Cl. In effect, the ionic strength of FPW in the end is not significantly different when either freshwater or RPW is used, and only differs during the first few

hours of flowback. The saturation limit of $NaCl^0_{(aq)}$ in solution is approximately 5 mol/L (Lee et al. 2018), while their concentrations are 2.2 mol/L and 2.5 mol/L in the Freshwater FPW and RPW FPW, respectively. As all the FPW is undersaturated with respect to halite, we know that it is unlikely that sufficient halite is present in the formation to fully saturate FPW, given the rapid kinetics of halite dissolution. While there are higher concentrations of most elements in the RPW FPW, after the concentrations have been normalized with respect to TDS, they are relatively equal to the freshwater FPW and so the SI of both the freshwater FPW and the RPW FPW are similar (Table 7, Table 8, Fig. 21).

4.2 Effect of Temperature on the Saturation Indices

The SI values from the core experiments are comparable with SI calculations for FPW samples with respect to most minerals, with the exception of celestite. While there were notable differences between the mineralogical and aqueous chemistry data between the cores and outcrop samples, the saturation indices of the outcrop were comparable to the cores, with a few exceptions (Table 9). Table 9 is coloured to indicate the degree of matching between the core and outcrop SI values: green indicates the SI for the outcrop and the core were a close match (within 0.2), yellow indicates a moderate match (0.21 – 0.5), and red indicates a poor match (>0.5 difference). Because the saturation indices of the outcrop were in most cases similar to those of the core samples, the outcrop experiments provided a reasonable indication of the influence of temperature on resulting FPW chemistry and SI values.

Table 9: Saturation indices of minerals at T_{48hr} for Core 1 (95 °C), Core 2 (140 °C), and Outcrop (95 °C and 140 °C) for both pure water and NaCl spiked experiments.

	Pure Water				NaCl			
	Core 1 95 °C	Outcrop 95 °C	Core 2 140 °C	Outcrop 140 °C	Core 1 95 °C	Outcrop 95 °C	Core 2 140 °C	Outcrop 140 °C
Quartz	-0.30	0.05	-0.13	-0.21	-0.12	0.21	0.01	0.01
$SiO_{2(am)}$	-1.21	-0.85	-0.84	-0.95	-1.07	-0.73	-0.75	-0.74
Calcite	-0.22	0.03	0.47	0.61	-0.71	n.d.	0.24	0.67
Gypsum	-1.73	-0.77	-1.73	-1.21	-2.84	-2.26	-2.45	-1.97
Anhydrite	-1.37	-0.39	-0.97	-0.50	-2.47	-1.87	-1.69	-1.21
Barite	-0.32	-0.19	-0.09	1.00	-0.53	-0.95	-0.22	-0.10
Celestite	-1.51	-1.37	-1.39	-1.64	-2.49	-2.75	-2.11	-2.16

4.2.1 Major Minerals

As quartz composed 52.4 % of the outcrop sample (Fig. 4), the saturation indices (SI) for both quartz and amorphous silica ($SiO_{2(am)}$) were calculated at 25 °C, 95 °C, and 140 °C to determine how the SI varied as a function of temperature (Fig. 26). Because Si was only detected in the freshwater FPW at one time point, saturation indices was only calculated for that point at 3 different temperatures. The results are of the similar values for both quartz and $SiO_{2(am)}$ and have a similar trend to both the solubility of quartz and $SiO_{2(am)}$, with solubility increasing with temperature. Although it cannot be determined if the FPW values have plateaued to reach equilibrium, they do coincide with the plateaued values from the pure water outcrop experiments for both quartz and amorphous silica.

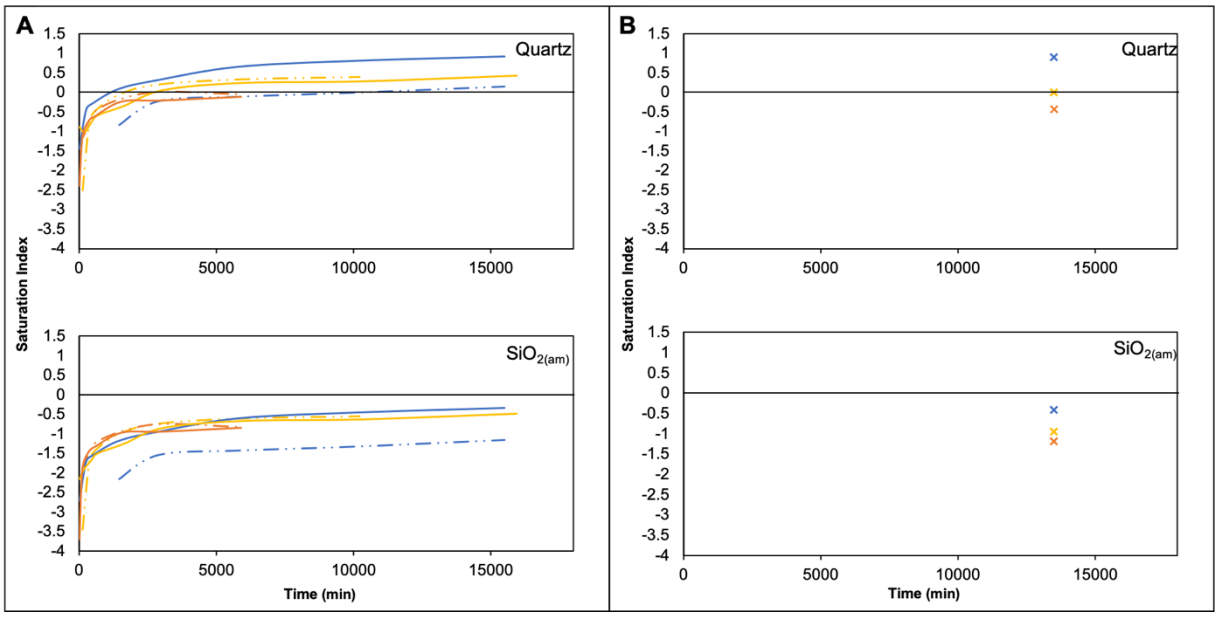

Figure 26: Saturation indices of quartz and $SiO_{2(am)}$ for both A) outcrop experiments compared B) FPW geochemical data. Modelling was conducted at the temperatures of experiments: 25°C (blue), and 95°C (yellow), 140°C (orange). Both freshwater (solid line) and NaCl spiked (dashed line) experiments are shown.

The second most common mineral in the outcrop sample was calcite, making up 14.6 % of the bulk mineral composition. The calculated calcite SI values varied over time for both the reactor experiments and FPW, and show that equilibrium was not established between the solution and calcite (Fig. 27). The biggest difference was in the higher temperature experiments, where calcite became oversaturated within the first 120 min. In general, the calcite SI modelled for the RPW FPW was lower than those for the reactor experiments. This likely resulted from formation water contributing to the composition of the RPW FPW or the fact that the DIC inherent to the RPW FPW was not measured before the fluid degassed at the surface. As this effect was only observed for the DIC and the Ca concentrations are comparable, degassing is the most likely cause of the disparity. Coincidentally, the DIC concentrations from outcrop experiments were comparable to

that of the RPW FPW, despite their differences in TDS. DIC makes up a much smaller fraction of the FPW (Zhong et al. 2018), and therefore limits the precipitation of calcite and other carbonate minerals. This finding suggests that DIC in FPW is nearly entirely due to leaching from the formation or interactions with the atmosphere and not from the HFF. It is more likely that the DIC is from the dissolution of carbonate minerals in the formation as previous studies have found (Paukert Vankeuren et al. 2018) and match the reactor experiments which were closed to atmospheric CO_2 aside from that in the fluid or headspace at the beginning of the experiment.

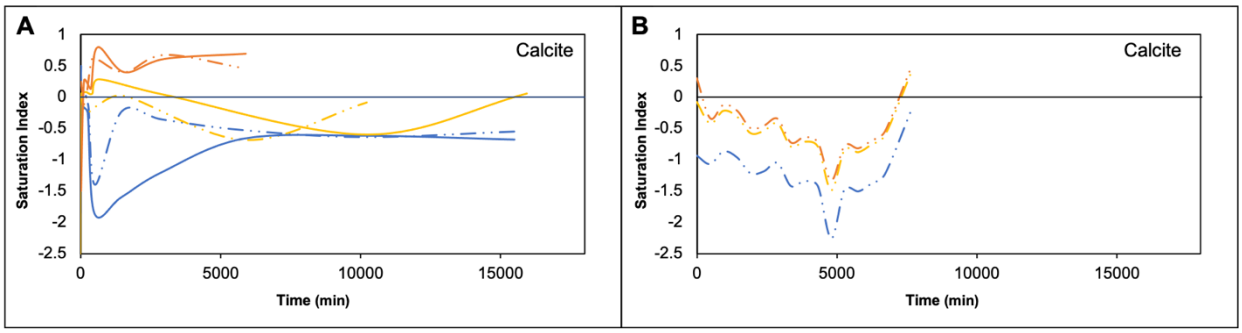

Figure 27: Saturation indices of calcite for both A) outcrop experiments compared B) FPW geochemical data. Modelling was conducted at the temperatures of experiments: 25°C (blue), and 95°C (yellow), 140°C (orange). Both freshwater (solid line) and NaCl spiked (dashed line) experiments are shown.

Unlike the core samples which had no measurable gypsum, gypsum was found to compose 0.5-2.2 % of the outcrop samples. Similar to core sample experiments (Fig. 24), neither gypsum nor anhydrite reached equilibrium over the course of the experiments, reaching an SI of -1.5 to -0.5 in pure water experiments and -2.5 to -2.0 in the NaCl spiked experiments. This range in SI in the outcrop experiments was not observed in the FPW samples, which all hovered around -1.5 for gypsum and -0.5 to -1.5 for anhydrite. The noise in the reactor experimental SI values is likely a product of analytical error in measurements and modelling. The effect of temperature on both

gypsum and anhydrite SI appears to be mostly camped in the kinetics of leaching elements from the minerals and not so much the solubility of those minerals. Although there are some differences in SI of the FPW samples relating to temperature at equilibrium (-1.5 to -1.1 and -1.6 to -0.5 for gypsum and anhydrite, respectively) they are much less pronounced than those of the reactor experiments (-0.5 to -2.5 and -0.4 to -2.6 for gypsum and anhydrite, respectively), that are still reaching equilibrium with the rock. These differences in SI between my experiments and that of FPW could also potentially be explained by the presence of additives in the HFF during the fracturing for the real FPW samples.

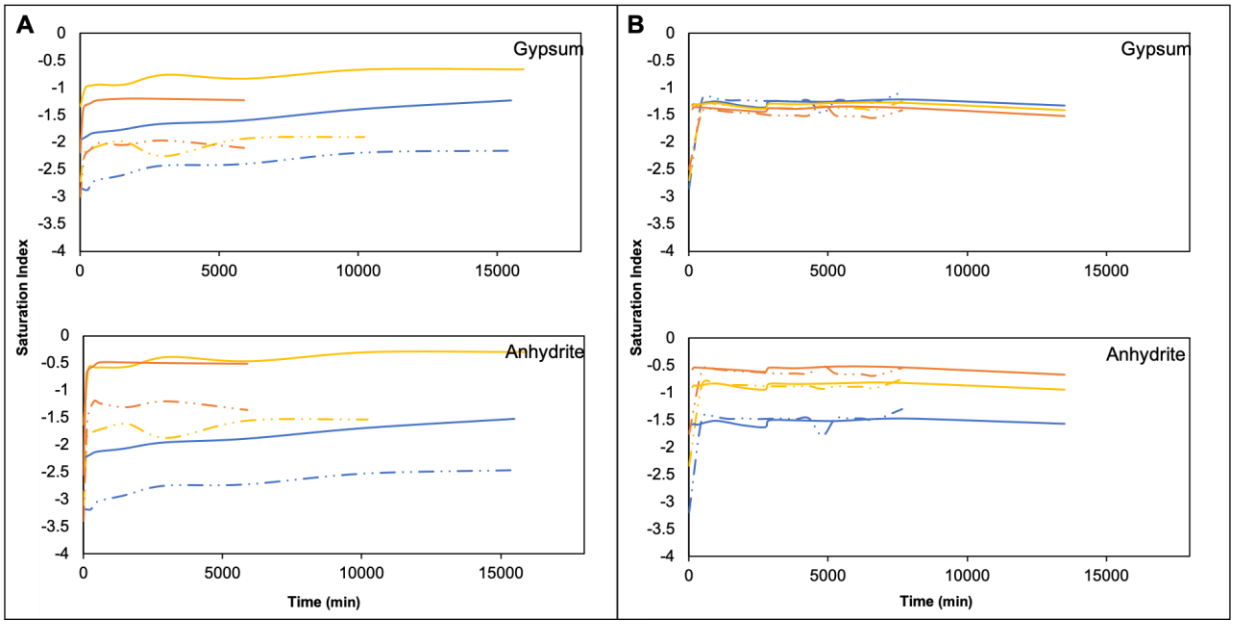

Figure 28: Saturation indices of gypsum and anhydrite for both A) outcrop experiments compared B) FPW geochemical data. Modelling was conducted at the temperatures of experiments: 25°C (blue), and 95°C (yellow), 140°C (orange). Both freshwater (solid line) and NaCl spiked (dashed line) experiments are shown.

4.2.2 Trace Minerals

The calculated SI for celestite for the outcrop samples showed an exaggeration of the trend as a function of temperature as seen in the FPW samples, with values ranging over a much greater range (-1.4 to -2.5) after 1 week than seen with the FPW samples, which all fell between -0.4 and -0.6 after the same amount of time (Fig. 29). As with the core experiments, the SI of celestite appear to be approaching that of the SI of both FPW samples, with the Na Cl experiment lagging even further behind. This lag in kinetics is likely the same reason as that of the core experiments, that hydration of Na and Cl ions has slowed the kinetics of leaching elements from the rock formation. The calculated SI values for barite however, disagreed in both the trend with temperature and values, with the outcrop experiments showing an increase in saturation with temperature while the modelled FPW SI values showed the opposite with a decrease in saturation with increasing temperature (Fig. 29). This opposite trend of barite SI values with temperature could also be a product of reaching equilibrium although the kinetics of the reactions are accelerated with increasing temperature, their SI values are lower. In contrast, celestite demonstrated the same trends with temperature as FPW.

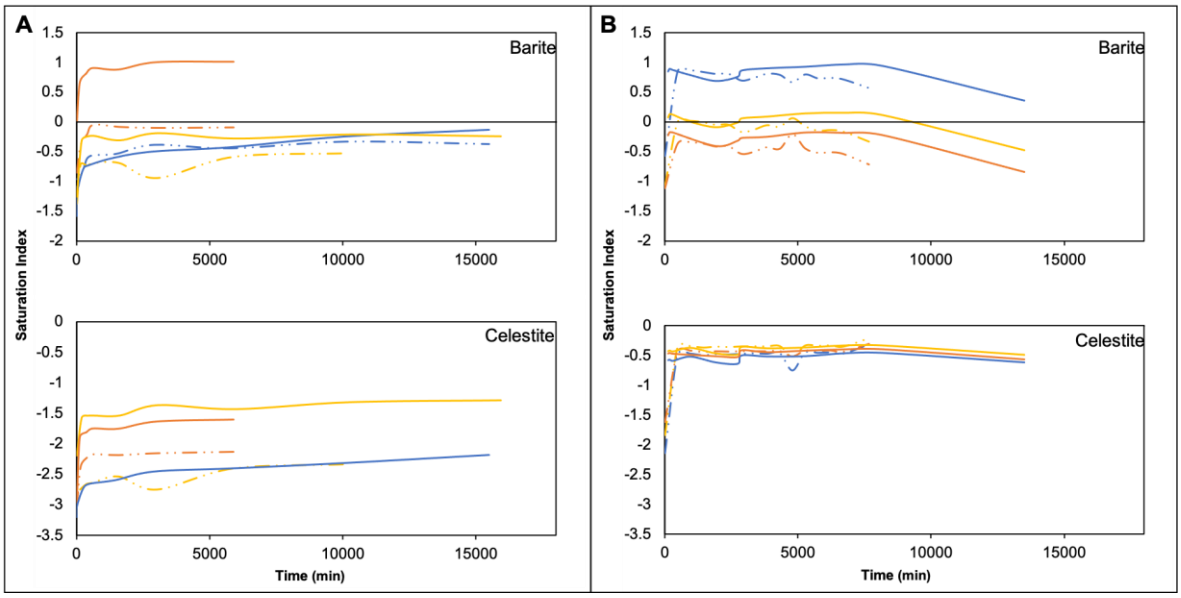

Figure 29: Saturation indices of barite and celestite for both A) outcrop experiments compared B) FPW geochemical data. Modelling was conducted at the temperatures of experiments: 25°C (blue), and 95°C (yellow), 140°C (orange). Both freshwater (solid line) and NaCl spiked (dashed line) experiments are shown.

4.3 Environmental implications

Many of the SI calculated from our experiments coincided well with those of FPW, revealing that formation minerals were the source of many of the elements found in solution, particularly Si, Ca, Ba, Sr, DIC, and SO_4. While other elements, such as Na and Cl, are more likely attributed to formation water or HFF, there was also substantial leaching of other trace elements from the formation, including additional potentially toxic heavy metals (PTHM). For this study, the PTHM of focus were As, Sr, and Ba. As seen in both the absolute concentrations (Table 7, Table 8, Appendix B) and the SI of the calculated minerals (Fig. 22 to Fig. 25), increasing the ionic strength of the simulated HFF using 0.5 mol/L NaCl had a substantial effect on the leachability of many of the metals by reducing the SI of their associated minerals.

There was enhanced leaching of PTHM, such as Ba, Sr, and As, and many of the other elements (B, Mg, Si, K, S, Ca, Mo, and U) in our experiments that were also measured in the field-collected RPW FPW (Table 8, Table 10). In some cases, the salting-in effect was pronounced enough to increase the concentrations in the reactor experiments to above that of the CCME guidelines, given the higher rock-water ratio of actual hydraulic fracturing operations when compared with my reactor experiments, this could lead to a much greater disparity in leached PTHM from the formation. For example, the CCME guidelines for aquatic life in freshwater systems for As is 5 µg/L or 0.067 µmol/L (CCME 1997), which was exceeded in all the reactor experiments spiked with NaCl, with an increase of up to 900 % from the freshwater experiments. If this relationship holds true for hydraulic fracturing, the potential increased As concentration could be up as much as 900 % in a well using a higher ionic strength solution (RPW FPW for example) from a well using only freshwater as its source water. Similar effects were observed with Sr, and although leaching from the formation is unlikely the sole source of the metal during hydraulic fracturing, the enhanced leaching seen with Sr indicated there was still a substantial contribution of Sr from the formation itself. Consistently across both the cores and the outcrops and across nearly all temperatures, the salting in effect was greatest for Ba. Ba does not have a CCME guideline for aquatic life, but it does have one for drinking water, 1.0 mg/L (7.3 µmol/L) (CCME 1997). My experiments revealed that the salting-in effect was enough to exceed this level in experiments conducted with the core samples, but not those with the outcrop samples (Table 8). It is important to note that because these experiments were conducted at a far higher water-rock ratio than in the subsurface during hydraulic fracturing, and so the concentrations from leaching from the formation in a real hydraulic fracturing operation would likely be much greater than those observed here, as the water would have access to more rock material and therefore more PTHM.

Table 10: Percent increase in leached ions in NaCl spiked experiments.

Element	Units	Outcrop 25 °C	Outcrop 95 °C	Outcrop 140 °C	EOG I 95 °C	EOG II 95 °C	ECA I 140 °C	ECA II 140 °C
B	mmol/L	5.53	163.26	223.91	61.37	-45.85	181.17	83.52
Mg	mmol/L	20.70	4.00	75.18	55.81	88.78	114.40	138.08
Si	mmol/L	-73.71	32.12	75.51	65.56	-1.49	41.22	3.18
K	mmol/L	54.93	65.12	31.01	35.39	44.64	81.53	49.62
S	mmol/L	33.10	-39.17	34.81	-65.56	-54.77	91.68	60.51
Ca	mmol/L	59.20	-23.06	84.41	50.81	58.98	163.32	150.27
As	µmol/L	BDL	486.20	100.71	937.80	225.69	138.89	-10.33
Sr	µmol/L	BDL	14.80	284.22	134.83	154.72	165.26	178.32
Mo	µmol/L	5.67	31.00	8.12	382.44	379.63	8.16	-14.30
Ba	µmol/L	1199.47	377.02	1379.64	1873.94	1192.92	1133.34	998.46
U	µmol/L	216.80	493.31	676.52	BDL	BDL	BDL	BDL

BDL = below detection limit in either pure water or NaCl spiked experiments, or both

5. Conclusions and Future Directions

5.1 Conclusions

The primary purpose of this study was to determine if hydraulic fracturing processes could be accurately represented in a small scale, inexpensive reactor system for the purposes of understanding geochemical problems. From the work here, it is clear that the intended goal was achieved, with some limitations. And although an accurate water-rock ratio cannot be achieved and the resulting aqueous solutions have far lower TDS than field-collected FPW, and steady state was not achieved in many of the chemical profiles during the experiments, the overall trends are similar and can be made comparable with the use of saturation indices. The systems also revealed the importance of formation water in many of the geochemical interactions that result in the composition of FPW. Assuming the necessary conditions are met, such as using a well-mixed core sample from the area of study and using a temperature appropriate for the depth of the reservoir, geochemical tasks such as determining the order of precipitation of amorphous minerals and the relative rates of metals leaching can be accurately predicted using this method.

I also determined that the use of an outcrop as a proxy for core samples of a formation should be used sparingly and only when the mineralogy and bulk geochemistry can be confirmed to be similar enough for the purposes of the study. In the case of this study, the Perdrix Formation outcrop in Jasper National Park, Alberta was found to be too different for direct geochemical comparisons, but still valuable to determine trends in saturation indices over a range of temperatures. Additionally, the differences in composition between the two sub-basin core samples was significant but did not translate much to the aqueous data like with the outcrop sample. This was likely because the mineralogy was substantially different between the outcrop and core

samples with not only proportions but also the presence of secondary weathering minerals appearing in the outcrop samples when not seen in the core samples.

Finally, the usability of the small-scale batch reactors to predict solutions to geochemical problems was tested by determining the effect of RPW on the resultant wastewaters from hydraulic fracturing. The trends revealed a strong salting-in effect on many of the trace metals, including numerous potentially toxic heavy metals (PTHM). This revealed that there is a potential environmental risk of using RPW in hydraulic fracturing processes, which is that there is a potential to leach more of potentially toxic metals, such as As, Ba, Mo, and Sr into the resultant wastewaters that is then brought to the surface. This becomes a potential spill risk with higher than normal potential dangers to surface and near-surface aquatic ecosystems.

5.2 Future Directions

My study has shown that it is possible to determine the leachability of a formation during hydraulic fracturing using a simple stirred batch reactor, with a primary focus on methodology there is room to expand the work conducted with the reactors developed here. For example, studies testing the viability of using the method outline in this study of simple reactors under atmospheric conditions with rocks from other formations that are typically targeted by hydraulic fracturing operations, such as the Marcellus Shale in the United States or the Montney formation in Alberta and British Columbia, would provide confidence in the repeatability of using these simple reactors. Furthermore, experimentation into the effects of individual or combinations of organic compounds typically found in HFF should be conducted to determine if these organic and inorganic compounds have a substantial effect on the leachability of metals from the formations during hydraulic fracturing. This second avenue has already begun to be explored by looking at the degradation rates and patterns of numerous compounds, such as benzoic acid, ethyl acetate,

glutaraldehyde, and propylene carbonate (Sumner and Plata 2018, Tasker et al. 2016, Xiong et al. 2018), finding that these compounds generally degrade, but their effect on the leaching of metals has not been well documented. These studies also used complex commercial or bespoke reactors that required a substantial financial investment, and the only study that used simplified reactor systems, in the form of serum bottles did not assess the effect of additives on the leachability of elements from the formations it studied. While these studies, and others such as Harrison et al. (2017), Jew et al. (2017), Li et al. (2019), and Li et al. (2020) have begun to systematically explore water-rock-fracturing fluid interactions many questions remain largely driven by the variability in fracturing fluid chemistry, inter-formation compositional differences and even heterogeneity within a single formation. A few follow-up studies should include:

1. Testing this method with a more representative rock sample by either selecting a greater length of the core or selecting samples from numerous cores from within a small geographical area. This would account for formation and formation water heterogeneity and likely produce results more comparable to that of FPW from the same area.
2. Testing the effect of biocides on both the leaching of metals as well as their impacts on the microbiological community and function during the hydraulic fracturing process. Some work has been done on this front by Cliffe et al. (2020) and Zhong et al. (2019), and both have concluded that sulfidogenic and halotolerant bacteria are dominantly present FPW. Further work on this could be done to determine if these bacteria could also thrive in downhole conditions following hydraulic fracturing. This could be achieved by running experiment with and without glutaraldehyde at reservoir temperatures, a common biocide in HF (Table 1).

3. Adjusting the particle size and quantity of rock sample to increase or decrease the reactive surface area to determine if these small modifications can improve the quality of the raw chemical data. By decreasing the particle size to a fine powder, the reactive surface area will be higher and with added rock samples and small adjustments to the sampling protocol, an increase the rate of elements leaching could be achieved, leading to equilibrium achieved much sooner to improve the geochemical profiles of kinetically slower leaching elements, such as Si. Li et al. (2019) has investigated the opposite, by submerging whole core samples into a simulated HFF solution to determine the thickness of the alteration zone, but work on much finer powders would provide information on more brittle formations that break off in fine pieces during fracturing.
4. Longer term experiments, on the order of months, as done in Harrison et al. 2017, would allow equilibrium to be reached with even the slower leaching minerals, that take longest to reach equilibrium, such as quartz and $SiO_{2(am)}$. Although due to the limited amount of sampling points, coarser geochemical profiles would be obtained, such a study would be invaluable in determining the full order of leaching from the host rock and would be useful in predicting the trends associated with later produced waters.
5. Adjusting the headspace gas to simulate anaerobic conditions with argon, CO_2, or N_2 gas bubbling, while keeping the initial water oxic with pCO_2 as would be the case during hydraulic fracturing. This could provide insight into the interactions occurring deep in the wells, along the edges of the fractures where minimal oxygen is usually present during hydraulic fracturing. By adjusting the amount of available

O_2 in the reactors, a lateral wellbore leaching profile could be obtained. Jew et al. (2017) and Li et al. (2019) have investigated the effect of the oxic and anoxic conditions on the leaching of Fe from pyrite, but a further study on other redox sensitive elements could also be valuable.

6. Using the full suite of HFF additives at the correct ratio with and without breakers to determine the effect the combination has on the leachability of the host rocks and subsequent reprecipitation of amorphous minerals and polymer degradation. This would require a previously characterized solution of HFF polymers and access to breakers and proppants used on a well where core samples are available. This type of study would give a more accurate representation of true FPW and its formation with time during the shut-in period of a well.

References

Abualfaraj, N., Guarian, P. L., and Olson, M.S. (2014) Characterization of Marcellus Shale Flowback water. Environmental Engineering Science, 31(9), 514-524.

AER (Alberta Energy Regulator). (2016) Duvernay Reserves and Resources Report: A Comprehensive Analysis of Alberta's Foremost Liquids-Rich Shale Resource. Retrieved from: https://www.aer.ca/documents/reports/DuvernayReserves_2016.pdf on May 10, 2020.

AER (Alberta Energy Regulator). (2019) Hydraulic Fracturing. Retrieved from: https://www.aer.ca/protecting-what-matters/holding-industry-accountable/industry-performance/hydraulic-fracturing-water-use on April 2, 2020.

Ahmadun, F., Pendashteh, A., Abdullah, L. C., Biak, D. R. A., Madaeni, S. S., and Abidin, Z. Z. (2009) Review of technologies for oil and gas produced water treatment. Journal of Hazardous Materials, 170(2-3), 530-551.

Ahmed, S. B., Tlili, M. M., Amami, M., and Amor, M. B. (2014) Gypsum Precipitation Kinetics and Solubility in the NaCl−$MgCl_2$−$CaSO_4$-H_2O System, Industrial and Engineering Chemistry Research, 53, 9554-9560.

Alessi, D. S., Zolfaghari, A., Kletke, S., Gehman, J., Allen, D. M., and Goss, G. G. (2017) Comparative analysis of hydraulic fracturing wastewater practices in unconventional shale development: Water sourcing, treatment, and disposal practices. Canadian Water Resources Journal, 42(2), 105-121.

Arthur, J. D., B. Bohm, and M. Layne. (2008) ALL Consulting. Hydraulic Fracturing Considerations for Natural Gas Wells of the Marcellus Shale. Presented at the GWPC Annual Forum in Cincinnati, OH. September 2008.

Azimi, G. (2010) Evaluating the Potential of Scaling due to Calcium Compounds in Hydrometallurgical Processes [PhD. Dissertation] University of Toronto, 156p.

Bish, D. L. and Howard, S. A. (1988) Quantitative phase analysis using the Rietveld method. Journal of Applied Crystallography, 21, 86-91.

Birdwell, J. E. (2017) Development of new shale geochemical reference materials: results from Boquillas Shale interlaboratory testing and other status updates, GSA Annual Meeting in Seattle Washington, USA, 69-8. https://gsa.confex.com/gsa/2017AM/webprogram/Paper304400.html on July 9, 2019.

Busenberg, E. Plummer, L. N., and Parker, V. B. (1984) The solubility of strontianite ($SrCO_3$) in CO_2-H_2O solutions between 2 and 91°C, the association constants of $SrHCO^+_3$(aq) and $SrCO^0_3$(aq) between 5 and 80°C, and an evaluation of the thermodynamic properties of Sr^{2+}(aq) and $SrCO_3$(cr) at 25°C and 1 atm total pressure. Geochimica et Cosmochimica Acta, 48(10), 2021-2035.

Blount, C. W. (1974) Synthesis of Barite Celestite, Anglesite, Witherite, and Strontianite from Aqueous Solutions. American Mineralogist, 59, 1209-1219

Brower, E. (1973) Synthesis of barite, celestite, and barium-strontium sulfate solid solution crystals. Geochemica et Cosmochimica Acta, 37(1), 155-158.

CAPP (Canadian Association of Petroliam Producers). (2018) Water use for hydraulic fracturing in Alberta. (Report No. 2018-0033) Retrieved from: https://www.capp.ca/publications-and-statistics/publications/322611 on May 2, 2020.

Cheary, R. W. and Coelho, A. (1992) A fundamental parameters approach to X-ray line-profile fitting. Journal of Applied Crystallography, 25, 109-121.

Clark, C. E., Horner, R. M., and Harto, C. B. (2013) Life cycle water consumption for shale gas and conventional natural gas, Environment Science and Technology, 47(20), 11829-11836.

CCME (Canadian Council of Ministers of the Environment). (1997) Appendix XXII – Canadian water quality guidelines: Updates (June 1997), arsenic, bromacil, carbaryl, chlorpyrifos, deltamethin, and glycols. In: Canadian water quality guidelines, Canadian Council of Resource and Environment Ministers. 1987. Prepared by the Task Force on Water Quality Guidelines.

Dwyer, F.J., S.A. Burch, C.G. Ingersoll, and J.B. Hunn. (1992) Toxicity of trace element and salinity mixtures to striped b(aMssorone saxatilis) andDaphnia magna. Environmental Toxicology and Chemistry 11(4): 513– 520.

Delompré, P. L. M., Blewett, T. A., Snihur, K. N., Flynn, S. L., Alessi, D. S., Glover, C. N., and Goss, G. G. (2019) The osmotic effect of hyper-saline hydraulic fracturing fluid on rainbow trout, *Oncorhynchus mykiss*. Aquatic Toxicology, 211, 1-10.

Dong, T., Harris, N. B., Knapp, L. J., McMillan, J. M., and Bish, D. L. (2018) The effect of thermal maturity on geomechanical properties in shale reservoirs: An example from the Upper Devonian Duvernay Formation, Western Canada Sedimentary Basin. Marine and Petroleum Geology, 97, 137-153.

Dong T., Harris, N. B., McMillan J. M., Twemlow, C. E., Nassichuk, B. R., and Bish D. L. (2019) A model for porosity evolution in shale reservoirs: An example from the Upper Devonian Duvernay Formation, Western Canada Sedimentary Basin. AAPG (American Association of Petroleum Geologists) Bulletin, 103(5), 1017-1044.

Dyer, S. J., and Graham G.M. (2002) The effect of temperature and pressure on oilfield scale formation. Journal of Petroleum Science and Engineering, 35, 95-107.

Finch, A. A. and Allison, N. (2007) Coordination of Sr and Mg in calcite and aragonite. Mineralogical Magazine, 71(5), 539-552.

Flynn S. L., von Gunten, K., Warchola, T., Snihur, K., Forbes, T. Z., Goss, G. G., Gingras, M. K., Konhauser, K. O., and Alessi, D. S. (2019) Characterization and implications of solids associated with hydraulic fracturing flowback and produced water from the Duvernay Formation, Alberta, Canada. Environmental Science Processes and Impacts, 21, 242-255.

Folkerts, E., Goss, G. G., and Blewett, T. A. (2020) Investigating the Potential Toxicity of Hydraulic Fracturing Flowback and Produced Water Spills to Aquatic Animals in Freshwater Environments: A North American Perspective. In: Reviews of Environmental Contamination and Toxicology (Continuation of Residue Reviews) Springer, Cham., pp. 1-56.

Fox, F. G. (1951) Devonian Stratigraphy of Rocky Mountains and the Foothills Between Crowsnest Pass and Athabasca River, Alberta, Canada, 34(4), 822-843.

Freedman, D. E., Riley, S. M., Jones, Z. L., Rosenblum, J. S., Sharp, J. O., Spear, J. R., and Cath, T. Y. (2017) Biologically active filtration for fracturing flowback and produced water treatment. Journal of Water Process Engineering, 18, 29-40.

Gallegos, T. J., Varela, B. A., Haines, S. S., and Engle, M. A. (2015) Hydraulic fracturing water use variability in the United States and potential environmental implications. Water Resources Research: Technical Reports, 51(7) 5839-5845.

Goss, G., Alessi, D. S., Allen, D., Gehman, J., Brisbois, J., Kletke, S., Zolfaghari-Sharak, A., Notte, D., Thompson, D.Y., Hong,K., Junes, C. R. V., Guedes de Arujo, B., Neto, W., and Prosser, D. (2015) Unconventional Wastewater Management: a Comparative Review and Analysis of Hydraulic Fracturing Wastewater Management Practices Across Four North

American Basins, 186pp. Retrieved from: https://cwn-rce.ca/wp-content/uploads/2015/10/Goss-et-al.-2015-CWN-Report-Unconventional-Wastewater-Management.pdf on May 22, 2020.

Gregory, K. B., Vidic, R. D., and Dzomback, D. A. (2011) Water management challenges associated with production of shale gas by hydraulic fracturing, Elements, 7(3), 181-186.

Hackley, P. C. and Cardott, B. J. (2016) Application of organic petrography in North American shale petroleum systems: A review. International Journal of Coal Geology, 163, 8-51.

Harris N. B., McMillan. J. M., Knapp L. J., and Mastalerz, M. (2018) Organic matter accumulation in the Upper Devonian Duvernay Formation, Western Canada Sedimentary Basin, from sequence stratigraphic analysis and geochemical proxies. Sedimentary Geology, 376, 185-203.

Harrison, A. L., Jew, A. D., Dusting, M. K., Thomas, D. L., Joe-Wang, C. M., Barger, J. R., Johnson, N., Brown, G. E., and Maher, K. (2017) Element release and reaction-induced porosity alteration during shale-hydraulic fracturing fluid interactions. Applied Geochemistry, 82, 47-62.

He, C., Wang, X., Liu, W., Barbot, E., and Vidic, R. D., (2014) Microfiltration in recycling of Marcellus Shale flowback water: Solids removal and potential fouling of polymeric microfiltration membranes. Journal of Membrane Science, 462, 88-95.

He, Y., Flynn, S. L., Folkerts, E., Zhang, Y., Ruan, D., Alessi, D. S., Martin, J. W., and Goss, G. G. (2017) Chemical and toxicological characterizations of hydraulic fracturing flowback and produced water. Water Research, 114, 78-87.

Helz, G. R. and Holland, H.D. (1965) The solubility and geologic occurrence of strontianite. Geochimica et Cosmochimica Acta, 29(12), 1303-1315.

Hill, R. J., Howard, C. J. (1987) Quantitative phase analysis from neutron powder diffraction data using the Rietveld method. Journal of Applied Crystallography, 20, 467-474.

Holland, H. D. and Zimmerman, H. (2000) The Dolomite Problem Revisited, International Geology Review, 42(6), 481-490.

Hörbrand, T., Baumann, T., and Moog, H.C. (2018) Validation of hydrogeochemical databases for problems in deep geothermal energy. Geothermal Energy, 6(2), 30pp.

Icenhower, J. P. and Dove, P. M. (2000) The dissolution kinetics of amorphous silica into sodium chloride solutions: Effects of temperature and ionic strength. Geochimica et Cosmochimica Acta, 64(24), 4193-4203.

Jew, A. D., Dustin, M. K., Harrison, A. L., Joe-Wang, C. M., Thomas, D. L., Maher, K., Brown Jr., G. E., and Bargar, J. R. (2017) Impact of Organics and Carbonates on the Oxidation and Precipitation of Iron during Hydraulic Fracturing of Shale, Energy and Fuels, 31, 3643-3658.

Kim, S., Omur_Ozbek, P., Dhanasekar, A., Prior, A., and Carlson, K. (2016) Temporal analysis of flowback and produced water composition from shale oil and gas operations: Impact of frac fluid characteristics. Journal of Petroleum Science and Engineering, 147, 202-210.

Kondash, A. J., Albright, E., and Vengosh, A. (2017) Quantity of flowback and produced waters from unconventional oil and gas exploration. Science of the Total Environment, 574, 314-321.

Knapp, L. J., McMillan, J. M., and Harris, N. B. (2017) A depositional model for organic rich Duvernay Formation mudstones. Sedimentary Geology, 347, 160-182.

Krumgalz, B. S. (2018) Temperature Dependence of Mineral Solubility in Water. Part 3. Alkaline and Alkaline Earth Sulfates. Journal of Physical and Chemical Reference, 47, 023101. 30pp.

Lee, C. J. D., McMullan, P. E., O'Kane, C. J., Stevenson, A., Santos, I. C., Roy, C., Ghosh, W., Mancinelli, R. L., Mormile, M. R., McMullan, G., Banciu, H. L., Fares, M. A., Benison, K. C., Oren, A., Dyall-Smith, M. L., and Hallsworth, J. E. (2018) NaCl-saturated brines are thermodynamically moderate, rather than extreme, microbial habitats. FEMS Microbiology Reviews, 42(5), 672-693.

Li, Q., Jew, A. D., Kohli, A, Maher, K., Brown Jr, G. E., and Bargar, J. R. (2019) Thickness of Chemically Altered Zones in Shale Matrices Resulting from Interactions with Hydraulic Fracturing Fluid, Energy and Fuels, 33, 6878-6889.

Li, Q., Jew, A. D., Brown Jr, G. E., Bargar, J. R., and Maher, K. (2020) Reactive Transport Modeling of Shale-Fluid Interactions after Imbibition of Fracturing Fluids, Energy and Fuels, 34, 5511-5523.

Locock, A. J., Chesterman, D., Caird, D., and Duke, M. J. M. (2012) Miniaturization of mechanical million for powder X-ray diffraction. Powder Diffraction 27, 189–193.

MacKay, M. K., Eaton, D. W., Pedersen, P. K., and Clarkson, C. R. (2018) Integration of outcrop, subsurface, and microseismic interpretation for rock-mass characterization: An example from the Duvernay Formation, Western Canada. Interpretation: Technical Papers, 6(4): T919-T936.

May, H. M., Helmke, P. A., and Jackson, M. L. (1979) Gibbsite solubility and thermodynamic properties of hydroxy-aluminum ions in aqueous solution at 25°C. Geochimica et Cosmochimica Acta, 44, 861-868.

McKean, S. H., Priest, J. A., and Eaton, D. W. (2018) A geomechanical comparison of the Duvernay and the Montney, Geoconvention 2018, 5pp.

Mehler, W.T., Nagel, A., Flynn, S., Zhang, Y., Sun, C., Martin, J., Alessi, D., and Goss, G. G. (2020) Understanding the effects of hydraulic fracturing flowback and produced water (FPW) to the aquatic vertebrate, *Lumbriculus variegatus* under various exposure regimes. Environmental Pollution, 259, 113889.

Meijer, J. A. M. and Van Rosmalen, G. M. (1984) Solubilities and supersaturations of calcium sulfate and its hydrates in seawater. Desalination, 51, 255-305.

Morey, G. W., Fournier, R. O., and Rowe, J. J. (1962) The solubility of quartz in water in the temperature interval from 25° to 300°C. Geochimica et Cosmochimica Acta, 26, 1029-1043.

Nicholson, R. V., Gillam, R. W., and Rearson, E. J. (1989) Pyrite oxidation in carbonate-buffered solution: 2. Rate control by oxide coatings. Geochimica et Cosmochimica Acta, 54, 395-402.

Owen, J., Bustin,, R. M., and Bustin, A. M. M. (2020) Insights from mixing calculations and geochemical modeling of Montney Formation post hydraulic fracturing flowback water chemistry. Journal of Petroleum Science and Engineering, 195, 107589, 18pp.

Paktinat, J., O'Neil, B. J., and Tulissi, M. G. (2011) Case studies: impact of high salt tolerant friction reducers on freshwater conversation in Canadian shale fracturing treatments. In Canadian unconventional resources conference. Society of Petroleum Engineers. Alberta, Canada. SPE-149272-MS, 14pp.

Parkhurst, D. and Appelo, C. A. J. (2013) PHREEQC (Version 3) -A Computer Program for Speciation, Batch Reaction, One-Dimensional Transport, and Inverse Geochemical Calculations. US Geologic Survey, Water Resources Division, Denver, Co.

Paukert Vankeuren, A. N. P., Hakala, J. A., Jarvis, K., and Moore, J. E. (2017) Mineral Reactions in Shale Gas Reservoirs: Barite Scale Formation from Reusing Produced Water as Hydraulic Fracturing Fluid. Environmental Science and Technology, 51, 9391-9402.

Phillips, W. J. (1972) Hydraulic fracturing and mineralization. Journal of the Geological Society 128(4), 337-359.

Pilkington, M., Snyder, D. B., and Hemant, K. (2006) Weakly magnetic crust in the Canadian Cordillera. Earth and Planetary Science Letters, 248, 461-470.

Pingitore, N. E. Jr (1987) Modes of Coprecipitation of Ba^{2+} and Sr^{2+} with Calcite, ACS Symposium Series, 323(27), 574-586.

Plata Enriquez, I. (2018) A combined Membrane Filtration – Aeration Approach for the Treatment of Hydraulic Fracturing-Flowback and Produced Water from the Duvernay Formation [MSc. Thesis]: Alberta, Canada, University of Alberta, 126p.

Rietveld, H. (1969) A profile refinement method for nuclear and magnetic structures. Journal of Applied Crystallography, 2, 65-71.

Rimstidt, J. D. and Vaughan D. J. (2003) Pyrite oxidation: A state-of-the-art assessment of the reaction mechanism. Geochimica et Cosmochimica Acta, 67(5), 873-880.

Rosenbauer, R. J., Koksalan, T., and Palandri, J. L. (2005) Experimental investigation of CO_2-brine-rock interactions at elevated temperatures and pressure: Implications for CO_2 sequestration in deep-saline aquifers, 86, 1581-1597.

Rowan, E. L., Engle, M. A., Kraemer, T. F., Schroeder, K. T., Hammack, R. W., and Doughten, M. W., (2015) Geochemical and isotopic evolution of water produced from Middle Devonian Marcellus shale gas wells, Appalachian basin, Pennsylvania. AAPG (American Association of Petroleum Geology) Bulletin, 99, 181–206.

Shaffer, D. L., Chavez, L. H. A., Ben-Sasson, M., Castrillón, S. R., Yip, N. Y., and Elimelech, M. (2013) Desalination and Reuse of High-Salinity Shale Gas Produced Water: Drivers, technologies, and Future Directions. Environmental Science & Technology, 47, 9569-9583.

Shen, L., Schmitt, D. R., and Haug, K. (2018) Measurements of the states of in situ stress for the Duvernay Formation near Fox Creek, west-central Alberta; Alberta Energy Regulator / Alberta Geological Survey, AER/AGS Report 97, 29 pp.

Siever, R. (1962) Silica solubility, 0°-200°C, and the diagenesis of siliceous sediments. Geology, 70(2), 127 – 150.

Sumner, A. J. and Plata, D. L. (2018) Exploring the hydraulic fracturing parameter space: a novel high-pressure, high-throughput reactor system for investigating subsurface chemical transformations. Environmental Science: Processes & Impacts, 20, 318-331.

Sun, Y., Want, D., Tsang, D. C. W., Wang, L., Ok, Y. S., and Feng, Y. (2019) A critical review of risks, characteristics, and treatment strategies for potentially toxic elements in wastewater from shale gas extraction. Environment International, 125, 452-469.

Szramek, K., McIntosh, J. C., Williams, E. L., Kanduc, T., Ogrinc, N., and Walter, L. M. (2007) Relative weathering intensity of calcite versus dolomite in carbonate-bearing temperate zone watersheds: Carbonate geochemistry and fluxes from catchments within the St. Lawrence and Danube river basins, Geochemistry, Geophysics, Geosystems, 8(4), 1-26.

Tasker, T. L., Piotrowski, P. K., Dorman, F. L., and Burgos, W. D. (2016) Metal Associations in Marcellus Shale and Fate of Synthetic Hydraulic Fracturing Fluids Reacted at High Pressure and Temperature. Environmental Engineering Science, 33(10), 753-765.

Taylor, R. S., Stobo, B., Niebergall, G., Aguilera, R., Walter, J., and Hards, E. (2014) Optimization of Duvernay fracturing treatment design using fully compositional dual permeability numeric reservoir simulations. SPE/CSUR Unconventional Resources Conference, Society of Petroleum Engineers, Canada.

US EPA (United States Environmental Protection Agency). (2016) Hydraulic Fracturing for Oil and Gas: Impacts from the Hydraulic Fracturing Water Cycle on Drinking Water Resources in the United States. (Report No. EPA-600-R-16-236ES). Retrieved from: https://www.epa.gov/sites/production/files/2016-12/documents/hfdwa_executive_summary.pdf on April 23, 2020.

Vidic, R. D., Brantley, S. L., Vandenbossche, J. M., Yoxtheimer, D., and Abad, J. D. (2013) Impact of Shale Gas Development on Regional Water Quality. Science 340(6134), 1235009, 11pp.

Wang, Y., von Gunten, K., Bartova, B., Meisser, N., Astner, M., Burger, M., and Bernier-Latmani, R. (2016) Products of in Situ Corrosion of Depleted Uranium Ammunition in Bosnia and Herzegovina Soils. Environmental Science & Technology 50, 12266-12274.

Weides, S. and Majorowicz, J. (2014) Implications of Spatial Variability in Heat Flow for Geothermal Resource Evaluation in Large Foreland Basins: The Case of the Western Canadian Sedimentary Basin. Energies 7, 2573-2594.

Wilson, M.A., Burt, R., and Lee, C.W. (2006) Improved Elemental Recoveries in Soils with Heating Boric Acid Following Microwave Total Digestion. Communications in Soil Science and Plant Analysis, 27(3-4), 513-524.

Worley, W. G., Tester, J. W., and Grigsby, C. O. (1996) Quartz dissolution Kinetics from 100-200°C as a function of pH and Ionic Strength. AIChE Journal, 42(12), 3442-3457.

Xiong, B., Miller, Z., Roman-White, S., Tasker, T., Farina, B., Piechowicz, B., Burgos, W. D., Joshi, P., Zhu, L., Gorski, C. A., Zydney, A. L., and Kumar, M. (2018) Chemical Degradation of Polyacrylamide during Hydraulic Fracturing. Environmental Science & Technology, 52, 327-336.

Xiong, W., Gill, M., Moore, J., Crandall, D., Hakala, J. A., and Lopano, C. (2020) Influence of Reactive Flow Conditions on Barite Scaling in Marcellus Shale during Stimulation and Shut-In Periods of Hydraulic Fracturing. Energy and Fuels, 34(11), 13625-13635.

Zhang, F, Dai, Z., Yan, C., Bhandari, N., Yan, F., Liu, Y., Zhang, Z., Ruan, G., Kan, A. T., and Tomson, M. B. (2017) Barite-Scaling Risk and Inhibition at High Temperature. Society of Petroleum Engineers, 22(1), 69-79.

Zetaware Utilities (2003a) BHT correction, I Only Have Time Since Circulation. Retrieved from http://www.zetaware.com/utilities/bht/timesince.html on June 4, 2019.

Zetaware Utilities (2003b) BHT Correction, The Last Resort. Retrieved from http://www.zetaware.com/utilities/bht/lastresort.html on June 4, 2019.

Ziemkiewicz, P.F. and He, Y.T. (2015) Evolution of water chemistry during Marcellus Shale gas development: A case study in West Virginia. Chemosphere, 134, 224-231.

Zhong, C., Li, J., Flynn, S. L., Nesbø, C. L., Sun, C., von Gunten, K., Lanoil, B. D., Goss, G. G., Martin, J. W., and Alessi, D. S. (2019) Temporal Changes in Microbial Community Composition and Geochemistry in Flowback and Produced Water from the Duvernay Formation. ACS Earth and Space Chemistry, 3, 1047-1057.

Appendix A

Supplemental Methodology

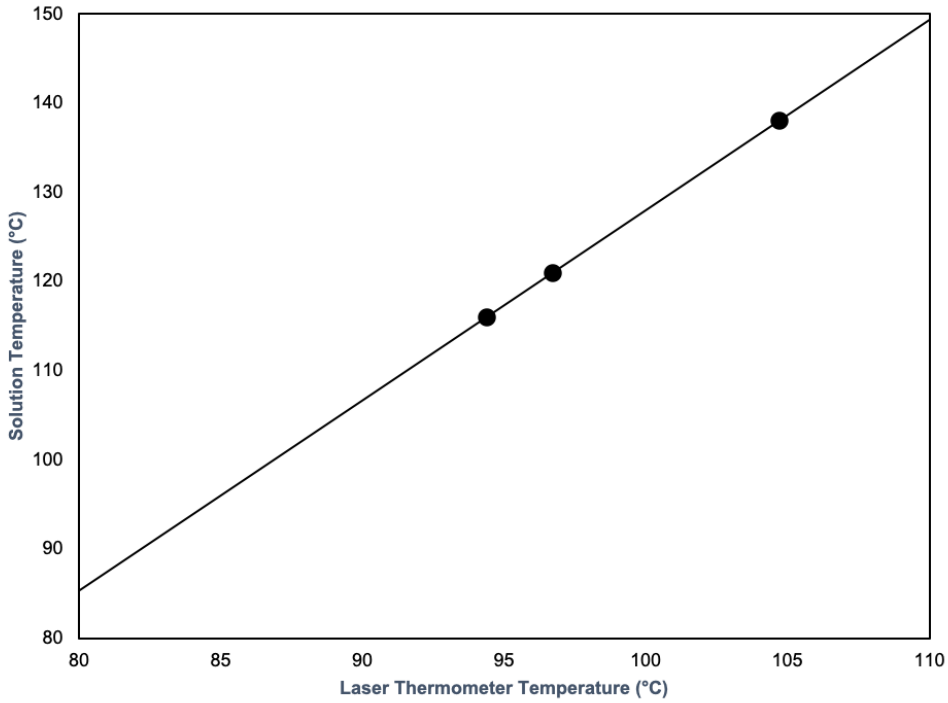

A-1 Temperature calibration curve, for Vessel B. Control points were collected with irreversible temperature dots.

A-2 PHREEQC Parameters used in modelling

Experiment		Concentration (mg/L)															pH	Temp	Number
		Li	B	Na	Mg	Si	K	Ca	Mn	Fe	Br	Sr	Ba	Cl-	S	CO32-			
Outcrop Freshwater @ 25C	Input	0.00	0.00	0.00	0.00	0.00	0.00	0.00	0.00	0.00	0.00	0.00	0.00	0.00	0.00	3.04	4.56	21.70	1.00
	$T_{0'}$	0.00	0.00	0.00	6.51	0.00	2.41	41.14	0.00	0.00	0.00	0.05	0.00	0.00	44.39	18.32	8.11	22.00	2.00
	T_0	0.00	0.00	0.00	8.26	0.24	2.79	45.26	0.00	0.00	0.00	0.07	0.01	0.00	49.36	20.33	8.29	26.50	5.00
	T_{4hrs}	0.00	0.13	4.07	12.41	2.35	5.73	51.75	0.00	0.00	0.00	0.14	0.01	10.56	56.20	24.63	8.07	26.50	245.00
	T_{8hrs}	0.00	0.21	1.74	11.95	3.35	6.62	53.58	0.00	0.00	0.00	0.15	0.01	0.00	62.41	31.98	6.53	26.00	485.00
	T_{24hrs}	0.00	1.04	2.78	12.68	7.90	8.59	61.52	0.00	0.00	0.00	0.17	0.02	0.00	64.37	44.61	6.57	26.00	1440.00
	T_{48hrs}	0.00	1.98	3.54	13.88	13.64	11.26	65.28	0.00	0.00	0.00	0.19	0.02	0.00	82.00	43.05	6.88	26.50	2885.00
	T_{96hrs}	0.00	5.44	8.30	14.01	30.29	14.47	75.18	0.03	0.00	0.00	0.22	0.02	0.00	86.54	56.88	7.19	27.00	5785.00
	T_{168hrs}	0.00	8.71	11.39	16.22	41.69	16.37	122.49	0.00	0.00	0.00	0.27	0.04	0.00	101.66	75.40	6.98	26.00	10085.00
	T_{264hrs}	0.05	13.36	17.33	16.65	55.58	20.13	143.69	0.03	0.05	0.00	0.29	0.04	0.00	137.12	98.69	6.78	27.00	15485.00
Outcrop NaCl @ 25C	Input	0.00	1.58	10192.82	0.00	0.00	0.00	0.00	0.00	0.00	0.00	0.00	0.00	13606.35	0.00	6.40	5.08	21.30	1.00
	$T_{0'}$	0.00	1.38	10968.18	6.01	0.00	0.00	57.68	0.00	0.00	0.00	0.00	0.05	15176.18	62.76	57.70	9.07	23.00	2.00
	T_0	0.00	1.29	12927.83	11.21	0.00	0.00	67.19	0.00	0.00	0.00	0.00	0.15	18383.39	74.19	36.56	8.87	25.00	20.00
	T_{4hrs}	0.00	1.27	16352.18	13.91	0.00	0.00	73.57	0.00	0.00	0.00	0.00	0.23	17794.72	75.54	46.84	8.36	27.00	260.00
	T_{8hrs}	0.00	1.25	11434.24	14.42	0.00	0.00	77.28	0.00	0.00	0.00	0.00	0.25	15743.26	79.33	39.57	7.12	26.00	500.00
	T_{24hrs}	0.00	1.62	10876.82	15.00	0.88	14.36	89.00	0.00	0.00	0.00	0.00	0.25	16934.29	85.63	62.41	7.97	27.00	1460.00
	T_{48hrs}	0.00	2.09	10951.54	16.75	3.59	17.44	103.92	0.00	0.00	0.00	0.00	0.27	14877.45	109.15	61.61	7.79	27.00	2900.00
	T_{96hrs}	0.00	2.66	11612.78	16.02	4.49	19.18	117.56	0.00	0.00	0.00	0.00	0.25	17323.42	110.17	85.49	7.44	26.50	5800.00
	T_{168hrs}	0.00	3.00	10266.56	17.53	5.70	22.13	143.69	0.00	0.00	0.00	0.00	0.24	14055.02	130.79	90.26	7.23	26.00	10100.00
	T_{264hrs}	0.00	3.90	11559.05	17.85	8.57	24.20	156.31	0.00	0.00	0.00	0.00	0.23	17750.82	147.47	116.54	7.15	28.00	15500.00
Outcrop Fresh water @ 95C	Input	0.00	0.03	0.00	0.70	0.00	0.00	0.86	0.02	0.00	0.00	0.00	0.00	0.00	0.00	5.16	5.96	24.00	1.00
	$T_{0'}$	0.00	0.00	0.00	11.18	0.86	2.10	106.74	0.01	0.00	0.00	0.27	0.00	0.00	122.91	12.25	8.40	26.00	2.00
	T_0	0.00	0.19	5.31	17.66	4.77	7.99	141.65	0.02	0.00	0.00	0.44	0.06	0.00	167.46	16.26	7.36	101.50	180.00
	T_{4hrs}	0.00	0.36	5.77	18.27	7.10	9.41	155.93	0.07	0.04	0.00	0.48	0.07	0.00	186.92	20.09	7.28	96.00	420.00
	T_{8hrs}	0.00	0.63	6.26	18.41	10.81	11.42	160.86	0.07	0.00	0.00	0.49	0.07	0.00	194.60	36.65	7.26	94.50	660.00
	T_{24hrs}	0.00	1.83	7.81	18.00	19.11	10.35	175.04	0.12	0.00	0.00	0.51	0.06	72.47	242.15	0.00	3.00	96.00	1620.00
	T_{48hrs}	0.00	4.94	10.31	19.28	49.32	16.01	192.75	0.03	0.00	0.00	0.57	0.06	0.00	270.45	28.76	7.07	96.00	3060.00
	T_{96hrs}	0.00	9.12	15.96	17.87	72.61	18.50	201.33	0.10	0.00	0.00	0.59	0.06	80.75	298.14	0.00	2.95	95.00	5960.00
	T_{168hrs}	0.00	11.85	18.72	17.41	79.72	18.17	224.80	0.05	0.00	0.00	0.60	0.06	0.00	314.93	44.54	6.40	95.00	10260.00
	$T_{262.5hrs}$	0.00	21.08	29.03	17.94	111.92	26.55	254.34	0.07	0.06	0.00	0.73	0.06	0.00	296.46	41.16	6.89	95.00	15930.00
Outcrop NaCl @ 95C	Input	0.00	0.00	12133.31	0.00	0.00	0.00	0.00	0.00	0.00	0.00	0.00	0.00	10838.98	0.00	4.46	5.39	19.50	1.00
	$T_{0'}$	0.00	0.00	11100.59	8.18	0.00	0.00	58.16	0.00	0.00	0.00	0.00	0.03	18593.72	104.32	24.77	8.99	21.00	2.00
	T_0	0.00	0.00	10968.83	20.18	0.13	0.00	101.29	0.00	0.00	0.00	0.40	0.30	11780.78	138.36	41.67	7.39	95.00	140.00
	T_{4hrs}	0.00	0.00	11243.35	20.06	6.99	17.44	114.52	0.00	0.00	0.00	0.47	0.28	11781.94	145.92	48.87	7.28	95.50	380.00
	T_{8hrs}	0.00	0.00	11324.25	21.58	13.84	19.66	128.79	0.00	0.00	0.00	0.49	0.30	11723.08	149.88	51.37	7.31	94.00	620.00
	T_{24hrs}	0.00	4.50	11008.36	20.24	38.84	20.68	143.32	0.00	0.00	0.00	0.57	0.28	12294.99	163.94	74.85	7.23	95.00	1580.00
	T_{48hrs}	0.00	13.01	11317.80	20.05	65.16	26.44	148.30	0.00	0.00	0.00	0.66	0.30	13259.69	164.52	0.00	2.24	96.00	3020.00
	T_{96hrs}	0.00	19.56	11362.13	20.22	86.86	36.43	161.97	0.00	0.00	0.00	0.77	0.36	12645.43	167.42	68.20	6.60	96.00	5900.00
	T_{168hrs}	0.00	28.52	11512.87	17.47	99.40	45.09	170.05	0.00	0.00	0.00	0.88	0.40	12679.29	174.04	65.29	7.13	95.00	10220.00
Outcrop Freshwater @ 140C	Input	0.00	0.00	0.00	0.00	0.00	0.00	0.00	0.00	0.00	0.00	0.00	0.01	0.00	0.00	4.08	4.60	21.60	1.00
	$T_{0'}$	0.00	0.00	0.00	6.07	0.02	2.47	36.99	0.00	0.00	0.00	0.13	0.10	0.00	32.81	12.42	7.34	20.00	2.00
	T_0	0.00	0.13	0.00	12.36	7.01	7.48	71.89	0.01	0.00	0.00	0.25	1.01	0.00	67.94	34.68	7.09	134.60	110.00
	T_{4hrs}	0.00	0.36	0.00	10.46	19.83	9.34	78.78	0.01	0.00	0.00	0.27	1.34	0.00	71.72	49.03	6.81	139.29	350.00
	T_{8hrs}	0.00	1.11	0.00	9.53	27.86	11.34	79.66	0.00	0.00	0.00	0.29	1.51	0.00	77.43	42.18	7.38	141.85	590.00
	T_{24hrs}	0.00	2.85	0.00	5.45	59.17	13.61	102.50	0.00	0.00	0.00	0.32	1.60	0.00	69.48	28.40	7.14	137.37	1550.00
	T_{48hrs}	0.00	5.00	8.00	3.65	62.32	16.33	82.87	0.02	0.00	0.00	0.35	1.75	0.00	79.56	33.18	7.35	136.31	2990.00
	T_{96hrs}	0.00	8.90	12.08	2.92	79.92	19.38	82.07	0.00	0.00	0.00	0.40	1.87	0.00	73.56	33.34	7.41	137.80	5890.00
	Input	0.00	0.00	9900.71	0.00	0.00	0.00	0.00	0.07	0.00	0.00	0.00	0.02	14651.66	0.00	5.09	4.59	20.50	1.00

Outcrop NaCl @ 140C	$T_{0'}$	0.00	0.00	9863.41	3.98	0.00	0.00	45.87	0.00	0.00	0.00	0.87	0.13	14885.47	62.36	34.60	9.19	20.00	2.00
	T_0	0.00	0.00	11365.19	13.79	6.53	0.00	98.59	0.00	0.00	0.00	1.07	1.23	16035.80	102.22	48.27	7.12	137.16	140.00
	T_{4hrs}	0.00	1.56	10084.56	10.57	23.95	15.40	103.31	0.21	0.00	0.00	1.13	1.58	14147.48	104.28	49.89	7.53	160.62	380.00
	T_{8hrs}	4.22	2.41	9523.54	12.97	37.06	18.20	127.76	0.00	0.00	0.00	1.21	1.98	14437.84	121.20	54.39	7.55	141.00	620.00
	T_{24hrs}	0.00	6.09	9560.57	8.06	68.08	19.55	126.01	0.00	0.00	0.00	1.26	1.91	13746.54	113.18	57.87	7.38	137.37	1580.00
	T_{48hrs}	0.00	16.20	9114.00	6.39	109.37	21.40	152.82	0.22	0.00	0.00	1.36	1.89	13560.39	107.25	65.72	7.47	140.57	3020.00
	T_{96hrs}	0.00	20.64	10116.73	6.20	86.99	30.07	121.41	0.07	0.00	0.00	1.56	2.05	14876.54	110.35	75.00	7.35	137.59	5900.00
Core 1 Freshwater Exp. I	Input	0.00	0.00	0.00	0.00	0.00	0.00	0.00	0.00	0.00	0.00	0.00	0.00	0.00	0.00	0.00	4.72	22.20	1.00
	$T_{0'}$	0.00	0.06	13.03	0.72	0.96	2.79	6.82	0.00	0.00	0.00	0.12	0.00	13.32	1.51	10.20	9.13	23.50	2.00
	$T_{0.5hrs'}$	0.00	0.21	28.86	1.49	2.66	7.08	13.13	0.01	0.00	0.00	0.28	0.02	30.43	7.81	19.67	8.71	57.00	30.00
	$T_{1hr'}$	0.00	0.32	23.07	1.46	4.22	9.70	11.25	0.01	0.00	0.00	0.35	0.04	23.27	11.93	16.84	8.36	76.00	60.00
	T_0	0.00	0.47	23.71	3.23	5.07	12.81	18.88	0.01	0.00	0.00	0.65	0.13	39.08	20.57	28.28	6.89	94.50	160.00
	T_{1hrs}	0.00	0.53	25.65	4.09	5.26	13.08	23.31	0.03	0.00	0.00	0.78	0.18	95.23	24.63	34.90	2.98	95.00	220.00
	T_{2hrs}	0.00	0.59	23.71	4.60	5.65	13.28	22.81	0.01	0.00	0.00	0.82	0.19	47.95	24.90	34.16	6.77	94.50	280.00
	T_{4hrs}	0.00	0.72	24.19	6.11	6.25	13.27	28.14	0.01	0.00	0.00	0.95	0.22	71.75	30.09	42.14	6.27	95.00	400.00
	T_{8hrs}	0.00	0.98	23.43	7.07	7.61	13.83	28.06	0.01	0.00	0.00	0.95	0.20	57.96	35.48	42.02	5.75	94.00	640.00
	T_{16hrs}	0.00	1.68	25.70	8.46	10.78	18.95	32.73	0.02	0.00	0.00	0.98	0.17	60.03	41.36	49.00	6.48	97.00	1105.00
	T_{24hrs}	0.00	2.37	25.34	10.38	13.98	17.18	38.05	0.01	0.00	0.00	1.05	0.14	40.97	54.01	56.98	6.96	95.50	1600.00
	T_{48hrs}	0.11	3.70	27.13	14.51	19.93	15.78	54.50	0.01	0.00	0.00	1.14	0.11	39.45	69.66	81.60	7.01	95.00	3040.00
Core 1 NaCl Exp. I	Input	0.00	0.22	10883.77	0.00	0.00	0.00	0.00	0.00	0.00	0.00	0	0	19053.29	0.00	0.00	5.61	21.90	1.00
	$T_{0'}$	0.00	0.67	10531.89	6.08	9.77	0.00	29.81	0.00	0.00	0.00	0.85	0.06	18838.38	0.00	37.36	9.29	24.00	2.00
	$T_{0.5hrs'}$	0.00	0.51	10627.14	7.24	10.69	12.87	34.32	0.00	0.00	0.00	1.53	0.90	18916.06	0.00	43.01	8.71	53.50	30.00
	$T_{1hr'}$	0.00	0.59	10355.68	8.52	11.60	17.42	43.76	0.00	0.00	0.00	1.88	1.63	18705.07	0.00	54.84	8.22	75.00	60.00
	T_0	0.00	0.74	10242.33	11.62	12.56	18.09	48.39	0.00	0.00	0.00	2.23	2.99	18666.45	0.00	60.64	3.43	94.50	165.00
	T_{1hrs}	0.00	0.80	10500.50	12.57	12.94	18.87	50.11	0.00	0.00	0.00	2.34	3.37	19086.19	0.00	62.80	7.30	94.50	225.00
	T_{2hrs}	0.00	0.93	10762.82	13.36	13.44	18.50	51.86	0.00	0.00	0.00	2.37	3.53	18977.68	0.00	65.00	7.45	95.50	285.00
	T_{4hrs}	0.00	1.29	10499.85	14.72	14.23	20.07	54.81	0.00	0.00	0.00	2.49	3.65	18525.53	0.00	68.69	7.59	95.00	405.00
	T_{8hrs}	0.00	1.84	10633.07	16.34	16.78	21.69	59.47	0.00	0.00	0.00	2.53	3.45	18766.61	0.00	74.53	7.28	95.00	645.00
	T_{16hrs}	0.00	2.77	9188.67	16.56	20.47	21.24	58.67	0.00	0.00	0.00	2.33	2.87	18421.40	0.00	73.53	6.02	93.00	1105.00
	T_{24hrs}	0.00	4.00	10011.58	20.09	26.04	21.45	70.06	0.00	0.00	0.00	2.59	2.81	18652.86	14.59	87.80	7.24	92.00	1605.00
	T_{48hrs}	0.00	5.97	10273.68	22.61	32.99	21.37	82.19	0.00	0.00	0.00	2.67	2.27	19245.90	23.99	103.00	7.12	95.00	3045.00
Core 1 Freshwater Exp. II	Input	0.00	0.00	0.00	0.00	0.00	0.00	0.00	0.00	0.00	0.00	0.00	0.00	0.00	0.00	0.00	4.64	22.60	1.00
	$T_{0'}$	0.00	0.06	13.92	0.73	0.97	3.12	7.02	0.00	0.00	0.00	0.12	0.00	1.84	1.84	8.80	8.84	20.00	2.00
	T_0	0.00	0.44	23.18	2.83	4.89	12.90	17.96	0.01	0.00	0.00	0.64	0.12	17.36	17.36	22.51	7.67	94.50	135.00
	T_{4hrs}	0.00	0.68	23.62	4.35	6.48	13.06	22.92	0.01	0.00	0.00	0.85	0.21	24.27	24.27	28.72	6.11	95.00	375.00
	T_{8hrs}	0.00	1.28	23.79	5.98	8.71	14.95	33.73	0.01	0.00	0.00	0.99	0.25	28.54	28.54	42.27	6.67	93.50	615.00
	T_{24hrs}	0.00	3.13	25.18	8.52	18.58	14.42	34.49	0.01	0.00	0.00	1.01	0.17	42.15	42.15	43.23	6.70	95.50	1575.00
	T_{48hrs}	0.00	5.09	26.52	15.15	22.26	14.61	55.35	0.02	0.00	0.00	1.09	0.11	79.50	79.50	69.37	6.92	93.50	3015.00
	T_{96hrs}	0.00	7.13	28.38	23.21	22.81	15.18	87.43	0.02	0.00	0.00	1.19	0.08	127.60	127.60	109.57	3.24	95.00	5915.00
	T_{168hrs}	0.00	9.40	30.41	26.08	30.52	15.73	107.32	0.01	0.00	0.00	1.23	0.07	155.36	155.36	134.51	6.57	95.00	10215.00
Core 1 NaCl Exp. II	Input	0.00	0.22	10418.25	0.00	0.00	0.00	0.00	0.00	0.00	0.00	0.00	0.00	0.00	0.00	0.00	5.61	21.70	1.00
	$T_{0'}$	0.00	1.36	10664.93	6.47	10.01	0.00	33.70	0.00	0.00	0.00	1.00	0.18	0.00	0.00	42.23	9.15	25.00	2.00
	T_0	0.00	0.78	10613.75	11.21	14.03	17.59	64.35	0.00	0.00	0.00	2.24	3.34	0.00	0.00	80.65	6.75	93.00	140.00
	T_{4hrs}	0.00	0.93	11039.13	14.57	13.28	18.38	55.58	0.00	0.00	0.00	2.46	3.70	0.00	0.00	69.66	6.56	94.50	380.00
	T_{8hrs}	0.00	1.20	10631.11	15.92	14.46	19.55	58.10	0.00	0.00	0.00	2.57	3.58	0.00	0.00	72.82	7.16	93.50	620.00
	T_{24hrs}	0.00	1.85	10286.58	27.06	16.08	21.68	81.84	0.03	0.00	0.00	2.61	1.81	29.69	29.69	102.57	7.16	94.00	1580.00
	T_{48hrs}	0.00	2.76	10605.32	28.60	21.93	21.13	87.99	0.00	0.00	0.00	2.79	1.45	35.95	35.95	110.28	7.14	94.00	3020.00
	T_{96hrs}	0.00	4.06	10436.98	28.57	28.28	21.62	92.07	0.00	0.00	0.00	2.90	1.33	39.36	39.36	115.39	6.30	94.00	5920.00
	T_{168hrs}	0.00	5.94	11525.51	30.54	34.05	21.99	103.63	0.00	0.00	0.00	3.00	1.14	62.75	62.75	129.87	7.12	95.00	10220.00
Core 2 Freshwater Exp. I	Input	0.00	0.00	0.00	0.00	0.00	0.00	0.00	0.00	0.00	0.00	0.00	0.00	0.00	0.00	0.00	6.67	19.80	1.00
	$T_{0'}$	0.00	0.00	0.00	0.29	0.00	0.00	6.47	0.00	0.00	0.00	0.00	0.01	0.00	1.91	25.59	9.76	20.00	2.00
	$T_{0.5hrs'}$	0.00	0.10	2.58	1.52	1.78	2.85	10.72	0.02	0.01	0.00	0.21	0.08	0.00	8.08	17.80	8.89	55.76	30.00
	$T_{1hr'}$	0.00	0.13	2.05	2.34	4.34	6.09	16.91	0.01	0.03	0.00	0.32	0.17	0.00	15.91	25.29	7.40	94.92	60.00
	T_0	0.00	0.16	2.20	3.28	6.89	7.27	26.04	0.02	0.00	0.00	0.42	0.21	0.00	27.61	32.32	7.23	140.15	110.00

	T_{1hrs}	0.00	0.20	2.37	3.90	10.55	7.74	30.93	0.02	0.00	0.00	0.51	0.20	0.00	34.68	36.63	7.07	143.13	170.00
	T_{2hrs}	0.00	0.28	2.88	4.26	14.19	8.08	34.04	0.02	0.00	0.00	0.55	0.20	0.00	37.25	36.77	6.98	150.81	230.00
	T_{4hrs}	0.00	0.78	2.62	4.29	20.47	7.63	33.85	0.12	0.00	0.00	0.61	0.18	0.00	38.05	39.46	6.97	146.55	350.00
	T_{8hrs}	0.00	1.59	3.49	4.35	30.92	8.20	33.67	0.01	0.00	0.00	0.65	0.20	0.00	41.47	39.71	7.16	147.40	590.00
	T_{16hrs}	0.00	3.29	4.60	3.80	45.97	9.66	34.12	0.03	0.00	0.00	0.70	0.17	0.00	41.65	47.68	7.18	141.00	1055.00
	T_{24hrs}	0.00	5.59	8.31	4.01	58.60	10.41	36.91	0.03	0.00	0.00	0.86	0.17	34.15	41.01	50.21	7.33	146.12	1550.00
	T_{48hrs}	0.00	9.77	12.24	4.11	78.57	12.81	31.49	0.02	0.00	0.00	0.90	0.19	0.00	42.60	52.90	7.41	137.16	2990.00
	Input	0.00	1.36	10093.91	0.00	0.00	0.00	0.00	0.00	0.00	0.00	0.00	0.00	13794.66	0.00	2.57	6.16	18.60	1.00
	$T_{0'}$	0.00	1.31	9710.56	1.20	0.00	0.00	27.34	0.00	0.00	0.00	0.00	0.29	13783.86	0.00	49.87	9.45	20.00	2.00
	$T_{0.5hrs'}$	0.00	0.00	9942.82	2.56	0.00	0.00	20.88	0.00	0.00	0.00	0.00	0.80	14322.47	0.00	53.24	8.89	49.91	30.00
	$T_{1hr'}$	0.00	0.00	9123.89	4.20	2.43	0.00	29.56	0.00	0.00	0.00	0.00	1.16	14294.03	0.00	50.26	8.22	81.49	60.00
	T_0	0.00	1.32	10347.16	6.15	5.64	0.00	41.41	0.00	0.00	0.00	0.00	1.64	14425.90	28.85	58.02	7.62	138.65	125.00
Core 2 NaCl	T_{1hrs}	0.00	1.68	9841.49	8.79	13.35	15.37	60.47	0.00	0.00	0.00	0.75	2.22	14961.41	47.64	60.85	7.47	141.21	185.00
Exp. I	T_{2hrs}	0.00	2.00	9886.24	9.94	19.17	14.06	64.70	0.00	0.00	0.00	0.89	2.26	14357.04	56.83	61.41	7.58	139.72	245.00
	T_{4hrs}	0.00	2.50	9801.16	8.96	26.51	12.61	59.62	0.00	0.00	0.00	0.89	2.01	14539.22	55.74	64.51	7.44	142.49	365.00
	T_{8hrs}	0.00	4.27	9538.26	8.05	45.82	13.11	62.18	0.00	0.00	0.00	0.98	1.94	14034.84	51.61	66.77	7.38	138.87	605.00
	T_{16hrs}	0.00	14.03	9337.15	8.39	88.84	17.45	78.50	0.00	0.00	0.00	1.42	2.21	14181.43	55.60	70.90	7.39	138.87	1065.00
	T_{24hrs}	0.00	14.67	9496.04	7.48	80.09	16.50	63.79	0.00	0.00	0.00	1.37	1.79	14717.02	54.88	80.10	7.20	135.88	1565.00
	T_{48hrs}	0.00	27.48	9814.29	8.81	110.95	23.26	82.92	0.00	0.00	0.00	2.38	2.36	17586.78	81.66	87.70	7.20	139.08	3005.00
	Input	0.00	0.00	0.00	0.00	0.00	0.00	0.00	0.00	0.00	0.00	0.00	0.00	0.00	0.00	4.47	4.63	19.50	1.00
	$T_{0'}$	0.00	0.00	0.00	0.31	0.00	0.00	6.46	0.01	0.00	0.00	0.00	0.01	0.00	2.18	27.09	8.83	18.80	2.00
	T_0	0.00	0.20	5.96	4.03	8.93	5.47	29.71	0.01	0.00	0.00	0.50	0.22	0.00	35.74	33.24	7.47	136.31	130.00
Core 2	T_{4hrs}	0.00	0.42	2.74	4.75	16.66	8.33	33.42	0.03	0.00	0.00	0.58	0.19	0.00	39.15	39.22	7.43	135.03	370.00
Freshwater	T_{8hrs}	0.00	1.09	2.65	5.01	22.96	6.70	32.41	0.06	0.00	0.00	0.66	0.18	0.00	40.90	35.37	7.11	136.73	610.00
Exp. II	T_{24hrs}	0.00	3.82	6.88	4.51	48.47	10.27	32.17	0.09	0.01	0.00	0.80	0.18	0.00	40.11	45.11	7.22	136.09	1570.00
	T_{48hrs}	0.00	11.89	13.55	3.11	92.09	12.28	31.01	0.05	0.00	0.00	0.83	0.20	0.00	44.15	51.25	7.20	149.53	3010.00
	T_{96hrs}	0.03	17.43	18.68	3.15	103.65	15.11	29.39	0.16	0.00	0.00	0.86	0.18	0.00	45.74	52.15	7.21	136.95	5890.00
	Input	0.00	0.00	9940.90	0.00	0.00	0.00	0.00	0.00	0.00	0.00	0.00	0.00	14142.79	0.00	4.28	4.98	20.70	1.00
	$T_{0'}$	0.00	0.00	9950.86	0.00	0.00	0.00	21.41	0.00	0.00	0.00	0.00	0.06	13842.07	0.00	66.10	9.41	18.80	2.00
	T_0	0.00	1.05	10039.11	6.38	4.51	0.00	55.68	0.00	0.00	0.00	0.69	1.90	14762.86	48.01	59.05	7.65	136.52	140.00
Core 2 NaCl	T_{4hrs}	0.00	2.19	10039.10	7.08	23.00	0.00	62.56	2.33	0.00	0.00	0.81	1.94	14932.54	61.60	65.85	7.41	139.93	380.00
Exp. II	T_{8hrs}	0.00	3.61	9870.56	6.88	39.07	0.00	64.45	0.00	0.00	0.00	0.96	1.90	14087.03	57.19	63.42	7.41	136.09	620.00
	T_{24hrs}	0.00	15.94	10217.98	6.26	85.55	14.60	74.94	0.00	0.00	0.00	1.59	2.04	14325.01	65.00	85.06	7.22	134.17	1580.00
	T_{48hrs}	0.00	21.81	10393.87	7.41	95.02	18.37	77.61	0.00	0.00	0.00	2.31	2.15	14316.69	70.87	91.66	7.24	140.36	3020.00
	T_{96hrs}	0.00	32.78	10724.43	7.19	93.47	21.87	84.39	0.00	0.00	0.00	2.70	2.31	15707.68	73.31	99.54	7.05	136.31	5900.00

Appendix B

Supplemental Results

B-1 Aqueous concentrations from experiments, BDL = below detection limit. The complete aqueous data with errors is reported in:

https://docs.google.com/spreadsheets/d/1ou4hHdse_TjVwPFMsT-p5XGK7CKkNvbYbC_l3o-u2rg/edit?usp=sharing

Outcrop Experimental Data											
H2O Type II 25°C											
Sample ID		Input	T0'	T0	T4hrs	T8hrs	T24hrs	T48hrs	T96hrs	T168hrs	T264hrs
Time (min)		0	1	5	245	485	1445	2885	5785	10085	15485
Li	µmol/L	BDL	BDL	BDL	BDL	BDL	BDL	BDL	BDL	BDL	6.54
B	µmol/L	BDL	BDL	BDL	11.9	19.5	96.0	183.3	502.8	805.4	1235.7
Na	mmol/L	BDL	BDL	BDL	0.18	0.08	0.12	0.15	0.36	0.50	0.75
Mg	mmol/L	BDL	0.27	0.34	0.51	0.49	0.52	0.57	0.58	0.67	0.69
Al	µmol/L	BDL	0.63	1.33	1.72	0.88	0.48	0.29	0.67	0.69	3.57
Si	mmol/L	BDL	BDL	0.01	0.08	0.12	0.28	0.49	1.08	1.48	1.98
K	mmol/L	BDL	0.06	0.07	0.15	0.17	0.22	0.29	0.37	0.42	0.51
P	µmol/L	BDL	BDL	BDL	BDL	BDL	BDL	BDL	2.45	0.28	0.31
S	mmol/L	BDL	1.38	1.54	1.75	1.95	2.01	2.56	2.70	3.17	4.28
Cl	mmol/L	BDL	BDL	BDL	0.30	BDL	BDL	BDL	BDL	BDL	BDL
Ca	mmol/L	BDL	1.03	1.13	1.29	1.34	1.53	1.63	1.88	3.06	3.59
Ti	µmol/L	BDL	BDL	BDL	BDL	BDL	BDL	BDL	BDL	BDL	BDL
Cr	µmol/L	BDL	BDL	BDL	BDL	BDL	BDL	BDL	BDL	BDL	BDL
Mn	µmol/L	BDL	BDL	BDL	BDL	BDL	BDL	BDL	0.46	BDL	0.57
Fe	µmol/L	BDL	BDL	BDL	BDL	BDL	BDL	BDL	BDL	BDL	0.95
Co	µmol/L	BDL	BDL	BDL	BDL	BDL	BDL	BDL	BDL	0.03	0.06
Ni	µmol/L	BDL	0.02	0.02	0.06	0.08	0.12	0.14	0.21	0.56	0.86
Cu	µmol/L	BDL	BDL	BDL	BDL	BDL	BDL	BDL	BDL	BDL	BDL
Zn	µmol/L	BDL	BDL	BDL	BDL	BDL	BDL	BDL	0.14	BDL	0.28
As	µmol/L	BDL	BDL	0.01	0.01	0.03	0.05	0.06	0.05	0.04	0.07
Br	µmol/L	BDL	BDL	BDL	BDL	BDL	BDL	BDL	BDL	BDL	BDL
Sr	µmol/L	BDL	0.61	0.81	1.56	1.68	1.94	2.21	2.47	3.08	3.36
Mo	µmol/L	BDL	1.20	2.38	8.98	10.76	13.15	14.51	15.52	16.18	16.44
Cd	µmol/L	BDL	BDL	BDL	BDL	BDL	BDL	BDL	BDL	BDL	BDL
Ba	µmol/L	BDL	0.02	0.04	0.10	0.11	0.14	0.15	0.18	0.27	0.30
Pb	µmol/L	BDL	BDL	BDL	BDL	BDL	BDL	BDL	BDL	BDL	0.01

U	µmol/L	BDL	0.01	0.01	0.01	0.02	0.03	0.04	0.07	0.14	0.17
DIC	mmol/L	0.05	0.31	0.34	0.41	0.53	0.74	0.72	0.95	1.26	1.64
NaCl Type II 25°C											
Sample ID		Input	T0'	T0	T4hrs	T8hrs	T24hrs	T48hrs	T96hrs	T168hrs	T264hrs
Time (min)		0	1	20	260	500	1460	2900	5800	10100	15500
Li	µmol/L	BDL	BDL	BDL	BDL	BDL	BDL	BDL	BDL	BDL	BDL
B	µmol/L	145.9	127.4	118.9	117.0	115.5	149.8	193.4	246.1	277.3	361.0
Na	mmol/L	443.4	477.1	562.3	711.3	497.4	473.1	476.4	505.1	446.6	502.8
Mg	mmol/L	BDL	0.25	0.46	0.57	0.59	0.62	0.69	0.66	0.72	0.73
Al	µmol/L	BDL	BDL	BDL	BDL	BDL	BDL	BDL	BDL	BDL	BDL
Si	mmol/L	BDL	BDL	BDL	BDL	BDL	0.03	0.13	0.16	0.20	0.31
K	mmol/L	BDL	BDL	BDL	BDL	BDL	0.37	0.45	0.49	0.57	0.62
P	µmol/L	BDL	BDL	BDL	BDL	BDL	BDL	BDL	BDL	BDL	BDL
S	mmol/L	BDL	1.96	2.31	2.36	2.47	2.67	3.40	3.44	4.08	4.60
Cl	mmol/L	384	428	519	502	444	478	420	489	396	501
Ca	mmol/L	BDL	1.44	1.68	1.84	1.93	2.22	2.59	2.93	3.59	3.90
Ti	µmol/L	BDL	BDL	BDL	BDL	BDL	BDL	BDL	BDL	BDL	BDL
Cr	µmol/L	BDL	BDL	BDL	BDL	BDL	BDL	BDL	BDL	BDL	BDL
Mn	µmol/L	BDL	BDL	BDL	BDL	BDL	BDL	BDL	BDL	BDL	BDL
Fe	µmol/L	BDL	BDL	BDL	BDL	BDL	BDL	BDL	BDL	BDL	BDL
Co	µmol/L	BDL	BDL	BDL	BDL	BDL	BDL	BDL	BDL	BDL	BDL
Ni	µmol/L	BDL	BDL	BDL	BDL	BDL	BDL	BDL	BDL	0.20	0.34
Cu	µmol/L	BDL	BDL	BDL	BDL	BDL	BDL	BDL	BDL	BDL	BDL
Zn	µmol/L	BDL	BDL	BDL	BDL	BDL	BDL	BDL	BDL	BDL	BDL
As	µmol/L	BDL	BDL	BDL	BDL	BDL	BDL	BDL	BDL	BDL	BDL
Br	µmol/L	BDL	BDL	BDL	BDL	BDL	BDL	BDL	BDL	BDL	BDL
Sr	µmol/L	BDL	BDL	BDL	BDL	BDL	BDL	BDL	BDL	BDL	BDL
Mo	µmol/L	BDL	1.33	4.50	11.32	12.73	13.94	15.34	15.53	16.82	16.26
Cd	µmol/L	BDL	BDL	BDL	BDL	BDL	BDL	BDL	BDL	BDL	BDL
Ba	µmol/L	BDL	0.36	1.06	1.64	1.79	1.82	1.97	1.83	1.74	1.69
Pb	µmol/L	BDL	BDL	BDL	BDL	BDL	BDL	BDL	BDL	BDL	BDL
U	µmol/L	BDL	0.07	0.07	0.08	0.09	0.11	0.14	0.17	0.19	0.21
DIC	mmol/L	0.11	0.96	0.61	0.78	0.66	1.04	1.03	1.42	1.50	1.94
H2O Type II 95°C											
Sample ID		Input	T0'	T0	T4hrs	T8hrs	T24hrs	T48hrs	T96hrs	T168hrs	T262.5hr
Time (min)		0	1	180	420	660	1620	3060	5960	10260	15660
Li	µmol/L	BDL	BDL	BDL	BDL	BDL	BDL	BDL	BDL	BDL	BDL
B	µmol/L	2.6	BDL	17.6	33.0	57.8	169.1	457.1	843.6	1096.3	1950.2
Na	mmol/L	BDL	BDL	0.2	0.3	0.3	0.3	0.4	0.7	0.8	1.3
Mg	mmol/L	0.03	0.46	0.73	0.75	0.76	0.74	0.79	0.74	0.72	0.74
Al	µmol/L	BDL	0.41	2.35	1.83	1.93	1.33	1.49	1.63	1.09	1.61
Si	mmol/L	BDL	0.03	0.17	0.25	0.38	0.68	1.76	2.59	2.84	3.98
K	mmol/L	BDL	0.05	0.20	0.24	0.29	0.26	0.41	0.47	0.46	0.68
P	µmol/L	BDL	BDL	0.24	0.81	0.47	0.39	0.32	0.46	0.58	1.62
S	mmol/L	BDL	3.83	5.22	5.83	6.07	7.55	8.43	9.30	9.82	9.25

Cl	mmol/L	BDL	BDL	BDL	BDL	BDL	2.04	BDL	2.28	BDL	BDL
Ca	mmol/L	0.02	2.66	3.53	3.89	4.01	4.37	4.81	5.02	5.61	6.35
Ti	µmol/L	0.18	0.20	BDL	BDL	0.18	0.18	0.18	0.20	0.19	BDL
Cr	µmol/L	BDL	BDL	BDL	BDL	BDL	BDL	BDL	BDL	BDL	BDL
Mn	µmol/L	0.34	0.13	0.42	1.28	1.36	2.18	0.50	1.91	0.86	1.35
Fe	µmol/L	BDL	BDL	BDL	0.72	BDL	BDL	BDL	BDL	BDL	1.08
Co	µmol/L	BDL	BDL	BDL	BDL	BDL	BDL	BDL	BDL	BDL	BDL
Ni	µmol/L	BDL	BDL	BDL	BDL	BDL	BDL	BDL	BDL	BDL	BDL
Cu	µmol/L	BDL	BDL	0.17	0.25	0.33	0.53	0.45	0.72	0.79	1.13
Zn	µmol/L	BDL	BDL	BDL	BDL	BDL	1.31	0.16	0.24	BDL	2.00
As	µmol/L	0.04	0.01	0.02	0.05	0.04	0.06	0.14	0.27	0.40	0.49
Br	µmol/L	BDL	BDL	BDL	BDL	BDL	BDL	BDL	BDL	BDL	BDL
Sr	µmol/L	BDL	3.08	4.99	5.49	5.59	5.78	6.56	6.68	6.89	8.34
Mo	µmol/L	1.12	2.32	5.32	11.76	13.09	14.25	15.54	15.74	16.96	16.43
Cd	µmol/L	BDL	BDL	BDL	BDL	BDL	BDL	BDL	BDL	BDL	BDL
Ba	µmol/L	BDL	0.02	0.46	0.50	0.50	0.46	0.46	0.44	0.41	0.42
Pb	µmol/L	BDL	BDL	BDL	BDL	BDL	0.01	BDL	0.00	BDL	BDL
U	µmol/L	BDL	0.01	BDL	0.00	0.01	0.01	0.01	0.01	0.01	0.01
DIC	mmol/L	0.09	0.20	0.27	0.33	0.61	0.00	0.48	0.00	0.74	0.69

NaCl Type II 95°C										
Sample ID		Input	T0'	T0	T4hrs	T8hrs	T24hrs	T48hrs	T96hrs	T168hrs
Time (min)		0	1	140	380	620	1580	3020	5900	10220
Li	µmol/L	BDL	BDL	BDL	BDL	BDL	BDL	BDL	BDL	BDL
B	µmol/L	BDL	BDL	BDL	BDL	BDL	416.1	1203.4	1809.7	2637.7
Na	mmol/L	527.8	482.8	477.1	489.1	492.6	478.8	492.3	494.2	500.8
Mg	mmol/L	BDL	0.34	0.83	0.83	0.89	0.83	0.82	0.83	0.72
Al	µmol/L	BDL	42.15	4.09	BDL	BDL	BDL	BDL	BDL	BDL
Si	mmol/L	BDL	BDL	0.00	0.25	0.49	1.38	2.32	3.09	3.54
K	mmol/L	BDL	BDL	BDL	0.45	0.50	0.53	0.68	0.93	1.15
P	µmol/L	BDL	BDL	BDL	BDL	BDL	BDL	BDL	BDL	BDL
S	mmol/L	BDL	3.25	4.31	4.55	4.67	5.11	5.13	5.22	5.43
Cl	mmol/L	306	525	332	332	331	347	374	357	358
Ca	mmol/L	BDL	1.45	2.53	2.86	3.21	3.58	3.70	4.04	4.24
Ti	µmol/L	BDL	2.57	BDL	BDL	BDL	BDL	1.52	BDL	BDL
Cr	µmol/L	BDL	BDL	BDL	BDL	BDL	BDL	BDL	BDL	BDL
Mn	µmol/L	BDL	BDL	BDL	BDL	BDL	BDL	BDL	BDL	BDL
Fe	µmol/L	BDL	BDL	BDL	BDL	BDL	BDL	BDL	BDL	BDL
Co	µmol/L	BDL	BDL	BDL	BDL	BDL	BDL	BDL	BDL	BDL
Ni	µmol/L	BDL	BDL	BDL	BDL	BDL	BDL	BDL	BDL	BDL
Cu	µmol/L	BDL	BDL	BDL	BDL	BDL	BDL	BDL	BDL	BDL
Zn	µmol/L	BDL	BDL	BDL	BDL	BDL	BDL	BDL	BDL	BDL
As	µmol/L	BDL	BDL	0.35	0.43	0.51	0.59	0.83	0.92	1.11
Br	µmol/L	BDL	BDL	BDL	BDL	BDL	BDL	BDL	BDL	BDL
Sr	µmol/L	BDL	BDL	4.55	5.40	5.64	6.46	7.53	8.78	10.08
Mo	µmol/L	BDL	0.88	15.20	17.65	19.56	19.75	20.36	22.41	22.64

Cd	µmol/L	BDL	BDL	BDL	BDL	BDL	BDL	BDL	BDL	BDL
Ba	µmol/L	BDL	0.19	2.20	2.02	2.17	2.02	2.19	2.62	2.90
Pb	µmol/L	BDL	BDL	BDL	BDL	BDL	BDL	0.08	BDL	BDL
U	µmol/L	BDL	0.05	0.06	0.07	0.09	0.09	0.07	0.05	0.06
DIC	mmol/L	0.07	0.41	0.69	0.81	0.86	1.25	0.00	1.14	1.09
H2O Type II 140°C										
Sample ID		Input	T0'	T0	T4hrs	T8hrs	T24hrs	T48hrs	T96hrs	
Time (min)		0	1	110	350	590	1550	2990	5890	
Li	µmol/L	BDL	BDL	BDL	BDL	BDL	BDL	BDL	BDL	
B	µmol/L	BDL	BDL	12.2	33.4	102.7	263.9	462.6	823.5	
Na	mmol/L	BDL	BDL	BDL	BDL	BDL	BDL	0.35	0.53	
Mg	mmol/L	BDL	0.25	0.51	0.43	0.39	0.22	0.15	0.12	
Al	µmol/L	BDL	1.07	4.36	2.71	2.55	2.09	1.41	1.21	
Si	mmol/L	BDL	0.00	0.25	0.71	0.99	2.11	2.22	2.85	
K	mmol/L	BDL	0.06	0.19	0.24	0.29	0.35	0.42	0.50	
P	µmol/L	BDL	BDL	0.29	0.60	0.42	0.25	0.53	0.49	
S	mmol/L	BDL	1.02	2.12	2.24	2.41	2.17	2.48	2.29	
Cl	mmol/L	BDL	BDL	BDL	BDL	BDL	BDL	BDL	BDL	
Ca	mmol/L	BDL	0.92	1.79	1.97	1.99	2.56	2.07	2.05	
Ti	µmol/L	BDL	BDL	BDL	BDL	BDL	BDL	BDL	BDL	
Cr	µmol/L	BDL	BDL	BDL	BDL	BDL	BDL	BDL	BDL	
Mn	µmol/L	BDL	BDL	0.23	0.13	BDL	0.09	0.44	BDL	
Fe	µmol/L	BDL	BDL	BDL	BDL	BDL	BDL	BDL	BDL	
Co	µmol/L	BDL	0.02	0.02	0.02	0.02	0.02	0.02	0.02	
Ni	µmol/L	BDL	BDL	0.16	0.07	BDL	0.10	0.15	0.13	
Cu	µmol/L	BDL	BDL	BDL	BDL	BDL	BDL	BDL	BDL	
Zn	µmol/L	BDL	BDL	0.12	0.06	BDL	0.09	0.18	0.08	
As	µmol/L	0.02	0.03	0.04	0.10	0.13	0.30	0.43	0.55	
Br	µmol/L	BDL	BDL	BDL	BDL	BDL	BDL	BDL	BDL	
Sr	µmol/L	BDL	1.54	2.86	3.13	3.32	3.63	4.03	4.54	
Mo	µmol/L	0.11	1.09	10.55	13.99	15.75	16.65	18.20	19.54	
Cd	µmol/L	BDL	BDL	BDL	BDL	BDL	BDL	BDL	BDL	
Ba	µmol/L	0.01	0.03	0.23	0.20	0.20	0.15	0.13	0.19	
Pb	µmol/L	BDL	BDL	BDL	0.00	BDL	BDL	0.00	BDL	
U	µmol/L	0.01	0.01	0.02	0.02	0.02	0.02	0.01	0.01	
DIC	mmol/L	0.07	0.21	0.58	0.82	0.70	0.47	0.55	0.56	
NaCl Type II 140°C										
Sample ID		Input	T0'	T0	T4hrs	T8hrs	T24hrs	T48hrs	T96hrs	
Time (min)		0	1	140	380	620	1580	3020	5900	
Li	µmol/L	BDL	BDL	BDL	BDL	607.46	BDL	BDL	BDL	
B	µmol/L	BDL	BDL	BDL	144.0	223.2	563.7	1498.4	1908.9	
Na	mmol/L	430.7	429.0	494.4	438.7	414.3	415.9	396.4	440.1	
Mg	mmol/L	BDL	0.16	0.57	0.43	0.53	0.33	0.26	0.26	
Al	µmol/L	1.33	0.52	11.05	5.57	2.78	1.01	BDL	BDL	
Si	mmol/L	BDL	BDL	0.23	0.85	1.32	2.42	3.89	3.10	

K	mmol/L	BDL	BDL	BDL	0.39	0.47	0.50	0.55	0.77
P	µmol/L	BDL	BDL	8.61	BDL	BDL	BDL	BDL	BDL
S	mmol/L	BDL	1.94	3.19	3.25	3.78	3.53	3.34	3.44
Cl	mmol/L	413	420	452	399	407	388	383	420
Ca	mmol/L	BDL	1.14	2.46	2.58	3.19	3.14	3.81	3.03
Ti	µmol/L	BDL	BDL	BDL	BDL	BDL	BDL	BDL	BDL
Cr	µmol/L	BDL	BDL	BDL	BDL	BDL	BDL	BDL	BDL
Mn	µmol/L	1.23	BDL	BDL	3.81	BDL	BDL	3.93	1.23
Fe	µmol/L	BDL	BDL	BDL	BDL	BDL	BDL	BDL	BDL
Co	µmol/L	BDL	BDL	BDL	BDL	0.24	BDL	BDL	BDL
Ni	µmol/L	BDL	BDL	BDL	BDL	BDL	BDL	BDL	BDL
Cu	µmol/L	BDL	BDL	BDL	BDL	BDL	BDL	BDL	BDL
Zn	µmol/L	BDL	BDL	BDL	BDL	1.22	BDL	BDL	BDL
As	µmol/L	0.27	BDL	0.34	0.56	0.63	0.86	0.87	1.22
Br	µmol/L	BDL	BDL	BDL	BDL	BDL	BDL	BDL	BDL
Sr	µmol/L	BDL	9.88	12.19	12.88	13.78	14.38	15.47	17.80
Mo	µmol/L	0.23	1.34	12.85	16.50	20.59	19.94	19.67	21.39
Cd	µmol/L	BDL	BDL	BDL	BDL	BDL	BDL	BDL	BDL
Ba	µmol/L	0.07	0.50	1.65	1.70	1.99	1.92	1.93	2.29
Pb	µmol/L	BDL	BDL	BDL	BDL	BDL	BDL	BDL	BDL
U	µmol/L	BDL	0.10	0.11	0.10	0.11	0.10	0.10	0.10
DIC	mmol/L	0.08	0.58	0.80	0.83	0.91	0.96	1.10	1.25

Core 1 Experimental Data

H2O Type I 95°C

Sample ID		Input	T0'	T0.5hrs'	T1hrs'	T0	T1hrs	T2hrs	T4hrs	T8hrs	T16hrs	T24hrs	T48hrs
Time (min)		0	1	30	60	160	220	280	400	640	1105	1600	3040
Li	µmol/L	BDL	BDL	BDL	BDL	BDL	BDL	BDL	BDL	BDL	BDL	BDL	16.23
B	µmol/L	BDL	5.5	19.6	29.8	43.5	48.9	54.8	66.9	90.7	155.5	218.9	342.2
Na	mmol/L	BDL	0.6	1.3	1.0	1.0	1.1	1.0	1.1	1.0	1.1	1.1	1.2
Mg	mmol/L	BDL	0.03	0.06	0.06	0.13	0.17	0.19	0.25	0.29	0.35	0.43	0.60
Al	µmol/L	BDL	3.15	14.83	30.90	9.48	6.39	4.11	2.63	2.31	1.70	1.09	0.76
Si	mmol/L	BDL	0.03	0.09	0.15	0.18	0.19	0.20	0.22	0.27	0.38	0.50	0.71
K	mmol/L	BDL	0.07	0.18	0.25	0.33	0.33	0.34	0.34	0.35	0.48	0.44	0.40
P	µmol/L	0.16	BDL	0.18	0.41	0.40	0.46	0.43	0.32	0.31	1.13	0.35	0.68
S	mmol/L	BDL	0.05	0.24	0.37	0.64	0.77	0.78	0.94	1.11	1.29	1.68	2.17
Cl	mmol/L	BDL	0.38	0.86	0.66	1.10	2.69	1.35	2.02	1.64	1.69	1.16	1.11
Ca	mmol/L	BDL	0.17	0.33	0.28	0.47	0.58	0.57	0.70	0.70	0.82	0.95	1.36
Ti	µmol/L	0.17	0.17	0.21	0.27	0.36	0.32	0.22	0.27	0.82	0.24	0.19	4.06
Cr	µmol/L	BDL	BDL	BDL	BDL	BDL	BDL	BDL	BDL	BDL	BDL	BDL	BDL
Mn	µmol/L	BDL	BDL	0.19	0.24	0.13	0.52	0.15	0.10	0.11	0.32	0.17	0.16
Fe	µmol/L	BDL	BDL	BDL	BDL	BDL	BDL	BDL	BDL	BDL	BDL	BDL	BDL
Co	µmol/L	BDL	BDL	BDL	BDL	BDL	BDL	BDL	BDL	BDL	BDL	BDL	BDL
Ni	µmol/L	BDL	BDL	BDL	BDL	BDL	BDL	BDL	BDL	BDL	BDL	BDL	BDL
Cu	µmol/L	BDL	BDL	BDL	BDL	BDL	0.10	BDL	0.17	0.17	0.18	0.18	0.12

Zn	µmol/L	BDL	BDL	0.34	BDL	BDL	0.45	0.14	0.40	BDL	BDL	0.11	0.97
As	µmol/L	0.01	0.01	0.01	0.02	0.02	0.02	0.02	0.02	0.02	0.02	0.03	0.02
Br	µmol/L	BDL	BDL	BDL	BDL	BDL	BDL	BDL	BDL	BDL	BDL	BDL	BDL
Sr	µmol/L	BDL	1.35	3.17	4.01	7.37	8.89	9.38	10.83	10.87	11.14	12.00	12.96
Mo	µmol/L	BDL	0.27	0.33	0.38	0.49	0.51	0.55	0.57	0.60	0.63	0.68	0.71
Cd	µmol/L	BDL	BDL	BDL	BDL	BDL	0.00	BDL	BDL	BDL	BDL	BDL	BDL
Ba	µmol/L	BDL	BDL	0.17	0.27	0.92	1.31	1.36	1.59	1.47	1.23	1.01	0.84
Pb	µmol/L	BDL	BDL	BDL	BDL	0.00	0.01	0.00	0.00	0.00	0.00	BDL	BDL
U	µmol/L	BDL	BDL	BDL	BDL	BDL	BDL	BDL	BDL	BDL	BDL	BDL	BDL
DIC	mmol/L	0.00	0.17	0.33	0.28	0.47	0.58	0.57	0.70	0.70	0.82	0.95	1.36
NaCl Type I 95°C													
Sample ID		Input	T0'	T0.5hrs'	Thrs'	T0	T1hrs	T2hrs	T4hrs	T8hrs	T16hrs	T24hrs	T48hrs
Time (min)		0	1	30	60	165	225	285	405	645	1105	1605	3045
Li	µmol/L	BDL	BDL	BDL	BDL	BDL	BDL	BDL	BDL	BDL	BDL	BDL	BDL
B	µmol/L	20.7	62.4	46.8	54.5	68.1	73.9	85.8	119.6	170.4	256.0	369.5	552.2
Na	mmol/L	473.4	458.1	462.3	450.4	445.5	456.7	468.2	456.7	462.5	399.7	435.5	446.9
Mg	mmol/L	BDL	0.25	0.30	0.35	0.48	0.52	0.55	0.61	0.67	0.68	0.83	0.93
Al	µmol/L	BDL	BDL	14.30	17.99	13.76	8.03	7.26	BDL	BDL	BDL	BDL	BDL
Si	mmol/L	BDL	0.35	0.38	0.41	0.45	0.46	0.48	0.51	0.60	0.73	0.93	1.17
K	mmol/L	BDL	BDL	0.33	0.45	0.46	0.48	0.47	0.51	0.55	0.54	0.55	0.55
P	µmol/L	BDL	BDL	BDL	1.53	BDL	BDL	BDL	1.33	2.00	1.48	6.17	BDL
S	mmol/L	BDL	BDL	BDL	BDL	BDL	BDL	BDL	BDL	BDL	BDL	0.46	0.75
Cl	mmol/L	537	531	534	528	527	538	535	523	529	520	526	543
Ca	mmol/L	BDL	0.74	0.86	1.09	1.21	1.25	1.29	1.37	1.48	1.46	1.75	2.05
Ti	µmol/L	BDL	2.07	BDL	BDL	BDL	BDL	BDL	BDL	BDL	1.85	BDL	2.16
Cr	µmol/L	BDL	BDL	BDL	BDL	BDL	BDL	BDL	BDL	BDL	BDL	BDL	BDL
Mn	µmol/L	BDL	BDL	BDL	BDL	BDL	BDL	BDL	BDL	BDL	BDL	BDL	BDL
Fe	µmol/L	BDL	BDL	BDL	BDL	BDL	BDL	BDL	BDL	BDL	BDL	BDL	BDL
Co	µmol/L	BDL	BDL	BDL	BDL	BDL	BDL	BDL	BDL	BDL	BDL	BDL	BDL
Ni	µmol/L	BDL	BDL	BDL	BDL	BDL	BDL	BDL	BDL	BDL	BDL	BDL	BDL
Cu	µmol/L	BDL	BDL	BDL	BDL	BDL	BDL	BDL	BDL	BDL	BDL	BDL	BDL
Zn	µmol/L	BDL	BDL	BDL	BDL	BDL	BDL	BDL	BDL	BDL	BDL	BDL	BDL
As	µmol/L	BDL	BDL	0.12	BDL	0.12	0.09	0.09	0.10	0.16	0.11	0.18	0.22
Br	µmol/L	BDL	BDL	BDL	BDL	BDL	BDL	BDL	BDL	BDL	BDL	BDL	BDL
Sr	µmol/L	BDL	9.71	17.42	21.44	25.50	26.71	27.04	28.44	28.92	26.57	29.58	30.45
Mo	µmol/L	BDL	3.02	3.07	3.10	3.21	3.28	3.32	3.33	3.31	3.01	3.38	3.41
Cd	µmol/L	BDL	BDL	BDL	BDL	BDL	BDL	BDL	BDL	BDL	BDL	BDL	BDL
Ba	µmol/L	BDL	0.47	6.55	11.87	21.79	24.51	25.72	26.59	25.09	20.87	20.44	16.51
Pb	µmol/L	BDL	BDL	BDL	BDL	BDL	BDL	BDL	BDL	BDL	BDL	BDL	BDL
U	µmol/L	BDL	BDL	BDL	BDL	BDL	BDL	BDL	BDL	BDL	BDL	BDL	BDL
DIC	mmol/L	0.00	0.62	0.72	0.91	1.01	1.05	1.08	1.14	1.24	1.23	1.46	1.72
H2O Type II 95°C													
Sample ID		Input	T0'	T0	T4hrs	T8hrs	T24hrs	T48hrs	T96hrs	T168hrs			
Time (min)		0	1	135	375	615	1575	3015	5915	10215			
Li	µmol/L	BDL	BDL	BDL	BDL	BDL	BDL	BDL	BDL	BDL			

B	µmol/L	BDL	5.9	40.4	62.9	118.1	289.6	470.7	660.0	869.9
Na	mmol/L	BDL	0.6	1.0	1.0	1.0	1.1	1.2	1.2	1.3
Mg	mmol/L	BDL	0.03	0.12	0.18	0.25	0.35	0.62	0.95	1.07
Al	µmol/L	BDL	3.47	11.15	4.21	2.04	1.23	0.63	0.59	0.52
Si	mmol/L	BDL	0.03	0.17	0.23	0.31	0.66	0.79	0.81	1.09
K	mmol/L	BDL	0.08	0.33	0.33	0.38	0.37	0.37	0.39	0.40
P	µmol/L	BDL	BDL	0.11	BDL	0.19	0.13	BDL	0.19	0.17
S	mmol/L	BDL	0.06	0.54	0.76	0.89	1.31	2.48	3.98	4.84
Cl	mmol/L	BDL	BDL	BDL	1.18	BDL	BDL	0.94	2.69	0.89
Ca	mmol/L	BDL	0.18	0.45	0.57	0.84	0.86	1.38	2.18	2.68
Ti	µmol/L	BDL	BDL	BDL	BDL	BDL	BDL	0.18	BDL	BDL
Cr	µmol/L	BDL	BDL	BDL	BDL	BDL	BDL	BDL	BDL	BDL
Mn	µmol/L	BDL	BDL	0.17	0.11	0.17	0.12	0.27	0.43	0.27
Fe	µmol/L	BDL	BDL	BDL	BDL	BDL	BDL	BDL	BDL	BDL
Co	µmol/L	BDL	BDL	BDL	BDL	BDL	BDL	BDL	BDL	BDL
Ni	µmol/L	BDL	BDL	BDL	BDL	BDL	BDL	BDL	BDL	BDL
Cu	µmol/L	BDL	BDL	BDL	0.12	0.14	0.22	0.13	BDL	BDL
Zn	µmol/L	BDL	BDL	BDL	0.29	BDL	0.19	BDL	0.65	0.11
As	µmol/L	BDL	0.01	0.02	0.02	0.03	0.04	0.05	0.03	0.05
Br	µmol/L	BDL	BDL	BDL	BDL	BDL	BDL	BDL	BDL	BDL
Sr	µmol/L	BDL	1.34	7.30	9.67	11.25	11.52	12.50	13.60	14.03
Mo	µmol/L	BDL	0.27	0.47	0.55	0.59	0.64	0.72	0.85	0.91
Cd	µmol/L	BDL	BDL	BDL	BDL	BDL	BDL	BDL	0.01	BDL
Ba	µmol/L	BDL	BDL	0.84	1.51	1.84	1.24	0.81	0.56	0.48
Pb	µmol/L	BDL	BDL	BDL	0.00	BDL	BDL	BDL	0.00	BDL
U	µmol/L	BDL	BDL	BDL	BDL	BDL	BDL	BDL	BDL	BDL
DIC	mmol/L	0.00	0.15	0.38	0.48	0.70	0.72	1.16	1.83	2.24

NaCl Type II 95°C

Sample ID		Input	T0'	T0	T4hrs	T8hrs	T24hrs	T48hrs	T96hrs	T168hrs
Time (min)		0	1	140	380	480	480	480	480	480
Li	µmol/L	BDL	BDL	BDL	BDL	BDL	BDL	BDL	BDL	BDL
B	µmol/L	20.8	126.1	72.2	85.6	110.8	170.7	254.9	375.4	549.7
Na	mmol/L	453.2	463.9	461.7	480.2	462.4	447.4	461.3	454.0	501.3
Mg	mmol/L	BDL	0.27	0.46	0.60	0.65	1.11	1.18	1.18	1.26
Al	µmol/L	BDL	BDL	17.26	6.07	BDL	BDL	BDL	BDL	BDL
Si	mmol/L	BDL	0.36	0.50	0.47	0.51	0.57	0.78	1.01	1.21
K	mmol/L	BDL	BDL	0.45	0.47	0.50	0.55	0.54	0.55	0.56
P	µmol/L	BDL	BDL	BDL	BDL	BDL	BDL	BDL	BDL	BDL
S	mmol/L	BDL	BDL	BDL	BDL	BDL	0.93	1.12	1.23	1.96
Cl	mmol/L	420	405	392	432	428	458	538	520	551
Ca	mmol/L	BDL	0.84	1.61	1.39	1.45	2.04	2.20	2.30	2.59
Ti	µmol/L	BDL	BDL	BDL	BDL	BDL	BDL	BDL	BDL	BDL
Cr	µmol/L	BDL	BDL	BDL	BDL	BDL	BDL	BDL	BDL	BDL
Mn	µmol/L	BDL	BDL	BDL	BDL	BDL	0.62	BDL	BDL	BDL
Fe	µmol/L	BDL	BDL	BDL	BDL	BDL	BDL	BDL	BDL	BDL

Co	µmol/L	BDL	BDL	BDL	BDL	BDL	BDL	BDL	BDL	BDL
Ni	µmol/L	BDL	BDL	BDL	BDL	BDL	BDL	BDL	BDL	BDL
Cu	µmol/L	BDL	BDL	BDL	BDL	BDL	BDL	BDL	BDL	BDL
Zn	µmol/L	BDL	BDL	BDL	BDL	BDL	BDL	BDL	BDL	BDL
As	µmol/L	BDL	0.11	0.10	0.17	0.11	0.10	0.17	0.21	0.21
Br	µmol/L	BDL	BDL	BDL	BDL	BDL	BDL	BDL	BDL	BDL
Sr	µmol/L	BDL	11.46	25.52	28.11	29.38	29.75	31.83	33.06	34.21
Mo	µmol/L	BDL	3.05	3.22	3.32	3.36	3.43	3.45	3.48	3.52
Cd	µmol/L	BDL	BDL	BDL	BDL	BDL	BDL	BDL	BDL	BDL
Ba	µmol/L	BDL	1.27	24.32	26.93	26.10	13.21	10.53	9.71	8.29
Pb	µmol/L	BDL	BDL	BDL	BDL	BDL	BDL	BDL	BDL	BDL
U	µmol/L	BDL	BDL	BDL	BDL	BDL	BDL	BDL	BDL	BDL
DIC	mmol/L	0.00	0.70	1.34	1.16	1.21	1.71	1.84	1.92	2.16

Core 2 Experimental Data

H2O Type I 140°C

Sample ID		Input	T0'	T0.5hrs'	Thrs'	T0	T1hrs	T2hrs	T4hrs	T8hrs	T16hrs	T24hrs	T48hrs
Time (min)		0	1	30	60	110	170	230	350	590	1055	1550	2990
Li	µmol/L	BDL	BDL	BDL	BDL	BDL	BDL	BDL	BDL	BDL	BDL	BDL	BDL
B	µmol/L	BDL	BDL	9.5	11.8	14.7	18.9	25.8	72.1	147.4	304.7	517.1	904.0
Na	mmol/L	BDL	BDL	0.11	0.09	0.10	0.10	0.13	0.11	0.15	0.20	0.36	0.53
Mg	mmol/L	BDL	0.01	0.06	0.10	0.14	0.16	0.18	0.18	0.18	0.16	0.16	0.17
Al	µmol/L	BDL	0.11	6.11	12.61	11.13	8.48	7.43	4.46	3.19	1.13	0.57	0.82
Si	mmol/L	BDL	BDL	0.06	0.15	0.25	0.38	0.51	0.73	1.10	1.64	2.09	2.80
K	mmol/L	BDL	BDL	0.07	0.16	0.19	0.20	0.21	0.20	0.21	0.25	0.27	0.33
P	µmol/L	BDL	BDL	BDL	BDL	BDL	BDL	BDL	BDL	BDL	BDL	BDL	BDL
S	mmol/L	BDL	0.06	0.25	0.50	0.86	1.08	1.16	1.19	1.29	1.30	1.28	1.33
Cl	mmol/L	BDL	BDL	BDL	BDL	BDL	BDL	BDL	BDL	BDL	BDL	0.96	BDL
Ca	mmol/L	BDL	0.16	0.27	0.42	0.65	0.77	0.85	0.84	0.84	0.85	0.92	0.79
Ti	µmol/L	BDL	BDL	0.00	0.01	0.01	0.00	BDL	0.01	0.01	0.00	0.00	0.00
Cr	µmol/L	BDL	BDL	BDL	BDL	BDL	BDL	BDL	BDL	BDL	BDL	BDL	BDL
Mn	µmol/L	BDL	BDL	0.30	0.26	0.36	0.45	0.34	2.10	0.24	0.61	0.47	0.28
Fe	µmol/L	BDL	BDL	0.22	0.60	BDL	BDL	BDL	BDL	BDL	BDL	BDL	BDL
Co	µmol/L	BDL	BDL	BDL	BDL	BDL	BDL	BDL	BDL	BDL	BDL	0.00	BDL
Ni	µmol/L	BDL	BDL	BDL	0.17	0.01	0.02	0.02	0.03	0.05	0.04	0.04	0.04
Cu	µmol/L	BDL	BDL	0.02	0.10	0.04	0.03	0.03	0.05	0.07	0.06	0.03	0.01
Zn	µmol/L	BDL	BDL	0.09	0.07	0.14	BDL	0.05	0.35	0.32	0.98	0.11	0.31
As	µmol/L	BDL	BDL	BDL	0.01	0.02	0.02	0.03	0.04	0.04	0.08	0.09	0.13
Br	µmol/L	BDL	BDL	BDL	BDL	BDL	BDL	BDL	BDL	BDL	BDL	BDL	BDL
Sr	µmol/L	BDL	BDL	2.41	3.61	4.83	5.82	6.26	6.95	7.45	8.03	9.81	10.26
Mo	µmol/L	BDL	0.01	0.11	0.20	0.31	0.42	0.47	0.49	0.58	0.62	0.62	0.69
Cd	µmol/L	BDL	BDL	BDL	BDL	BDL	BDL	BDL	BDL	BDL	BDL	BDL	BDL
Ba	µmol/L	BDL	0.06	0.57	1.22	1.55	1.43	1.42	1.29	1.46	1.21	1.26	1.39
Pb	µmol/L	BDL	BDL	BDL	BDL	BDL	BDL	BDL	BDL	BDL	BDL	BDL	BDL
U	µmol/L	BDL	BDL	BDL	BDL	BDL	BDL	BDL	BDL	BDL	BDL	BDL	BDL

DIC	mmol/L	0.00	0.43	0.30	0.42	0.54	0.61	0.61	0.66	0.66	0.79	0.84	0.88
NaCl Type I 140°C													
Sample ID		Input	T0'	T0.5hrs'	Thrs'	T0	T1hrs	T2hrs	T4hrs	T8hrs	T16hrs	T24hrs	T48hrs
Time (min)		0	1	30	60	125	185	245	365	605	1065	1565	3005
Li	µmol/L	BDL	BDL	BDL	BDL	BDL	BDL	BDL	BDL	BDL	BDL	BDL	BDL
B	µmol/L	125.8	121.4	BDL	BDL	122.2	155.5	185.1	231.0	394.7	1298.2	1357.2	2541.6
Na	mmol/L	439.1	422.4	432.5	396.9	450.1	428.1	430.0	426.3	414.9	406.1	413.1	426.9
Mg	mmol/L	BDL	0.05	0.11	0.17	0.25	0.36	0.41	0.37	0.33	0.35	0.31	0.36
Al	µmol/L	BDL	BDL	2.72	16.71	13.13	14.68	7.67	7.07	0.85	BDL	BDL	BDL
Si	mmol/L	BDL	BDL	BDL	0.09	0.20	0.48	0.68	0.94	1.63	3.16	2.85	3.95
K	mmol/L	BDL	BDL	BDL	BDL	BDL	0.39	0.36	0.32	0.34	0.45	0.42	0.59
P	µmol/L	BDL	BDL	BDL	BDL	BDL	BDL	BDL	BDL	BDL	BDL	BDL	BDL
S	mmol/L	BDL	BDL	BDL	BDL	0.90	1.49	1.77	1.74	1.61	1.73	1.71	2.55
Cl	mmol/L	389	389	404	403	407	422	405	410	396	400	415	496
Ca	mmol/L	BDL	0.68	0.52	0.74	1.03	1.51	1.61	1.49	1.55	1.96	1.59	2.07
Ti	µmol/L	BDL	BDL	BDL	BDL	BDL	BDL	BDL	0.06	BDL	BDL	0.06	BDL
Cr	µmol/L	BDL	BDL	BDL	BDL	BDL	BDL	BDL	BDL	BDL	BDL	BDL	BDL
Mn	µmol/L	BDL	BDL	BDL	BDL	BDL	BDL	BDL	BDL	BDL	BDL	BDL	BDL
Fe	µmol/L	BDL	BDL	BDL	BDL	BDL	BDL	BDL	BDL	BDL	BDL	BDL	BDL
Co	µmol/L	BDL	BDL	BDL	BDL	BDL	BDL	BDL	BDL	BDL	BDL	BDL	BDL
Ni	µmol/L	BDL	BDL	BDL	BDL	BDL	BDL	BDL	BDL	BDL	BDL	BDL	BDL
Cu	µmol/L	BDL	BDL	BDL	BDL	BDL	0.11	0.15	0.14	0.17	0.29	BDL	0.12
Zn	µmol/L	BDL	BDL	BDL	BDL	BDL	BDL	BDL	BDL	BDL	0.57	BDL	BDL
As	µmol/L	BDL	BDL	BDL	BDL	BDL	BDL	BDL	BDL	0.16	0.15	0.18	0.31
Br	µmol/L	BDL	BDL	BDL	BDL	BDL	BDL	BDL	BDL	BDL	BDL	BDL	BDL
Sr	µmol/L	BDL	BDL	BDL	BDL	BDL	8.58	10.21	10.21	11.16	16.24	15.58	27.21
Mo	µmol/L	BDL	BDL	BDL	0.20	0.34	0.51	0.57	0.65	0.59	0.67	0.66	0.75
Cd	µmol/L	BDL	BDL	BDL	BDL	BDL	BDL	BDL	BDL	BDL	BDL	BDL	BDL
Ba	µmol/L	BDL	2.14	5.80	8.45	11.93	16.14	16.45	14.60	14.16	16.08	13.05	17.20
Pb	µmol/L	BDL	BDL	BDL	BDL	BDL	BDL	BDL	BDL	BDL	BDL	BDL	BDL
U	µmol/L	BDL	BDL	BDL	BDL	BDL	BDL	BDL	BDL	BDL	BDL	BDL	BDL
DIC	mmol/L	0.04	0.83	0.89	0.84	0.97	1.01	1.02	1.08	1.11	1.18	1.34	1.46

H2O Type II 140°C									
Sample ID		Input	T0'	T0	T4hrs	T8hrs	T24hrs	T48hrs	T96hrs
Time (min)		0	1	130	370	610	1570	3010	5910
Li	µmol/L	BDL	BDL	BDL	BDL	BDL	BDL	BDL	4.30
B	µmol/L	BDL	BDL	18.7	38.4	101.1	353.1	1099.4	1612.7
Na	mmol/L	BDL	BDL	0.26	0.12	0.12	0.30	0.59	0.81
Mg	mmol/L	BDL	0.01	0.17	0.20	0.21	0.19	0.13	0.13
Al	µmol/L	BDL	0.21	8.15	6.07	3.57	1.23	0.95	0.79
Si	mmol/L	BDL	BDL	0.32	0.59	0.82	1.73	3.28	3.69
K	mmol/L	BDL	BDL	0.14	0.21	0.17	0.26	0.31	0.39
P	µmol/L	BDL	BDL	BDL	BDL	BDL	BDL	BDL	BDL
S	mmol/L	BDL	0.07	1.11	1.22	1.28	1.25	1.38	1.43
Cl	mmol/L	BDL	BDL	BDL	BDL	BDL	BDL	BDL	BDL

Ca	mmol/L	BDL	0.16	0.74	0.83	0.81	0.80	0.77	0.73
Ti	µmol/L	BDL	BDL	BDL	BDL	0.00	0.01	0.00	0.00
Cr	µmol/L	BDL	BDL	BDL	BDL	BDL	BDL	BDL	BDL
Mn	µmol/L	BDL	0.19	0.14	0.60	1.02	1.58	0.96	2.97
Fe	µmol/L	BDL	BDL	BDL	BDL	BDL	0.18	BDL	BDL
Co	µmol/L	BDL	BDL	BDL	BDL	BDL	BDL	BDL	BDL
Ni	µmol/L	BDL	BDL	BDL	BDL	BDL	0.02	0.02	0.03
Cu	µmol/L	BDL	BDL	BDL	0.03	0.03	0.02	BDL	0.01
Zn	µmol/L	BDL	0.04	BDL	BDL	BDL	0.07	BDL	BDL
As	µmol/L	BDL	BDL	0.01	0.02	0.04	0.07	0.17	0.19
Br	µmol/L	BDL	BDL	BDL	BDL	BDL	BDL	BDL	BDL
Sr	µmol/L	BDL	BDL	5.65	6.67	7.51	9.13	9.46	9.80
Mo	µmol/L	BDL	BDL	0.33	0.46	0.52	0.58	0.70	0.77
Cd	µmol/L	BDL	BDL	BDL	BDL	BDL	BDL	BDL	BDL
Ba	µmol/L	BDL	0.05	1.59	1.40	1.31	1.34	1.43	1.34
Pb	µmol/L	BDL	BDL	BDL	BDL	BDL	0.01	BDL	BDL
U	µmol/L	BDL	BDL	BDL	BDL	BDL	BDL	BDL	BDL
DIC	mmol/L	0.07	0.45	0.55	0.65	0.59	0.75	0.85	0.87

NaCl Type II 140°C									
Sample ID		Input	T0'	T0	T4hrs	T8hrs	T24hrs	T48hrs	T96hrs
Time (min)		0	1	140	380	620	1580	3020	5920
Li	µmol/L	BDL	BDL	BDL	BDL	BDL	BDL	BDL	BDL
B	µmol/L	BDL	BDL	97.5	203.0	334.0	1474.6	2017.5	3032.1
Na	mmol/L	432.4	432.8	436.7	436.7	429.3	444.5	452.1	466.5
Mg	mmol/L	BDL	BDL	0.26	0.29	0.28	0.26	0.30	0.30
Al	µmol/L	BDL	BDL	15.89	6.41	2.50	1.68	BDL	BDL
Si	mmol/L	BDL	BDL	0.16	0.82	1.39	3.05	3.38	3.33
K	mmol/L	BDL	BDL	BDL	BDL	BDL	0.37	0.47	0.56
P	µmol/L	BDL	BDL	BDL	BDL	BDL	BDL	BDL	BDL
S	mmol/L	BDL	BDL	1.50	1.92	1.78	2.03	2.21	2.29
Cl	mmol/L	399	390	416	421	397	404	404	443
Ca	mmol/L	BDL	0.53	1.39	1.56	1.61	1.87	1.94	2.11
Ti	µmol/L	BDL	BDL	BDL	BDL	BDL	BDL	BDL	BDL
Cr	µmol/L	BDL	BDL	BDL	BDL	BDL	BDL	BDL	BDL
Mn	µmol/L	BDL	BDL	BDL	42.37	BDL	BDL	BDL	BDL
Fe	µmol/L	BDL	BDL	BDL	BDL	BDL	BDL	BDL	BDL
Co	µmol/L	BDL	BDL	BDL	BDL	BDL	BDL	BDL	BDL
Ni	µmol/L	BDL	BDL	BDL	BDL	BDL	BDL	BDL	0.31
Cu	µmol/L	BDL	BDL	BDL	BDL	BDL	BDL	BDL	BDL
Zn	µmol/L	BDL	BDL	BDL	BDL	BDL	BDL	BDL	1.59
As	µmol/L	BDL	BDL	BDL	BDL	0.14	0.16	0.15	0.34
Br	µmol/L	BDL	BDL	BDL	BDL	BDL	BDL	BDL	BDL
Sr	µmol/L	BDL	BDL	7.91	9.28	10.94	18.17	26.32	30.87
Mo	µmol/L	BDL	BDL	0.43	0.45	0.50	0.51	0.60	0.70
Cd	µmol/L	BDL	BDL	BDL	BDL	BDL	BDL	BDL	BDL

Ba	µmol/L	BDL	0.42	13.81	14.11	13.86	14.87	15.68	16.85
Pb	µmol/L	BDL	BDL	0.12	BDL	BDL	BDL	BDL	0.12
U	µmol/L	BDL	BDL	0.06	0.05	BDL	0.05	0.05	0.05
DIC	mmol/L	0.07	1.10	0.98	1.10	1.06	1.42	1.53	1.66

B-2 Solid Concentrations from Experiments, BDL = below detection limit, a standard error of 5 % was used.

Outcrop Experimental Data											
H2O Type II 25°C											
Sample ID		Input	T0'	T0	T4hrs	T8hrs	T24hrs	T48hrs	T96hrs	T168hrs	T264hrs
Time (min)		0	1	5	245	485	1445	2885	5785	10085	15485
Li	mmol/L	6.4	3.5	BDL	1.0	BDL	BDL	1.1	BDL	BDL	BDL
Na	mol/L	0.077	0.021	0.031	0.038	0.027	0.023	0.029	0.025	0.029	0.031
Mg	mol/L	0.2	0.1	0.1	0.2	0.2	0.2	0.2	0.1	0.1	0.2
Al	mol/L	1.5	1.0	1.0	1.5	1.1	1.0	1.1	1.1	0.9	1.0
Si	mol/L	10.7	9.6	8.5	13.0	9.9	10.6	11.0	9.7	8.8	10.8
K	mol/L	0.7	0.6	0.6	0.8	0.6	0.6	0.7	0.6	0.5	0.6
P	mol/L	0.033	0.020	0.020	0.032	0.023	0.022	0.024	0.021	0.019	0.021
S	mol/L	0.7	0.4	0.4	0.6	0.5	0.5	0.5	0.4	0.4	0.4
Ca	mol/L	1.7	1.5	1.4	2.2	1.6	1.6	1.7	1.6	1.3	1.5
Ti	mol/L	0.031	0.030	0.030	0.040	0.031	0.029	0.031	0.029	0.025	0.028
Cr	mmol/L	1.0	0.8	0.8	1.2	0.9	0.8	0.9	0.8	0.7	0.8
Mn	mmol/L	1.8	19.3	4.5	9.6	3.4	5.2	10.0	1.4	6.5	1.9
Fe	mol/L	0.3	0.3	0.3	0.4	0.3	0.3	0.3	0.3	0.2	0.3
Co	mmol/L	0.1	0.1	0.1	0.2	0.1	0.1	0.1	0.1	0.1	0.1
Ni	mmol/L	1.8	1.6	1.6	2.3	1.7	1.6	1.7	1.5	1.3	1.5
Cu	mmol/L	1.0	0.7	0.7	1.1	0.8	0.7	0.8	0.7	0.6	0.7
Zn	mmol/L	0.4	0.1	0.1	0.2	0.1	0.1	0.1	0.1	0.1	0.1
As	mmol/L	0.3	0.2	0.2	0.3	0.2	0.2	0.2	0.2	0.2	0.2
Sr	mmol/L	1.2	1.1	1.1	1.6	1.2	1.1	1.2	1.1	0.9	1.0
Mo	µmol/L	858.8	362.9	311.0	400.1	303.1	257.7	249.1	224.6	173.1	201.2
Cd	µmol/L	3.1	41.1	4.4	12.7	30.2	1.6	3.1	1.7	3.7	1.4
Ba	mmol/L	3.1	2.7	2.7	3.6	2.8	2.5	2.7	2.6	2.1	2.6
Pb	µmol/L	91.5	54.9	53.2	82.8	64.8	58.7	63.0	62.1	52.5	58.4
U	µmol/L	88.3	57.0	56.8	91.2	66.2	58.1	62.2	64.0	48.9	55.4
NaCl Type II 25°C											
Sample ID		Input	T0'	T0	T4hrs	T8hrs	T24hrs	T48hrs	T96hrs	T168hrs	T264hrs
Time (min)		0	1	20	260	500	1460	2900	5800	10100	15500
Li	mmol/L	6.4	1.7	BDL	BDL	BDL	1.2	BDL	21.6	BDL	BDL
Na	mol/L	0.077	0.088	0.029	0.045	0.051	0.039	0.054	0.032	0.039	0.036
Mg	mol/L	0.2	0.2	0.2	0.2	0.2	0.1	0.2	0.1	0.2	0.2
Al	mol/L	1.5	1.4	1.1	1.2	1.1	0.9	1.1	0.9	1.2	1.0
Si	mol/L	10.7	11.9	10.4	10.4	10.5	8.6	9.8	8.7	12.3	10.0
K	mol/L	0.7	0.8	0.7	0.7	0.7	0.5	0.6	0.5	0.7	0.6
P	mol/L	0.033	0.028	0.022	0.026	0.024	0.018	0.023	0.018	0.025	0.021
S	mol/L	0.7	0.5	0.5	0.5	0.5	0.4	0.5	0.4	0.5	0.4

Ca	mol/L	1.7	1.8	1.6	1.9	1.8	1.3	1.7	1.3	1.9	1.6
Ti	mol/L	0.031	0.039	0.032	0.035	0.031	0.024	0.030	0.025	0.035	0.033
Cr	mmol/L	1.0	1.2	0.9	1.0	0.9	0.7	0.9	0.7	1.0	0.9
Mn	mmol/L	1.8	10.1	5.1	7.1	3.0	7.2	2.6	27.3	6.1	6.8
Fe	mol/L	0.3	0.3	0.3	0.3	0.3	0.2	0.3	0.2	0.3	0.3
Co	mmol/L	0.1	0.2	0.1	0.2	0.1	0.1	0.1	0.1	0.1	0.1
Ni	mmol/L	1.8	2.2	1.7	1.9	1.7	1.3	1.6	1.4	1.8	1.6
Cu	mmol/L	1.0	1.2	0.8	0.9	0.8	0.6	0.8	0.6	0.9	0.7
Zn	mmol/L	0.4	0.5	0.1	0.1	0.1	0.1	0.1	0.1	0.1	0.1
As	mmol/L	0.3	0.2	0.2	0.2	0.2	0.2	0.2	0.2	0.2	0.2
Sr	mmol/L	1.2	1.6	1.2	1.4	1.2	0.9	1.2	0.9	1.3	1.1
Mo	µmol/L	858.8	499.5	341.3	302.1	281.0	191.9	226.9	189.5	255.2	212.0
Cd	µmol/L	3.1	2.1	1.7	2.0	2.0	1.7	1.6	2.0	1.2	1.5
Ba	mmol/L	3.1	3.8	2.9	3.0	2.8	2.1	2.6	2.2	3.1	2.5
Pb	µmol/L	91.5	76.5	60.3	67.0	61.7	52.9	63.3	49.8	67.6	56.8
U	µmol/L	88.3	82.8	64.4	72.7	65.4	52.8	60.9	48.6	67.7	55.1
H2O Type II 95°C											
Sample ID		Input	T0'	T0	T4hrs	T8hrs	T24hrs	T48hrs	T96hrs	T168hrs	T262.5hrs
Time (min)		0	1	180	420	660	1620	3060	5960	10260	15660
Li	mmol/L	2.6	2.5	2.3	1.7	1.6	1.6	1.6	1.4	1.1	1.4
Na	mol/L	0.073	0.036	0.032	0.033	0.027	0.027	0.028	0.028	0.021	0.031
Mg	mol/L	0.2	0.1	0.1	0.1	0.1	0.1	0.1	0.1	0.1	0.2
Al	mol/L	1.6	0.8	0.8	0.8	0.8	0.8	0.8	0.8	0.7	0.9
Si	mol/L	12.8	8.3	8.7	8.6	8.2	8.5	8.9	9.2	8.0	9.9
K	mol/L	0.7	0.7	0.7	0.7	0.7	0.7	0.7	0.7	0.6	0.7
P	mol/L	0.023	0.016	0.016	0.017	0.016	0.016	0.016	0.016	0.014	0.017
S	mol/L	2.3	0.3	0.3	0.3	0.3	0.3	0.3	0.3	0.3	0.3
Ca	mol/L	1.5	1.0	1.2	1.2	1.3	1.3	1.2	1.2	1.0	1.2
Ti	mol/L	0.038	0.038	0.035	0.036	0.035	0.034	0.032	0.033	0.030	0.036
Cr	mmol/L	1.1	1.0	0.8	0.9	0.8	0.8	0.8	0.8	0.7	0.9
Mn	mmol/L	1.6	1.2	1.1	1.2	1.1	1.2	1.1	1.4	0.9	1.1
Fe	mol/L	0.4	0.3	0.3	0.3	0.3	0.3	0.3	0.3	0.2	0.3
Co	mmol/L	0.2	0.2	0.1	0.2	0.1	0.1	0.1	0.1	0.1	0.1
Ni	mmol/L	8.0	1.8	1.6	1.7	1.6	1.6	1.4	1.4	1.3	1.5
Cu	mmol/L	9.3	1.0	1.0	0.8	0.8	0.8	0.8	0.8	0.6	1.3
Zn	mmol/L	0.0	BDL	BDL	BDL	BDL	BDL	2.8	1.3	BDL	0.1
As	mmol/L	0.3	0.2	0.2	0.2	0.2	0.2	0.2	0.2	0.1	0.2
Sr	mmol/L	1.3	1.1	1.1	1.1	1.2	1.1	1.1	1.1	0.9	1.1
Mo	µmol/L	636.4	484.1	230.6	208.8	185.0	172.4	153.9	145.9	119.6	143.6
Cd	µmol/L	7.0	1.9	1.4	1.3	1.3	2.1	1.8	1.2	1.4	1.6
Ba	mmol/L	1.4	1.7	1.4	1.4	1.3	1.3	1.2	1.2	1.1	1.3
Pb	µmol/L	105.2	65.9	62.0	60.4	59.2	60.4	58.3	50.8	53.4	60.9
U	µmol/L	76.0	66.1	63.6	64.2	60.0	59.1	55.8	53.8	47.1	56.7
NaCl Type II 95°C											
Sample ID		Input	T0'	T0	T4hrs	T8hrs	T24hrs	T48hrs	T96hrs	T168hrs	

Time (min)		0	1	140	380	620	1580	3020	5900	10220
Li	mmol/L	BDL	0.5	0.7	1.1	1.2	1.6	1.1	1.3	1.1
Na	mol/L	0.060	0.040	0.032	0.040	0.070	0.072	0.047	0.086	0.113
Mg	mol/L	0.2	0.2	0.1	0.1	0.1	0.1	0.1	0.1	0.1
Al	mol/L	1.3	0.9	0.8	0.8	0.8	0.8	0.8	0.7	0.7
Si	mol/L	11.1	7.9	7.3	8.2	8.3	9.1	9.1	8.3	9.0
K	mol/L	0.6	0.7	0.6	0.7	0.6	0.7	0.6	0.6	0.6
P	mol/L	0.030	0.018	0.018	0.018	0.018	0.018	0.017	0.016	0.016
S	mol/L	1.8	0.3	0.3	0.4	0.4	0.4	0.3	0.3	0.3
Ca	mol/L	1.7	1.4	1.3	1.4	1.5	1.5	1.4	1.3	1.3
Ti	mol/L	0.030	0.042	0.036	0.036	0.035	0.037	0.033	0.034	0.031
Cr	mmol/L	1.0	0.9	0.8	0.8	0.8	0.9	0.8	0.8	0.7
Mn	mmol/L	1.5	1.2	1.2	1.2	1.4	1.2	1.1	1.1	1.1
Fe	mol/L	0.3	0.3	0.3	0.3	0.3	0.3	0.3	0.3	0.3
Co	mmol/L	0.2	0.2	0.1	0.1	0.1	0.1	0.1	0.1	0.1
Ni	mmol/L	5.8	2.1	1.8	1.7	1.7	1.6	1.5	1.4	1.5
Cu	mmol/L	6.9	1.1	0.8	0.8	0.8	0.8	0.7	0.7	0.7
Zn	mmol/L	BDL	BDL	BDL	BDL	BDL	BDL	BDL	BDL	0.0
As	mmol/L	0.3	0.2	0.2	0.2	0.2	0.2	0.2	0.2	0.2
Sr	mmol/L	1.2	1.2	1.1	1.1	1.2	1.2	1.1	1.0	1.0
Mo	µmol/L	527.4	555.3	190.9	165.3	163.6	152.9	128.6	113.6	109.5
Cd	µmol/L	4.1	1.3	1.3	1.4	1.6	3.3	1.2	1.1	1.7
Ba	mmol/L	1.1	1.5	1.1	1.1	1.1	1.1	1.1	1.0	1.0
Pb	µmol/L	70.6	82.8	63.1	57.9	58.7	62.6	52.5	52.1	53.8
U	µmol/L	70.3	73.5	65.4	64.1	60.7	61.8	57.9	55.1	54.2

H2O Type II 140°C									
Sample ID		Input	T0'	T0	T4hrs	T8hrs	T24hrs	T48hrs	T96hrs
Time (min)		0	1	110	350	590	1550	2990	5890
Li	mmol/L	6.4	1.2	BDL	BDL	BDL	BDL	BDL	BDL
Na	mol/L	0.077	0.079	0.080	0.057	0.082	0.069	0.062	0.086
Mg	mol/L	0.2	0.2	0.2	0.2	0.3	0.2	0.2	0.2
Al	mol/L	1.5	1.3	1.5	1.1	1.6	1.3	1.0	1.3
Si	mol/L	10.7	10.3	11.7	8.7	12.2	10.9	8.6	11.5
K	mol/L	0.7	0.7	0.8	0.6	0.8	0.7	0.5	0.7
P	mol/L	0.033	0.030	0.035	0.026	0.037	0.032	0.024	0.029
S	mol/L	0.7	0.6	0.7	0.5	0.7	0.6	0.5	0.6
Ca	mol/L	1.7	1.8	2.0	1.5	2.3	1.9	1.4	1.7
Ti	mol/L	0.031	0.035	0.042	0.030	0.044	0.034	0.026	0.033
Cr	mmol/L	1.0	1.2	1.4	1.0	1.5	1.2	0.9	1.1
Mn	mmol/L	1.8	3.2	2.7	2.2	4.8	3.4	2.6	2.9
Fe	mol/L	0.3	0.4	0.4	0.3	0.5	0.4	0.3	0.4
Co	mmol/L	0.1	0.2	0.2	0.1	0.2	0.2	0.1	0.2
Ni	mmol/L	1.8	2.2	2.6	1.8	2.7	2.1	1.5	2.1
Cu	mmol/L	1.0	1.2	1.3	0.9	1.4	1.1	0.7	1.2
Zn	mmol/L	0.4	0.8	7.0	0.4	0.6	0.5	1.1	0.5

As	mmol/L	0.3	0.3	0.4	0.3	0.4	0.3	0.2	0.3
Sr	mmol/L	1.2	1.3	1.5	1.1	1.7	1.4	1.0	1.3
Mo	µmol/L	858.8	635.7	358.4	216.4	287.3	238.7	158.7	220.1
Cd	µmol/L	3.1	12.3	2.2	5.5	11.3	9.0	4.1	2.4
Ba	mmol/L	3.1	3.8	4.2	3.0	4.4	3.6	2.5	3.4
Pb	µmol/L	91.5	178.1	88.9	101.1	204.2	150.0	80.7	76.8
U	µmol/L	88.3	79.5	96.6	68.7	103.5	81.2	57.9	79.6
NaCl Type II 140°C									
Sample ID		Input	T0'	T0	T4hrs	T8hrs	T24hrs	T48hrs	T96hrs
Time (min)		0	1	140	380	620	1580	3020	5900
Li	mmol/L	6.4	BDL	BDL	BDL	BDL	BDL	BDL	BDL
Na	mol/L	0.077	0.085	0.078	0.203	0.634	0.088	0.073	0.072
Mg	mol/L	0.2	0.2	0.2	0.3	0.2	0.2	0.2	0.1
Al	mol/L	1.5	1.3	1.4	1.6	1.4	1.3	1.1	0.9
Si	mol/L	10.7	9.3	9.5	12.6	11.3	11.0	9.5	6.5
K	mol/L	0.7	0.6	0.7	0.8	0.8	0.7	0.6	0.4
P	mol/L	0.033	0.037	0.030	0.039	0.034	0.030	0.026	0.017
S	mol/L	0.7	0.6	0.5	0.8	0.7	0.6	0.5	0.4
Ca	mol/L	1.7	1.6	1.7	2.3	2.1	1.8	1.6	1.0
Ti	mol/L	0.031	0.033	0.038	0.044	0.041	0.035	0.029	0.019
Cr	mmol/L	1.0	1.1	1.3	1.5	1.3	1.1	1.0	0.7
Mn	mmol/L	1.8	3.6	2.4	3.3	2.8	1.9	2.1	1.0
Fe	mol/L	0.3	0.3	0.4	0.5	0.4	0.4	0.3	0.2
Co	mmol/L	0.1	0.2	0.2	0.2	0.2	0.2	0.1	0.1
Ni	mmol/L	1.8	2.0	2.3	2.8	2.4	2.0	1.7	1.2
Cu	mmol/L	1.0	1.0	1.1	1.4	1.2	1.1	0.9	0.6
Zn	mmol/L	0.4	0.3	0.2	0.4	2.1	0.2	0.1	0.6
As	mmol/L	0.3	0.2	0.3	0.4	0.3	0.3	0.2	0.2
Sr	mmol/L	1.2	1.2	1.2	1.6	1.4	1.2	1.0	0.7
Mo	µmol/L	858.8	420.2	245.3	217.2	211.8	160.4	129.5	85.6
Cd	µmol/L	3.1	5.6	1.8	5.5	47.8	2.3	1.4	1.5
Ba	mmol/L	3.1	3.2	3.5	4.3	3.8	3.2	2.7	1.7
Pb	µmol/L	91.5	117.3	79.9	108.2	82.5	74.1	62.5	50.3
U	µmol/L	88.3	73.9	91.3	103.4	91.5	78.3	64.0	45.4

Core 1 Experimental Data

H2O Type I 95°C													
Sample ID		Input	T0'	T0.5hrs'	Thrs'	T0	T1hrs	T2hrs	T4hrs	T8hrs	T16hrs	T24hrs	T48hrs
Time (min)		0	1	30	60	160	220	280	400	640	1105	1600	3040
Li	mmol/L	BDL	3.8	3.7	4.4	4.7	4.8	4.8	4.9	4.8	4.8	4.8	4.9
Na	mol/L	0.061	0.019	0.014	0.013	0.014	0.014	0.019	0.015	0.013	0.028	0.015	0.020
Mg	mol/L	0.4	0.4	0.4	0.4	0.3	0.3	0.3	0.4	0.3	0.3	0.3	0.3
Al	mol/L	1.0	0.9	0.8	0.8	0.8	0.8	0.8	0.9	0.8	0.8	0.8	0.8
Si	mol/L	3.4	3.2	3.1	3.1	2.6	2.9	2.6	3.4	3.3	2.8	2.8	2.7
K	mol/L	0.5	0.6	0.5	0.5	0.5	0.5	0.5	0.6	0.5	0.5	0.5	0.5

P	mol/L	0.033	0.026	0.024	0.025	0.024	0.023	0.024	0.027	0.024	0.024	0.024	0.023
S	mol/L	0.6	0.2	0.1	0.1	0.1	0.1	0.1	0.2	0.1	0.1	0.1	0.1
Ca	mol/L	5.3	5.4	5.1	5.2	4.9	4.9	4.9	5.6	5.2	4.9	4.8	4.6
Ti	mol/L	0.027	0.030	0.028	0.029	0.028	0.028	0.027	0.032	0.029	0.027	0.029	0.030
Cr	mmol/L	0.8	0.7	0.6	0.6	0.6	0.6	0.6	0.6	0.6	0.6	0.6	0.6
Mn	mmol/L	5.4	5.4	4.9	5.1	4.8	5.0	5.0	5.5	4.8	5.0	5.0	4.8
Fe	mol/L	0.3	0.3	0.3	0.3	0.2	0.2	0.2	0.3	0.3	0.3	0.3	0.2
Co	mmol/L	0.2	0.2	0.2	0.2	0.2	0.2	0.2	0.2	0.2	0.2	0.2	0.2
Ni	mmol/L	0.9	0.7	0.7	0.7	0.7	0.7	0.7	0.8	0.7	0.8	0.7	0.7
Cu	mmol/L	1.3	0.5	0.6	0.5	0.5	0.5	0.4	0.6	0.4	0.5	0.5	0.4
Zn	mmol/L	1.9	0.4	2.8	BDL	BDL	0.1	BDL	0.8	BDL	BDL	BDL	0.9
As	mmol/L	0.2	0.1	0.1	0.1	0.1	0.1	0.1	0.1	0.1	0.1	0.1	0.1
Sr	mmol/L	3.8	4.6	4.1	4.2	3.9	3.9	3.9	4.4	3.8	4.0	3.9	3.7
Mo	µmol/L	33.7	10.6	11.4	8.4	8.4	10.1	7.0	11.7	13.6	8.6	7.6	8.8
Cd	µmol/L	5.2	3.4	0.8	0.4	0.8	1.9	2.0	0.3	1.3	0.8	0.8	0.6
Ba	mmol/L	1.9	2.4	2.2	2.2	2.0	2.1	2.1	2.3	2.1	2.2	2.1	2.2
Pb	µmol/L	63.9	58.7	51.6	53.8	52.0	58.7	64.2	59.3	54.4	53.5	53.0	52.0
U	µmol/L	15.3	17.2	26.9	80.4	120.6	116.3	124.1	119.9	121.4	120.1	120.7	121.4

NaCl Type I 95°C

Sample ID		Input	T0'	T0.5hrs'	Thrs'	T0	T1hrs	T2hrs	T4hrs	T8hrs	T16hrs	T24hrs	T48hrs
Time (min)		0	1	30	60	165	225	285	405	645	1105	1605	3045
Li	mmol/L	BDL	3.3	3.9	3.6	3.6	3.4	3.3	3.4	3.1	4.4	3.3	3.2
Na	mol/L	0.061	0.072	0.045	0.027	0.015	0.013	0.023	0.016	0.017	0.015	0.014	0.018
Mg	mol/L	0.4	0.3	0.4	0.4	0.4	0.3	0.3	0.3	0.3	0.4	0.3	0.3
Al	mol/L	1.0	0.8	1.0	0.9	0.9	0.8	0.8	0.8	0.8	0.9	0.8	0.8
Si	mol/L	3.4	2.8	3.7	3.6	3.4	3.1	3.0	2.8	3.2	3.3	3.1	3.0
K	mol/L	0.5	0.5	0.6	0.6	0.6	0.5	0.5	0.5	0.6	0.6	0.5	0.5
P	mol/L	0.033	0.023	0.029	0.027	0.026	0.023	0.023	0.023	0.024	0.025	0.023	0.023
S	mol/L	0.6	0.1	0.2	0.2	0.1	0.1	0.1	0.1	0.1	0.1	0.1	0.1
Ca	mol/L	5.3	4.8	6.2	5.9	5.6	4.9	5.0	4.9	5.1	5.2	4.9	4.7
Ti	mol/L	0.027	0.028	0.036	0.034	0.031	0.029	0.030	0.029	0.029	0.029	0.028	0.028
Cr	mmol/L	0.8	0.6	0.7	0.7	0.7	0.6	0.6	0.7	0.9	0.6	0.6	0.6
Mn	mmol/L	5.4	4.5	5.9	5.6	5.3	4.6	4.7	4.8	4.8	5.0	5.0	4.7
Fe	mol/L	0.3	0.2	0.3	0.3	0.3	0.2	0.2	0.3	0.3	0.3	0.3	0.2
Co	mmol/L	0.2	0.2	0.2	0.2	0.2	0.2	0.2	0.2	0.2	0.2	0.2	0.2
Ni	mmol/L	0.9	0.7	0.8	0.8	0.8	0.7	0.7	0.7	0.8	0.7	0.7	0.7
Cu	mmol/L	1.3	0.4	0.6	0.6	0.5	0.4	0.4	0.4	0.4	0.4	0.4	0.4
Zn	mmol/L	1.9	0.0	BDL	1.7	BDL	BDL	BDL	BDL	0.1	BDL	BDL	BDL
As	mmol/L	0.2	0.1	0.1	0.1	0.1	0.1	0.1	0.1	0.1	0.1	0.1	0.1
Sr	mmol/L	3.8	4.1	4.9	4.6	4.3	3.8	3.8	3.8	4.0	4.0	3.7	3.6
Mo	µmol/L	33.7	11.2	13.2	12.0	10.4	8.8	8.6	16.1	11.2	7.8	8.6	8.1
Cd	µmol/L	5.2	1.6	0.9	10.7	1.0	1.4	0.5	0.9	0.8	1.0	0.6	1.0
Ba	mmol/L	1.9	2.2	2.3	2.1	1.9	1.7	1.7	1.8	1.9	2.0	2.0	2.0
Pb	µmol/L	63.9	48.6	62.2	61.7	55.5	53.3	51.4	54.3	52.5	54.9	51.4	52.0
U	µmol/L	15.3	15.0	18.6	17.9	16.9	14.7	15.4	15.6	15.4	16.4	15.1	14.6

H2O Type II 95°C										
Sample ID		Input	T0'	T0	T4hrs	T8hrs	T24hrs	T48hrs	T96hrs	T168hrs
Time (min)		0	1	135	375	615	1575	3015	5915	10215
Li	mmol/L	BDL	20.2	11.8	7.3	5.5	4.5	4.5	4.1	BDL
Na	mol/L	0.061	0.048	0.044	0.043	0.038	0.034	0.064	0.031	0.018
Mg	mol/L	0.4	0.5	0.4	0.4	0.4	0.4	0.4	0.4	0.4
Al	mol/L	1.0	1.0	0.9	0.9	0.9	0.9	0.9	0.9	1.3
Si	mol/L	3.4	2.8	2.8	2.8	2.5	2.6	2.8	2.9	4.1
K	mol/L	0.5	0.5	0.5	0.5	0.5	0.5	0.5	0.5	0.5
P	mol/L	0.033	0.036	0.032	0.034	0.031	0.031	0.031	0.030	0.032
S	mol/L	0.6	0.2	0.2	0.2	0.2	0.2	0.2	0.2	BDL
Ca	mol/L	5.3	5.8	5.3	5.7	5.2	5.1	5.1	5.1	5.7
Ti	mol/L	0.027	0.031	0.030	0.031	0.028	0.030	0.029	0.029	0.029
Cr	mmol/L	0.8	0.8	0.7	0.8	0.7	0.7	0.8	0.8	0.8
Mn	mmol/L	5.4	5.8	5.2	5.7	5.1	5.0	5.3	5.4	5.4
Fe	mol/L	0.3	0.3	0.3	0.3	0.3	0.3	0.3	0.3	0.3
Co	mmol/L	0.2	0.2	0.2	0.2	0.2	0.2	0.2	0.2	0.2
Ni	mmol/L	0.9	0.9	0.8	0.9	0.9	0.9	0.9	0.9	BDL
Cu	mmol/L	1.3	1.3	1.3	1.4	1.2	1.1	1.2	1.2	BDL
Zn	mmol/L	1.9	BDL	BDL	BDL	BDL	BDL	BDL	0.3	0.2
As	mmol/L	0.2	0.2	0.1	0.1	0.1	0.1	0.1	0.1	0.1
Sr	mmol/L	3.8	4.5	4.0	4.3	3.8	3.8	3.9	3.9	4.0
Mo	µmol/L	33.7	698.6	253.4	137.9	77.5	57.7	65.1	36.0	9.7
Cd	µmol/L	5.2	6.9	3.9	3.7	3.9	2.3	807.2	1.5	0.4
Ba	mmol/L	1.9	2.5	2.2	2.4	2.3	2.2	2.3	2.2	2.2
Pb	µmol/L	63.9	74.4	61.6	62.2	64.6	61.8	78.1	59.2	67.3
U	µmol/L	15.3	20.2	17.3	17.7	16.8	17.1	17.6	17.1	17.1
NaCl Type II 95°C										
Sample ID		Input	T0'	T0	T4hrs	T8hrs	T24hrs	T48hrs	T96hrs	T168hrs
Time (min)		0	1	140	380	480	480	480	480	480
Li	mmol/L	BDL	153.0	37.6	3.6	3.2	3.1	3.2	2.7	BDL
Na	mol/L	0.061	3.391	0.596	0.047	0.052	0.047	0.052	0.037	0.029
Mg	mol/L	0.4	0.7	0.4	0.4	0.4	0.4	0.4	0.4	0.3
Al	mol/L	1.0	1.0	1.0	0.9	0.9	0.9	0.9	0.8	1.2
Si	mol/L	3.4	3.4	3.3	2.6	2.3	3.1	2.8	2.7	3.9
K	mol/L	0.5	0.9	0.6	0.5	0.5	0.6	0.6	0.5	0.5
P	mol/L	0.033	0.033	0.032	0.028	0.030	0.029	0.029	0.027	0.027
S	mol/L	0.6	0.5	0.3	0.2	0.2	0.2	0.2	0.2	BDL
Ca	mol/L	5.3	5.0	5.2	5.1	4.7	5.3	5.4	5.0	4.9
Ti	mol/L	0.027	0.039	0.028	0.029	0.031	0.033	0.032	0.031	0.026
Cr	mmol/L	0.8	1.5	0.9	0.7	0.7	0.7	0.7	0.7	0.6
Mn	mmol/L	5.4	7.5	5.9	5.4	5.3	5.4	5.6	5.2	4.5
Fe	mol/L	0.3	0.3	0.3	0.3	0.3	0.3	0.3	0.3	0.3
Co	mmol/L	0.2	0.2	0.2	0.2	0.2	0.2	0.2	0.2	0.1
Ni	mmol/L	0.9	0.7	BDL	0.9	0.9	0.8	0.9	0.8	BDL

Cu	mmol/L	1.3	1.3	1.0	1.1	1.1	1.0	1.3	0.9	BDL
Zn	mmol/L	1.9	5.7	3.0	BDL	BDL	BDL	0.0	BDL	0.2
As	mmol/L	0.2	BDL	BDL	0.1	0.1	0.1	0.1	0.1	0.1
Sr	mmol/L	3.8	4.3	3.6	3.7	3.8	3.8	4.0	3.7	3.2
Mo	µmol/L	33.7	72.7	25.1	21.3	19.5	18.8	15.8	15.6	8.3
Cd	µmol/L	5.2	73.1	23.5	1.8	1.5	1.0	1.1	2.3	BDL
Ba	mmol/L	1.9	2.2	1.6	1.9	2.0	2.2	2.3	2.2	1.9
Pb	µmol/L	63.9	61.6	59.8	65.1	60.1	61.7	63.1	70.2	55.7
U	µmol/L	15.3	4110.4	1991.1	16.8	17.4	17.7	18.3	17.2	15.2

Core 2 Experimental Data

H2O Type I 140°C

Sample ID		Input	T0'	T0.5hrs'	Thrs'	T0	T1hrs	T2hrs	T4hrs	T8hrs	T16hrs	T24hrs	T48hrs
Time (min)		0	1	30	60	110	170	230	350	590	1055	1550	2990
Li	mmol/L	BDL	BDL	BDL	BDL	BDL	BDL	BDL	BDL	BDL	BDL	BDL	BDL
Na	mol/L	0.019	0.043	0.041	0.040	0.044	0.038	0.033	0.042	0.031	0.023	0.021	0.032
Mg	mol/L	0.6	0.8	0.8	0.8	0.8	0.8	0.7	0.8	0.7	0.6	0.6	0.8
Al	mol/L	0.3	0.5	0.5	0.5	0.6	0.6	0.5	0.6	0.4	0.5	0.4	0.5
Si	mol/L	3.3	4.8	5.2	4.2	4.8	4.6	4.7	4.9	3.9	3.5	3.5	4.2
K	mol/L	0.2	0.2	0.2	0.2	0.2	0.2	0.2	0.3	0.2	0.2	0.2	0.2
P	mol/L	0.011	0.017	0.016	0.016	0.017	0.016	0.015	0.018	0.014	0.012	0.012	0.014
S	mol/L	0.4	0.6	0.5	0.5	0.5	0.5	0.4	0.5	0.4	0.4	0.4	0.5
Ca	mol/L	5.2	6.7	6.7	6.3	7.2	6.6	6.1	7.4	5.9	5.0	4.8	6.4
Ti	mol/L	0.011	0.014	0.015	0.014	0.015	0.015	0.014	0.016	0.014	0.010	0.013	0.014
Cr	mmol/L	0.2	0.4	0.4	0.4	0.5	0.4	0.4	0.5	0.3	0.3	0.3	0.4
Mn	mmol/L	11.2	15.7	14.8	14.6	16.2	14.7	13.2	20.1	14.7	11.3	11.0	15.5
Fe	mol/L	0.3	0.4	0.3	0.3	0.4	0.3	0.3	0.4	0.3	0.3	0.3	0.3
Co	mmol/L	0.1	0.1	0.1	0.1	0.1	0.1	0.1	0.1	0.1	0.1	0.1	0.1
Ni	mmol/L	0.2	0.3	0.3	0.3	0.5	0.4	0.3	0.4	0.3	0.3	0.2	0.3
Cu	mmol/L	0.2	0.4	0.4	0.4	8.9	0.4	0.3	0.4	0.3	0.2	0.2	0.3
Zn	mmol/L	0.0	0.0	0.1	0.0	3.8	0.0	0.1	0.1	0.1	0.0	0.0	0.1
As	mmol/L	0.1	0.1	0.1	0.1	0.1	0.1	0.1	0.1	0.1	0.1	0.1	0.1
Sr	mmol/L	4.0	5.1	4.8	4.6	5.2	4.9	4.3	5.3	4.2	3.6	3.5	4.5
Mo	µmol/L	25.7	39.1	31.3	30.5	31.5	25.7	24.7	32.1	22.3	18.2	19.6	23.9
Cd	µmol/L	0.9	1.4	0.7	1.1	1.3	0.9	0.9	1.1	30.8	1.1	2.3	4.9
Ba	mmol/L	2.1	3.2	4.6	4.1	5.0	4.3	3.9	4.2	3.0	2.1	1.9	2.1
Pb	µmol/L	44.8	70.4	60.0	65.5	159.3	67.6	56.6	69.3	68.7	61.2	56.1	75.2
U	µmol/L	5.5	7.0	6.4	6.0	7.4	7.4	6.3	7.3	5.9	5.6	4.8	6.5

NaCl Type I 140°C

Sample ID		Input	T0'	T0.5hrs'	Thrs'	T0	T1hrs	T2hrs	T4hrs	T8hrs	T16hrs	T24hrs	T48hrs
Time (min)		0	1	30	60	125	185	245	365	605	1065	1565	3005
Li	mmol/L	BDL	BDL	BDL	BDL	BDL	BDL	BDL	BDL	BDL	BDL	BDL	BDL
Na	mol/L	0.019	0.024	0.023	0.030	0.043	0.028	0.023	0.049	0.078	0.036	0.132	0.047
Mg	mol/L	0.6	0.6	0.6	0.5	0.6	0.5	0.6	0.9	0.8	0.7	0.7	0.6
Al	mol/L	0.3	0.4	0.7	0.4	0.8	0.4	0.3	1.0	0.5	0.5	0.5	0.3

Si	mol/L	3.3	3.5	3.8	3.7	3.9	3.9	4.8	5.3	4.4	4.6	4.1	3.2
K	mol/L	0.2	0.2	0.2	0.2	0.2	0.2	0.2	0.3	0.2	0.2	0.2	0.2
P	mol/L	0.011	0.011	0.013	0.012	0.013	0.013	0.011	0.018	0.015	0.014	0.013	0.010
S	mol/L	0.4	0.3	0.4	0.3	0.4	0.3	0.3	0.5	0.4	0.4	0.4	0.4
Ca	mol/L	5.2	4.8	5.1	4.9	5.4	5.3	4.8	7.3	6.7	6.0	6.1	4.8
Ti	mol/L	0.011	0.012	0.011	0.011	0.011	0.011	0.010	0.017	0.015	0.014	0.013	0.010
Cr	mmol/L	0.2	0.3	0.4	0.3	0.4	0.3	0.3	0.5	0.4	0.3	0.3	0.3
Mn	mmol/L	11.2	11.0	11.3	10.2	11.7	10.0	10.1	17.8	15.3	13.2	12.7	10.6
Fe	mol/L	0.3	0.2	0.3	0.2	0.3	0.3	0.2	0.4	0.3	0.3	0.3	0.2
Co	mmol/L	0.1	0.1	0.1	0.1	0.1	0.1	0.0	0.1	0.1	0.1	0.1	0.1
Ni	mmol/L	0.2	0.3	0.3	0.2	0.3	0.2	0.2	0.4	0.3	0.3	0.3	0.2
Cu	mmol/L	0.2	0.2	0.2	0.2	0.2	0.2	0.2	0.4	0.4	0.2	0.2	0.2
Zn	mmol/L	0.0	0.1	0.1	0.0	0.1	0.0	BDL	0.1	0.1	0.0	0.0	0.0
As	mmol/L	0.1	0.1	0.1	0.1	0.1	0.1	0.1	0.1	0.1	0.1	0.1	0.1
Sr	mmol/L	4.0	3.5	3.8	3.4	3.6	3.4	3.5	5.4	4.9	4.1	4.1	3.2
Mo	µmol/L	25.7	21.9	24.9	19.0	28.0	18.0	19.5	32.3	26.2	24.5	24.1	17.8
Cd	µmol/L	0.9	0.9	3.8	0.9	2.0	0.9	0.5	3.9	0.7	1.1	0.7	0.6
Ba	mmol/L	2.1	2.8	3.0	2.6	2.1	1.9	1.4	2.6	2.1	1.8	1.7	1.3
Pb	µmol/L	44.8	48.7	63.7	54.8	54.7	50.8	42.4	71.5	64.9	58.9	59.6	43.5
U	µmol/L	5.5	4.9	5.4	5.5	5.3	5.0	4.4	8.0	6.4	6.0	6.2	4.3

H2O Type II 140°C

Sample ID		Input	T0'	T0	T4hrs	T8hrs	T24hrs	T48hrs	T96hrs
Time (min)		0	1	130	370	610	1570	3010	5910
Li	mmol/L	BDL	56.9	BDL	BDL	BDL	1.0	7.7	BDL
Na	mol/L	0.019	0.018	0.011	0.016	0.026	0.029	0.024	0.035
Mg	mol/L	0.6	0.6	0.5	0.5	0.7	0.8	0.7	0.9
Al	mol/L	0.3	0.4	0.3	0.4	0.5	0.6	0.5	0.5
Si	mol/L	3.3	3.8	3.3	3.4	4.8	4.5	4.2	5.3
K	mol/L	0.2	0.2	0.2	0.2	0.2	0.2	0.2	0.2
P	mol/L	0.011	0.011	0.010	0.011	0.014	0.014	0.013	0.015
S	mol/L	0.4	0.4	0.3	0.3	0.4	0.5	0.4	0.5
Ca	mol/L	5.2	5.0	4.4	5.0	6.2	6.9	6.4	7.7
Ti	mol/L	0.011	0.010	0.010	0.011	0.013	0.014	0.013	0.017
Cr	mmol/L	0.2	0.2	1.2	0.3	0.3	0.4	0.4	0.4
Mn	mmol/L	11.2	11.9	9.8	10.4	13.7	19.8	17.7	17.0
Fe	mol/L	0.3	0.3	0.2	0.2	0.3	0.3	0.3	0.4
Co	mmol/L	0.1	0.1	0.1	0.1	0.1	0.1	0.1	0.1
Ni	mmol/L	0.2	0.2	0.6	0.3	0.3	0.3	0.3	0.3
Cu	mmol/L	0.2	0.2	0.2	0.2	0.3	0.3	0.3	0.4
Zn	mmol/L	0.0	BDL	0.0	0.0	0.0	0.1	0.0	0.1
As	mmol/L	0.1	0.1	0.1	0.1	0.1	0.1	0.1	0.1
Sr	mmol/L	4.0	3.8	3.2	3.6	4.6	5.1	4.7	5.6
Mo	µmol/L	25.7	26.7	22.0	17.8	23.9	26.8	24.9	26.7
Cd	µmol/L	0.9	0.8	1.4	1.1	0.8	1.5	0.6	0.8
Ba	mmol/L	2.1	2.3	2.8	2.7	2.9	2.7	2.1	2.5

Pb	µmol/L	44.8	43.3	39.3	47.4	55.5	71.1	56.4	64.6
U	µmol/L	5.5	4.5	4.1	5.1	5.7	7.2	6.4	7.2
NaCl Type II 140°C									
Sample ID		Input	T0'	T0	T4hrs	T8hrs	T24hrs	T48hrs	T96hrs
Time (min)		0	1	140	380	620	1580	3020	5920
Li	mmol/L	BDL	BDL	BDL	BDL	BDL	BDL	BDL	BDL
Na	mol/L	0.019	0.012	0.034	0.032	0.077	0.031	0.019	0.145
Mg	mol/L	0.6	0.6	0.7	0.5	0.6	0.6	0.6	0.7
Al	mol/L	0.3	0.4	0.5	0.4	0.4	0.4	0.3	0.4
Si	mol/L	3.3	3.7	4.3	3.3	3.8	4.0	3.6	4.5
K	mol/L	0.2	0.2	0.2	0.2	0.2	0.2	0.2	0.2
P	mol/L	0.011	0.011	0.014	0.011	0.012	0.012	0.010	0.013
S	mol/L	0.4	0.3	0.4	0.3	0.4	0.4	0.3	0.4
Ca	mol/L	5.2	5.1	6.5	4.9	5.6	5.6	4.8	6.3
Ti	mol/L	0.011	0.011	0.014	0.011	0.013	0.012	0.010	0.013
Cr	mmol/L	0.2	0.2	0.3	0.3	0.3	0.3	0.2	0.4
Mn	mmol/L	11.2	21.0	19.0	23.0	11.6	12.7	11.2	14.1
Fe	mol/L	0.3	0.2	0.3	0.2	0.3	0.3	0.2	0.3
Co	mmol/L	0.1	0.1	0.1	0.1	0.1	0.1	0.1	0.1
Ni	mmol/L	0.2	0.3	0.3	0.3	0.3	0.3	0.2	0.3
Cu	mmol/L	0.2	0.0	0.3	0.2	0.2	0.1	0.1	0.2
Zn	mmol/L	0.0	BDL	0.2	0.1	0.0	0.1	0.0	0.0
As	mmol/L	0.1	0.1	0.1	0.1	0.1	0.1	0.1	0.1
Sr	mmol/L	4.0	3.7	4.6	3.4	3.9	3.7	3.3	4.2
Mo	µmol/L	25.7	19.4	24.9	18.5	18.7	18.8	16.5	21.8
Cd	µmol/L	0.9	1.8	1.2	0.7	1.5	1.0	0.8	1.0
Ba	mmol/L	2.1	2.6	2.4	1.6	1.8	1.5	1.3	1.6
Pb	µmol/L	44.8	50.8	58.5	45.6	52.4	47.8	41.8	52.4
U	µmol/L	5.5	4.9	6.7	4.8	5.3	5.3	4.3	6.0

B-3 Measured XRD Values. Mineralogy is broken up into major (M), minor (m), and trace (t) minerals. In the event that a mineral was not detected it is noted as N.D.

Sample Name	Quartz	Calcite	Feldspar (Orthoclase)	Illite	Dolomite	Pyrite	Clinochlore	Kaolinite	Gypsum	Total	Rwp	GOF	Weighted Durbin-Watson
Core 1													
Input 1	m 7.7%	M 63.0%	M 12.6%	m 7.9%	m 4.8%	m 1.5%	m 2.2%	t 0.4%	N.D 0.0%	100.0%	9.35	2.49	0.39
Input 2	m 7.0%	M 59.5%	M 10.9%	M 14.1%	m 5.2%	m 1.4%	m 1.7%	t 0.2%	N.D 0.0%	100.0%	8.73	2.3	0.46
Freshwater Exp. Type I T0	M	M	M	M	m	m	m	t	N.D	Too little of sample - XRD done with ethanol slurry, therefore no quantitative data possible			
Freshwater Exp. Type I T4hr	m 6.5%	M 56.3%	M 8.3%	m 22.9%	m 3.4%	m 1.3%	m 1.1%	t 0.1%	N.D 0.0%	100.0%	9.34	2.37	0.47
Freshwater Exp. Type I T8hr	m 6.5%	M 58.4%	M 9.3%	m 19.4%	m 3.4%	m 1.3%	m 1.3%	t 0.6%	N.D 0.0%	100.0%	8.65	2.18	0.52
Freshwater Exp. Type II T0	m 6.8%	M 58.7%	M 10.0%	m 19.3%	m 2.5%	m 1.3%	m 1.2%	t 0.2%	N.D 0.0%	100.0%	8.74	2.2	0.5
Freshwater Exp. Type II T4hr	m 6.9%	M 63.3%	M 10.1%	m 13.9%	m 3.0%	m 1.3%	m 1.4%	t 0.1%	N.D 0.0%	100.0%	8.7	2.21	0.49
Freshwater Exp. Type II T8hr	m 7.0%	M 61.5%	M 10.6%	m 14.3%	m 3.1%	m 1.3%	m 1.8%	t 0.5%	N.D 0.0%	100.0%	8.58	2.18	0.49
NaCl Exp. Type I T0	m 6.7%	M 56.4%	M 7.0%	m 21.8%	m 4.6%	m 1.2%	m 1.9%	t 0.4%	N.D 0.0%	100.0%	9.92	2.53	0.47
NaCl Exp. Type I T4hr	m 7.4%	M 62.8%	M 10.2%	m 14.1%	m 2.2%	m 1.4%	m 1.8%	t 0.1%	N.D 0.0%	100.0%	8.37	2.12	0.51
NaCl Exp. Type I T8hr	m 7.0%	M 62.5%	M 10.4%	m 14.8%	m 2.0%	m 1.3%	m 1.6%	t 0.4%	N.D 0.0%	100.0%	8.61	2.17	0.48
NaCl Exp. Type II T0	m 6.6%	M 58.5%	M 9.8%	m 19.0%	m 3.6%	m 1.4%	m 1.1%	t 0.1%	N.D 0.0%	100.0%	8.77	2.25	0.5
NaCl Exp. Type II T4hr	m 6.6%	M 59.8%	M 8.7%	m 19.4%	m 3.0%	m 1.3%	m 1.1%	t 0.1%	N.D 0.0%	100.0%	8.32	2.08	0.54
NaCl Exp. Type II T8hr	m 6.6%	M 59.4%	M 9.7%	m 18.8%	m 2.0%	m 1.3%	m 1.7%	t 0.5%	N.D 0.0%	100.0%	8.64	2.2	0.52
Core 2													
Input 1	M 19.7%	M 56.4%	m 6.2%	m 3.3%	M 12.3%	m 2.1%	N.D 0.0%	N.D 0.0%	N.D 0.0%	100.0%	8.16	2.12	0.52
Input 2	M 19.2%	M 55.5%	m 5.7%	m 4.7%	M 12.6%	m 2.3%	N.D 0.0%	N.D 0.0%	N.D 0.0%	100.0%	8.23	2.12	0.5
Input 3	M 20.0%	M 56.2%	m 6.1%	m 3.2%	M 12.4%	m 2.1%	N.D 0.0%	N.D 0.0%	N.D 0.0%	100.0%	8.7	2.25	0.46
Freshwater Exp. Type I T0	M	M	M	m	M	m	N.D	N.D	N.D	Too little of sample - XRD done with ethanol slurry, therefore no quantitative data possible			
Freshwater Exp. Type I T4hr	M 19.6%	M 55.8%	m 5.8%	m 6.5%	M 10.5%	m 1.8%	N.D 0.0%	N.D 0.0%	N.D 0.0%	100.0%	9.98	2.48	0.44
Freshwater Exp. Type I T8hr	M 19.5%	M 57.3%	m 5.7%	m 3.9%	M 11.5%	m 2.1%	N.D 0.0%	N.D 0.0%	N.D 0.0%	100.0%	7.59	2.01	0.55
Freshwater Exp. Type II T0	M 20.1%	M 57.5%	m 6.1%	m 3.0%	M 11.3%	m 2.0%	N.D 0.0%	N.D 0.0%	N.D 0.0%	100.0%	8.7	2.17	0.5
Freshwater Exp. Type II T4hr	M 19.9%	M 57.4%	m 6.0%	m 3.7%	M 11.1%	m 2.0%	N.D 0.0%	N.D 0.0%	N.D 0.0%	100.0%	8.42	2.12	0.52
Freshwater Exp. Type II T8hr	M 20.0%	M 56.8%	m 4.4%	m 4.5%	M 12.2%	m 2.1%	N.D 0.0%	N.D 0.0%	N.D 0.0%	100.0%	8.12	2.09	0.53
NaCl Exp. Type I T0	M 19.1%	M 54.4%	m 5.1%	m 8.5%	M 11.3%	m 1.6%	N.D 0.0%	N.D 0.0%	N.D 0.0%	100.0%	10.24	2.58	0.42
NaCl Exp. Type I T4hr	M 19.2%	M 56.5%	m 5.9%	m 3.3%	M 13.4%	m 1.7%	N.D 0.0%	N.D 0.0%	N.D 0.0%	100.0%	10.5	2.64	0.41
NaCl Exp. Type I T8hr	M 19.5%	M 57.3%	m 5.9%	m 4.0%	M 11.3%	m 2.0%	N.D 0.0%	N.D 0.0%	N.D 0.0%	100.0%	8.19	2.13	0.52
NaCl Exp. Type II T0	M 19.5%	M 56.1%	m 5.8%	m 5.8%	M 10.8%	m 1.9%	N.D 0.0%	N.D 0.0%	N.D 0.0%	100.0%	8.29	2.07	0.54
NaCl Exp. Type II T4hr	M 19.7%	M 56.2%	m 6.1%	m 5.1%	M 10.9%	m 1.9%	N.D 0.0%	N.D 0.0%	N.D 0.0%	100.0%	8.11	2.02	0.55

NaCl Exp. Type II T8hr	M 20.0%	M 57.2%	m 5.9%	m 3.3%	M 11.4%	m 2.1%	N.D 0.0%	N.D 0.0%	N.D 0.0%	100.0%	7.93	2.05	0.54
Outcrop													
Input 1	M 52.6%	M 15.5%	M 16.8%	M 10.7%	m 1.0%	m 2.7%	N.D 0.0%	N.D 0.0%	t 0.6%	100.0%	6.85	2.06	0.58
Input 2	M 52.0%	M 15.5%	M 16.7%	M 10.7%	m 1.5%	m 2.9%	N.D 0.0%	N.D 0.0%	t 0.9%	100.0%	7.03	2.08	0.54
Input 3	M 50.9%	M 12.1%	M 17.1%	M 14.6%	t 0.4%	m 2.6%	N.D 0.0%	N.D 0.0%	m 2.2%	100.0%	7.14	2.16	0.54
Input 4	M 54.2%	M 15.2%	M 15.3%	M 10.5%	m 1.5%	m 2.8%	N.D 0.0%	N.D 0.0%	t 0.5%	100.0%	6.82	2.02	0.58
Input 5	M 51.4%	M 15.6%	M 13.4%	M 15.8%	t 1.0%	m 2.8%	N.D 0.0%	N.D 0.0%	N.D. 0.0%	100.0%	6.91	2.01	0.58
Freshwater 25C T0	M	M	M	M	m	m	N.D	N.D	N.D.	Too little of sample - XRD done with ethanol slurry, therefore no quantitative data possible			
Freshwater 25C T4hr	M 48.7%	M 17.6%	M 13.4%	M 16.0%	m 1.4%	m 3.0%	N.D 0.0%	N.D 0.0%	N.D. 0.0%	100.0%	7.43	2.14	0.56
Freshwater 25C T48hr	M 51.5%	M 15.9%	M 14.8%	M 13.6%	t 1.5%	m 2.8%	N.D 0.0%	N.D 0.0%	N.D. 0.0%	100.0%	6.95	2	0.62
Freshwater 95C T0	M 47.8%	M 13.5%	M 15.2%	M 19.7%	t 1.2%	m 2.7%	N.D 0.0%	N.D 0.0%	N.D. 0.0%	100.0%	7.86	2.33	0.45
Freshwater 95C T4hr	M 46.5%	M 14.3%	M 15.5%	M 20.1%	t 0.9%	m 2.7%	N.D 0.0%	N.D 0.0%	N.D. 0.0%	100.0%	9.37	2.76	0.36
Freshwater 95C T48hr	M 51.5%	M 13.8%	M 15.8%	M 15.4%	t 0.8%	m 2.7%	N.D 0.0%	N.D 0.0%	N.D. 0.0%	100.0%	8.88	2.61	0.39
Freshwater 140C T0	M 48.3%	M 16.6%	M 15.1%	M 15.7%	t 1.5%	m 2.9%	N.D 0.0%	N.D 0.0%	N.D. 0.0%	100.0%	6.88	1.99	0.59
Freshwater 140C T4hr	M 48.5%	M 17.1%	M 15.2%	M 15.3%	t 1.3%	m 2.8%	N.D 0.0%	N.D 0.0%	N.D. 0.0%	100.0%	8.42	2.45	0.45
Freshwater 140C T48hr	M 50.8%	M 16.1%	M 13.4%	M 15.3%	t 1.5%	m 2.9%	N.D 0.0%	N.D 0.0%	N.D. 0.0%	100.0%	6.76	1.93	0.62
NaCl 25C T0	M 50.7%	M 15.9%	M 13.7%	M 16.1%	m 1.1%	m 2.6%	N.D 0.0%	N.D 0.0%	N.D. 0.0%	100.0%	7.16	2.09	0.54
NaCl 25C T4hr	M 48.4%	M 17.1%	M 13.3%	M 18.0%	t 0.6%	m 2.7%	N.D 0.0%	N.D 0.0%	N.D. 0.0%	100.0%	8.3	2.39	0.45
NaCl 25C T48hr	M 50.2%	M 17.1%	M 11.9%	M 16.8%	m 1.2%	m 2.8%	N.D 0.0%	N.D 0.0%	N.D. 0.0%	100.0%	6.96	1.96	0.62
NaCl 95C T0	M	M	M	M	m	m	N.D	N.D	N.D.	Too little of sample - XRD done with ethanol slurry, therefore no quantitative data possible			
NaCl 95C T4hr	M 49.0%	M 18.5%	M 18.2%	M 10.7%	t 0.3%	m 3.2%	N.D 0.0%	N.D 0.0%	N.D. 0.0%	100.0%	8.16	2.38	0.43
NaCl 95C T48hr	M 50.9%	M 16.4%	M 18.2%	M 10.9%	t 0.7%	m 2.9%	N.D 0.0%	N.D 0.0%	N.D. 0.0%	100.0%	7.9	2.29	0.47
NaCl 140C T0	M 47.7%	M 16.9%	M 15.2%	M 17.0%	t 0.8%	m 2.5%	N.D 0.0%	N.D 0.0%	N.D. 0.0%	100.0%	9.18	2.67	0.38
NaCl 140C T4hr	M 48.5%	M 17.1%	M 15.2%	M 15.3%	t 1.3%	m 2.8%	N.D 0.0%	N.D 0.0%	N.D. 0.0%	100.0%	8.42	2.45	0.45
NaCl 140C T48hr	M 54.1%	M 16.3%	M 17.4%	M 8.2%	t 1.0%	m 2.9%	N.D 0.0%	N.D 0.0%	N.D. 0.0%	100.0%	7.37	2.22	0.48

Supplemental Geochemical Profiles

Core experiments are represented as blue for pure water experiments and orange for saline experiments. Outcrop experiments are color coded by temperature, 25°C (blue), 95°C (yellow), 140°C (orange) and organized by experiment: pure water (solid lines) and saline (dashed lines). When an element was below the detection limit, they were plotted as zero.

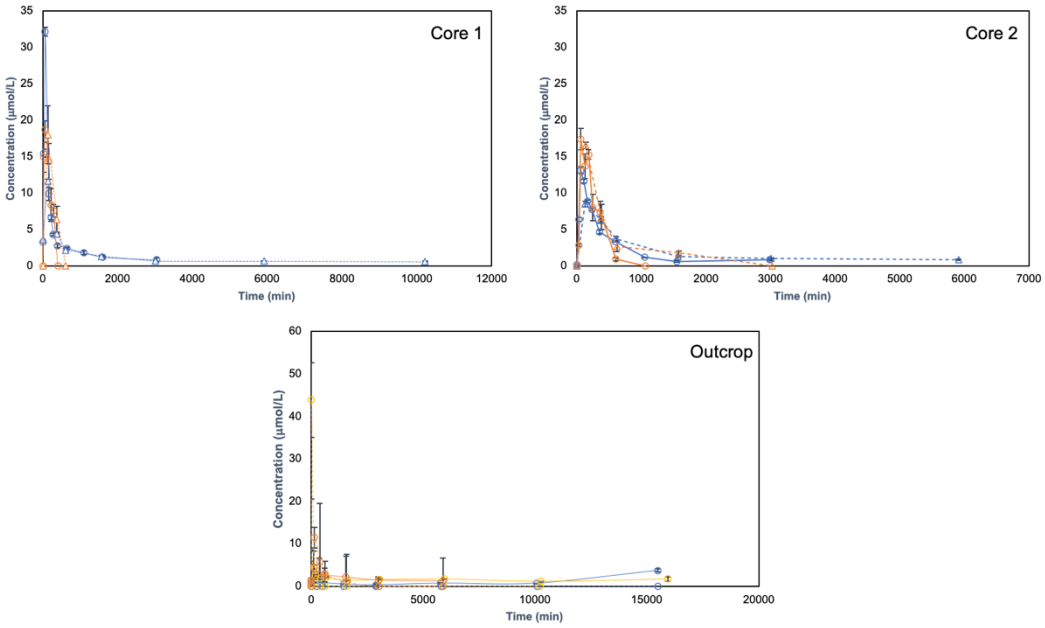

B-4 Geochemical profiles of $Al_{(aq)}$ for both cores and outcrop experiments in µmol/L.

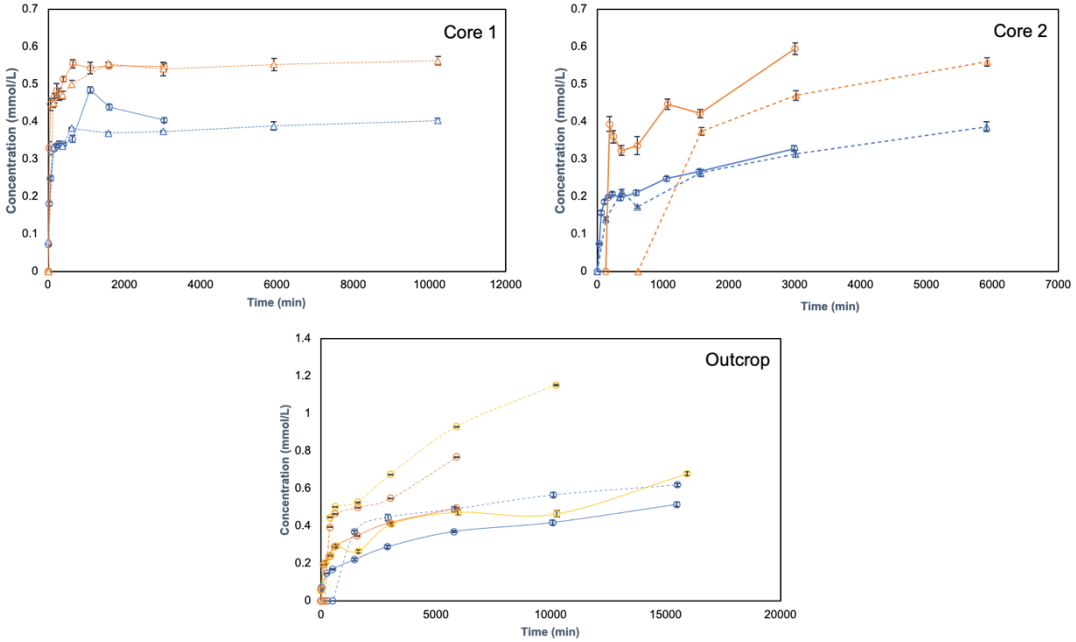

B-5 Geochemical profile of $K_{(aq)}$ for both cores and outcrop experiments in mmol/L.

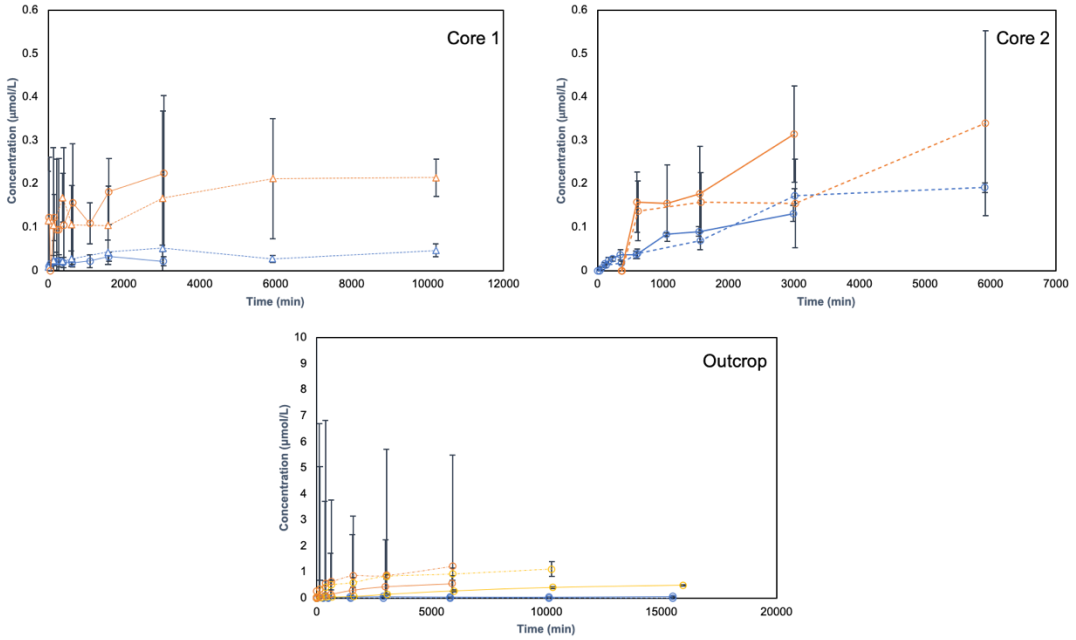

B-6 Geochemical profile of $As_{(aq)}$ for both cores and outcrop experiments in µmol/L.

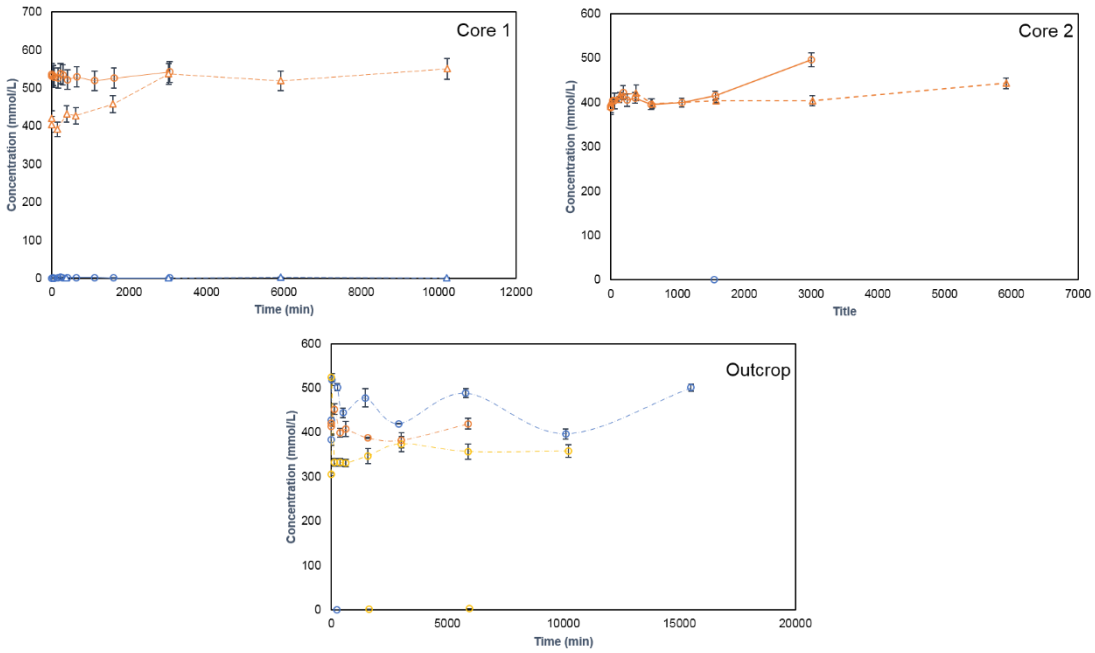

B-7 Geochemical profile of $Cl_{(aq)}$ for both cores and outcrop experiments in mmol/L.

Appendix C

Supplemental Information for FPW Samples from Zhong et al. 2019

C-1 FPW detection limits after dilution factor was applied, in ppm.

Na	271
Li	0.031
B	1.71
Mg	7.44
Al	0.18
Si	30.9
S	14.5
K	122
Ca	93.4
Mn	0.074
Fe	0.43
Ni	0.45
Cu	0.83
Zn	1.52
As	0.42
Br	20.0
Sr	4.1
Cd	0.01
Ba	0.02
Pb	0.01

C-2 Approximate detection limits for NaCl and freshwater reactor experiments in mg/L.

	Freshwater Reactor Experiments	NaCl experiments
Na	1.0	100
Cl (ICP)	66	6600
Cl (Colorimetry)	0.20	0.20
Li	0.044	0.60
B	0.067	0.91
Mg	0.049	0.66
Al	0.0033	0.04
Si	0.051	0.69
K	1.0	14
P	0.0045	0.060
Ti	0.00026	0.0035
S	1.8	24
Ca	0.34	4.5
Mn	0.013	0.17
Fe	0.015	0.21
Co	0.00062	0.0084
Ni	0.00062	0.0084
Cu	0.00062	0.0084
Zn	0.0070	0.094
Br	0.29	3.89
Sr	0.050	0.67
As	0.00062	0.0083
Mo	0.00061	0.0082
Cd	0.00060	0.0081
Ba	0.00062	0.0083
Pb	0.0018	0.025
U	0.00093	0.013

Appendix D

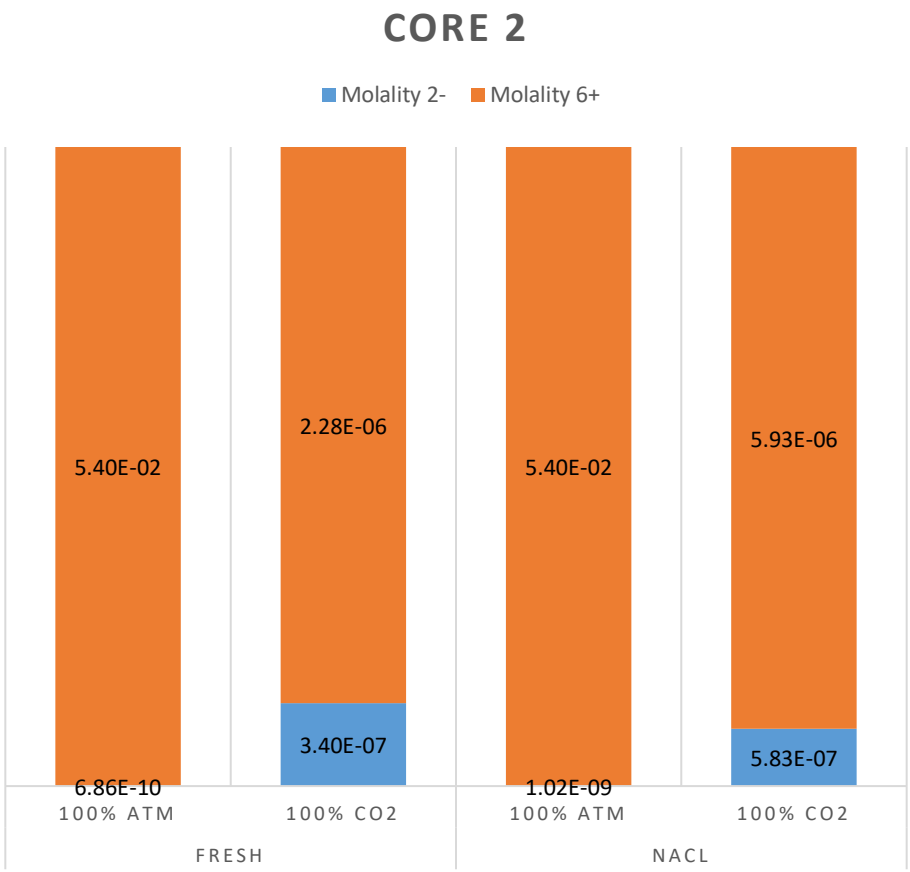

Figure D-1: Modelled speciation and molality of leached sulfur during experiments with Core 2 under atmospheric headspace conditions and 100 % CO_2 headspace, so simulate an anoxic environment.